Lecture Notes on

Wind Energy Systems

Summer Semester 2025

Moritz Diehl

Edition 2025

Contents

Preface

This manuscript is based on lecture notes of the Wind Energy Systems (WES) master course given by Moritz Diehl in the summer semesters 2018 and 2020 at the University of Freiburg. This course was supported by Rachel Leuthold and Nick Harder who gave the exercise sessions, but also contributed significantly to the organization and contents of this text, for which I want to very warmly thank them. The initial LaTeX typesetting and drawing of most of the figures in this manuscript was performed by Hsin Chen under a job student contract, whom I also want to thank. Finally, I want to also thank Paul Daum for proofreading of the manuscript. I hope that these lecture notes prove to be an additional useful resource for self study, in addition to the video recordings and the exercise sheets which are also released on the WES course webpage.

`https://www.syscop.de/teaching/ss2025/wind-energy-systems`

Moritz Diehl,

Freiburg, July 2020

Chapter 1

Introduction

1.1 Motivation and lecture overview

This course introduces the fundamentals of wind energy systems from resource analysis to aerodynamics, mechanical design, and control. The objective is to provide students with a thorough understanding of how wind energy can be harvested efficiently and integrated into modern power systems.

Wind energy is a rapidly growing sector of renewable energy, combining concepts from fluid dynamics, mechanical and electrical engineering, and control theory. These lecture notes serve as a companion to the slides, exercise sessions, and video lectures. For slides: Click here for slides (https://tinyurl.com/yb8xskhn).

1.2 Energy content of the wind

Consider a cylindrical volume of air flowing through an imaginary "window" of cross-sectional area A [m^2] with flow speed u [$\mathrm{m\,s}^{-1}$] and length L [m].

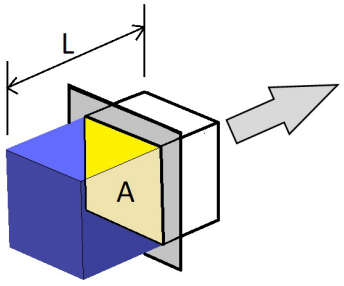

Figure 1.1: Power flowing through a 'window' of air.

The mass of air m [kg] in this volume is:

$$m = \rho L A, \tag{1.1}$$

where ρ is the air density [$\mathrm{kg\,m}^{-3}$], typically $\rho = 1.225\,\mathrm{kg/m}^3$.

The kinetic energy T [J] in this volume of air is:

$$T = \frac{1}{2}mu^2 = \frac{1}{2}\rho L A u^2. \tag{1.2}$$

The power P [W] is defined as the rate of energy transfer through the "window." And as an average speed is the distance traveled divided by the time to travel, the time t [s] for the air volume to pass through the window is $t = L/u$. So the power becomes:

$$P = \frac{T}{t} = \frac{1}{2}\rho A u^3. \tag{1.3}$$

The **key insight** here is that the power P is proportional to the cube of wind speed u.

The SI-unit consistency of this equation can be shown explicitly:

$$\underbrace{\frac{\mathrm{kg}}{\mathrm{m}^3}}_{\text{air density}} \cdot \underbrace{\left(\frac{\mathrm{m}}{\mathrm{s}}\right)^3}_{\text{flow speed cubed}} = \frac{\mathrm{kg}}{\mathrm{s}^3}$$

$$= \underbrace{\left(\frac{\mathrm{kg}\cdot\mathrm{m}}{\mathrm{s}^2}\right)}_{\mathrm{N}} \cdot \left(\frac{1}{\mathrm{m}\cdot\mathrm{s}}\right) = \underbrace{(\mathrm{N}\cdot\mathrm{m})}_{\mathrm{J}} \cdot \left(\frac{1}{\mathrm{m}^2\cdot\mathrm{s}}\right) = \underbrace{\frac{\mathrm{J}}{\mathrm{s}}}_{\mathrm{W}} \cdot \frac{1}{\mathrm{m}^2} = \frac{\mathrm{W}}{\mathrm{m}^2}$$

Strong winds constitute a fairly concentrated form of sustainable energy of a similar power density as solar power. Note that the cross-sectional area, A (shown in Figure 1.2), of wind turbines is given by the whole disc over which the rotor blades sweep.

If we compare the power available in the wind to the average European's power need of about 5 kW:

- **2** m^2 of cross-sectional area in very strong wind,
- **16** m^2 of area in good wind (of $u = 10\ \mathrm{m\,s^{-1}}$), or
- **128** m^2 of area in weak wind (of $u = 5\ \mathrm{m\,s^{-1}}$)

contains about 5 kW of power.

(Not all of this can be harvested due to the so-called "Betz-Limit," which we will derive and discuss in Chapter 3.)

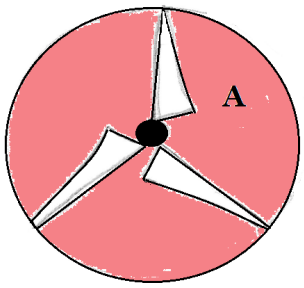

Figure 1.2: The rotor blades (white) and the swept area (pink).

So, wind turbines can harvest from the entire area with relatively little blade area; this is one explanation of why wind power is comparably cheap and competitive.

Example: For $u = 20$ m/s, the power density is:

$$\frac{P}{A} = \frac{1}{2}\rho u^3 = 4.8 \text{ kW/m}^2.$$

With a rotor radius of $R = 35$ m, the swept area is:

$$A = \pi R^2 = 3850 \text{ m}^2.$$

The total power is:

$$P = 4.8 \cdot 10^3 \text{ W/m}^2 \times 3850 \text{ m}^2 = 18.5 \text{ MW}.$$

At high wind speeds, a large amount of power is accessible to the wind turbine!

1.3 Power density and blade area

Let's try to estimate how much power can be captured by a given blade area A_B [m^2].

We consider only the outer part of a rotor blade (close to the wing tips) which moves with a blade speed V_B [m s^{-1}] in the cross-wind direction.

Note that the inner part of the blade moves slower, but they are not our focus for now.

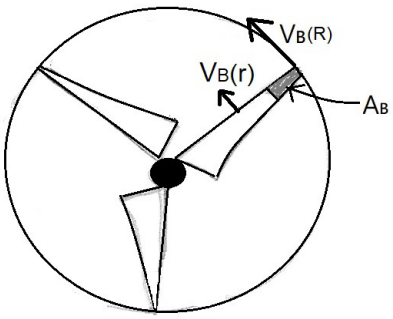

Figure 1.3: The outer part of the rotor blade near the tip moves at high speed V_B; the inner parts move slower.

We simplify further by assuming that the blade tip moves in a straight line (not along a circular path).

With this simplification, the motion of the blade tip can be compared to a sailing boat moving "half-wind" or "cross-wind." This situation can be depicted from the top view as shown in Figure 1.4.

The apparent wind $\mathbf{V}_A$ [m s^{-1}] is given by the vector difference between the true wind $\mathbf{V}$ [m s^{-1}] and the blade speed $\mathbf{V}_B$ [m s^{-1}]:

$$\mathbf{V}_A = \mathbf{V} - \mathbf{V}_B$$

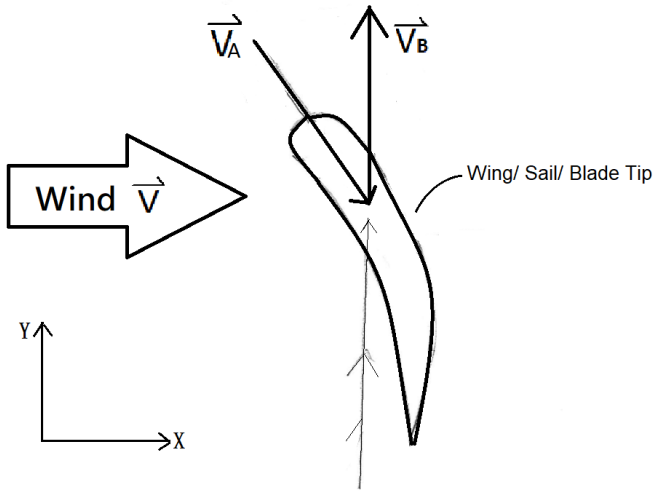

Figure 1.4: Top view analogy: the blade tip behaves like a sailboat moving "cross-wind."

In component form:

$$\mathbf{V}_A = \begin{pmatrix} V \\ 0 \end{pmatrix} - \begin{pmatrix} 0 \\ V_B \end{pmatrix} = \begin{pmatrix} V \\ -V_B \end{pmatrix}$$

The magnitude of the apparent wind is:

$$|V_A| = \sqrt{V_B^2 + V^2} := V_A \tag{1.4}$$

To determine the forces on the "wing" (we use this term for the blade tip with area A_B), we use a basic fact from aerodynamics: the aerodynamic force on a body in a moving fluid is proportional to the dynamic pressure $\frac{1}{2}\rho V_A^2$ and the reference area A_B.

The aerodynamic force can be decomposed into:

- the **lift force** L [N], which is perpendicular to $\mathbf{V}_A$
- the **drag force** D [N], which is aligned with $\mathbf{V}_A$

With the lift coefficient C_L [-] and drag coefficient C_D [-] we can express the aerodynamic forces on the blade tip as:

$$F_L = \frac{1}{2} C_L \, \rho \, A_B \, V_A^2 \tag{1.5}$$

$$F_D = \frac{1}{2} C_D \, \rho \, A_B \, V_A^2 \tag{1.6}$$

The coefficients C_L and C_D depend upon:

- the **angle of attack** (orientation of the blade section relative to the apparent wind)
- the **Reynolds number** (a dimensionless ratio of inertial forces to viscous forces)

Good wings are designed to produce high lift and low drag. A typical example is $C_L = 1.5$ and $C_D = 0.05$.

The lift-over-drag ratio $\frac{C_L}{C_D}$ has an important interpretation in sailplanes: it determines how far a sailplane can glide, depending on its initial altitude. Because of this, the ratio $\frac{C_L}{C_D}$ is also called the "gliding number".

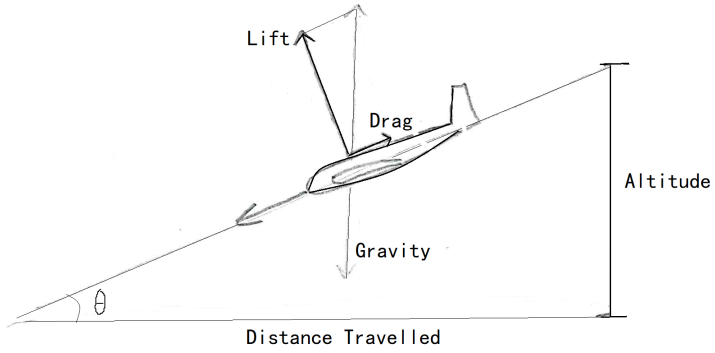

Figure 1.5: For a sailplane, the distance traveled equals the gliding number $\frac{C_L}{C_D}$ times the altitude.

For our rotor blade we obtain an analogous picture:

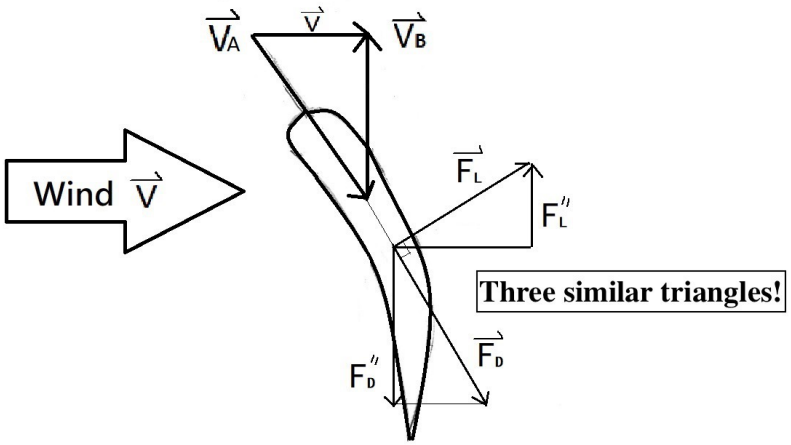

Figure 1.6: Illustration of lift and drag forces acting on the rotor blade tip.

For the rotation of the wind turbine, we are first interested only in the force component in the direction of motion of the wing, $F^{\parallel}$ [N], since its product with the blade speed V_B [$\mathrm{m\,s^{-1}}$] gives the mechanical power production:

$$P_B = F^{\parallel} \cdot (V_B) \tag{1.7}$$

Here $F^{\parallel}$ represents the component of aerodynamic force parallel to the blade's movement direction.

We decompose this as:

$$F^{\parallel} = F_L^{\parallel} + F_D^{\parallel} = F_L \cdot \frac{V}{V_A} - F_D \cdot \frac{V_B}{V_A}$$

where F_L and F_D are the lift and drag forces on the blade section, and the fractions $\frac{V}{V_A}$ and $\frac{V_B}{V_A}$ project these forces onto the direction of motion.

Bringing these together yields:

$$P_B = \frac{1}{2}\rho A_B \, V_A^2 \, V_B \left(C_L \frac{V}{V_A} - C_D \frac{V_B}{V_A} \right) \tag{1.8}$$

To simplify further, we introduce the tip speed ratio

$$\lambda_r = \frac{V_B(r)}{V}, \tag{1.9}$$

where $V_B(r)$ $[\mathrm{m\,s^{-1}}]$ is the local blade speed at radius r [m], and V $[\mathrm{m\,s^{-1}}]$ is the free-stream wind speed.

At the blade tip (at radius R), this simplifies to

$$\lambda = \frac{V_B}{V}.$$

Thus,

$$V_B = \lambda V$$

and

$$V_A = \sqrt{1 + \lambda^2}\, V.$$

Substituting these into Equation 1.8 simplifies the power expression to:

$$P_B = \frac{1}{2}\rho A_B \, V^3 \lambda^2 \underbrace{\sqrt{1 + \frac{1}{\lambda^2}} \left(C_L - C_D \cdot \lambda \right)}_{:=\zeta \text{ (Power Harvesting Factor)}} \tag{1.10}$$

This is often expressed in terms of the power harvesting factor ζ:

$$\zeta = \lambda \frac{1}{\sqrt{1 + \lambda^2}} \left(C_L - C_D \lambda \right),$$

so that the power can be written compactly as:

$$P_B = \frac{1}{2}\rho A_B V^3 \zeta.$$

At $\lambda = \frac{C_L}{C_D}$, no power is generated. This value $\frac{C_L}{C_D}$ represents the maximum possible tip speed ratio — it is realized if the generator is switched off, meaning there is no torque acting on the rotor.

Example: For a typical tip speed ratio of $\lambda = 7$, with $C_L = 1.5$ and $C_D = 0.05$, we can calculate the power harvesting factor ζ by evaluating the underbraced term in Equation 1.10.

$$\zeta = \lambda^2 \frac{1}{\sqrt{1+\lambda^2}} \left(C_L - C_D \lambda\right)$$

Plugging in the values:

$$\zeta \approx 49 \times 1 \times (1.5 - 0.05 \times 7) \approx 57.$$

(For $\lambda = 20$, we would even get $\zeta \approx 400 \times 0.5 = 200$.)

This is a remarkably high number. The factor ζ shows how many times more power a blade area can harvest compared to the energy in the wind which would pass through the "window" of the same size as the blade area.

Compared to the energy in the air, for $\zeta = 50$ and $V = 10$ m/s, we thus get a power density of

$$\frac{P_B}{A} = 50 \times 600 \text{ W m}^{-2} = 30 \text{ kW m}^{-2}.$$

For the inner parts of the blade we can calculate the local speed ratio

$$\lambda_r = \frac{V_B(r)}{V}.$$

As the inner parts of the blade move slower, their λ_r is smaller and therefore also their harvesting factors. This is one major reason why blades become thicker toward the center, as shown by Figure 1.7:

1.4 Components of a modern wind turbine

With its five joints (yaw, rotor, and three pitch joints), a wind turbine can be regarded as a gigantic robot arm, comparable to the six-joint robot arms used in car manufacturing. However, it is an "energy-harvesting robot."

For an illustration of the components of a modern wind turbine, refer to Figures 1.8, 1.9, and 1.10.

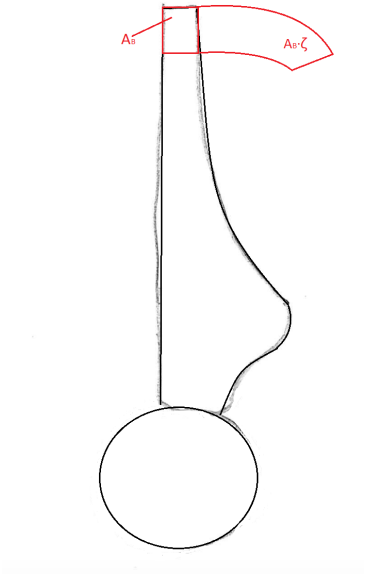

Figure 1.7: Blades become thicker toward the root because the local speed ratio λ_r is smaller there.

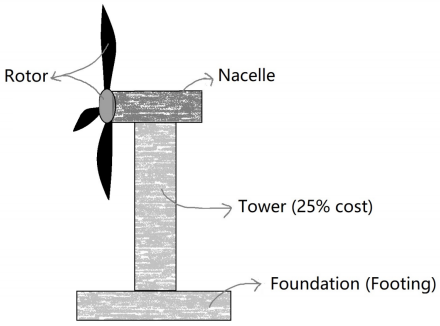

Figure 1.8: Wind turbine components.

1.5 Blade & airfoil nomenclature

Note: the **chordwise direction** is along the chord line. The **spanwise direction** is orthogonal, along the radial direction of the turbine.

The surface area of a blade element, dA, by definition, is the chord length $c(r)$ [m] multiplied by the span increment dr [m] (see Figure 1.12). Therefore, the whole blade area A [m^2] can be found by:

$$A = \int_0^R c(r)\, dr \tag{1.11}$$

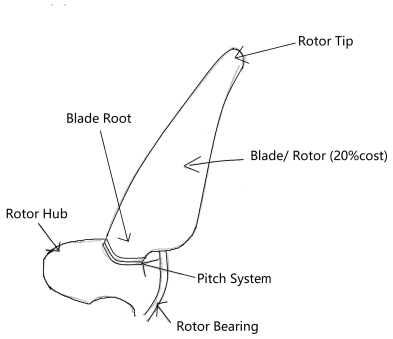

Figure 1.9: Rotor details.

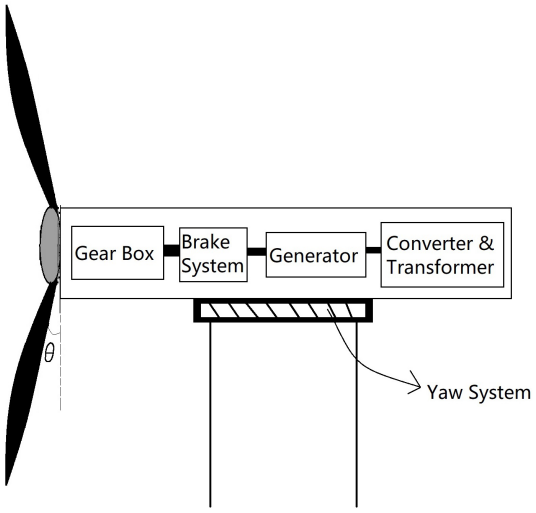

Figure 1.10: Inner details of the nacelle.

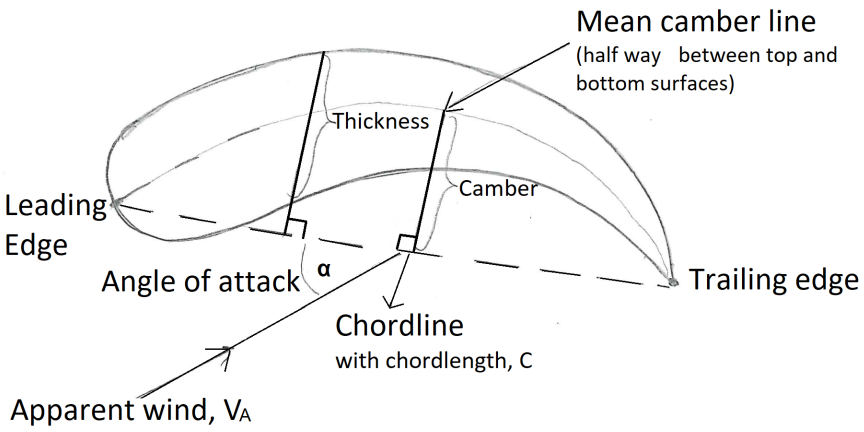

Figure 1.11: The parts of an airfoil.

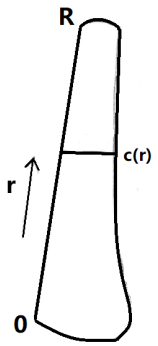

Figure 1.12: Surface area of a blade element.

Chapter 2

The Wind Resource

2.1 Origins

The movement of air that we experience as wind begins with heating from the sun. Solar energy warms different parts of the Earth's surface unevenly, and this imbalance sets the atmosphere in motion.

- Air is heated up (by the sun, directly or indirectly).
- The air density drops as it warms.
- The lighter, warmer air rises and creates a low-pressure region.
- Cooler, denser air rushes in to fill the gap — this flow of air is what we call "wind."

The contrast between land and water plays a major role in shaping local wind patterns. The heat capacity[1] of land is lower than that of water, meaning land heats up and cools down much faster than oceans or lakes.

During a sunny day, the ground temperature rises quickly. Air over land warms rapidly, becomes lighter, and begins to rise, creating a zone of lower pressure. Over water, the temperature rises more slowly, and the cooler, denser air remains closer to the surface. The warmer air from land can be cooled by the ocean and eventually sinks back down. This process is illustrated in Figure 2.1.

At night, the situation reverses. Land cools down much faster than water, so air over land becomes colder and denser. Over the water, the air remains relatively warmer and continues to rise, drawing the cooler air from land toward the sea. This reversal of air movement is shown in Figure 2.2.

2.2 Global patterns

Air in the atmosphere does not move randomly — it follows large-scale circulation patterns driven by solar heating, the Earth's rotation, and the shape of the planet. Within the troposphere, which extends from about 5–15 km above the Earth's surface, air moves

[1] Heat capacity is the amount of energy it takes to increase the temperature of 1 kg of a substance by 1 kelvin.

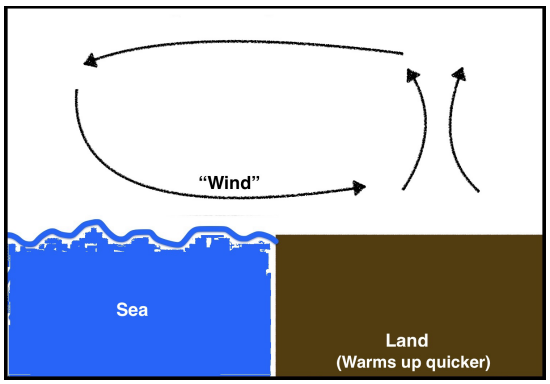

Figure 2.1: Sunny day at the coast: warm air rises over land, cooler air flows in from over the water.

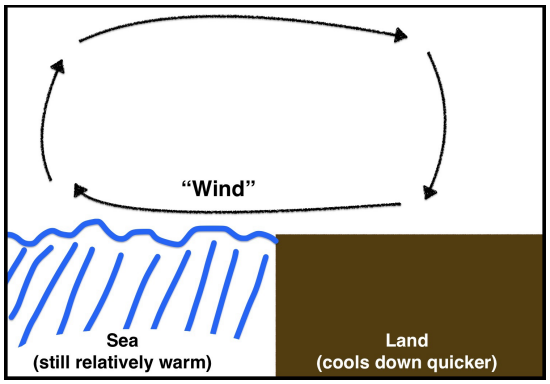

Figure 2.2: Clear night at the coast: the situation reverses, and cooler air flows out toward the water.

in three major "cells" per hemisphere: the Hadley cell near the equator, the Ferrel cell in the mid-latitudes, and the Polar cell closer to the poles (Figure 2.3).

Note 1: The Ferrel cell is indirectly driven by the Hadley cell and the Polar cell.

Note 2: The distance along the surface of the Earth between the North Pole and the equator is about 10,000 km. In comparison, the troposphere's thickness is only 5–15 km — very thin relative to the Earth's diameter.

Due to the Coriolis force, winds are diverted to the right in the northern hemisphere (relative to their direction of travel), and to the left in the southern hemisphere (Figure 2.4).

Closer to the Earth's surface, strong wind shear exists in the Atmospheric Boundary Layer (ABL). Both the magnitude and the direction of wind can change with altitude, and friction with the ground plays a significant role (Figure 2.5).

2.3 Mechanics of wind

Four main influences determine the movement of wind:

- pressure differences;
- Coriolis force;

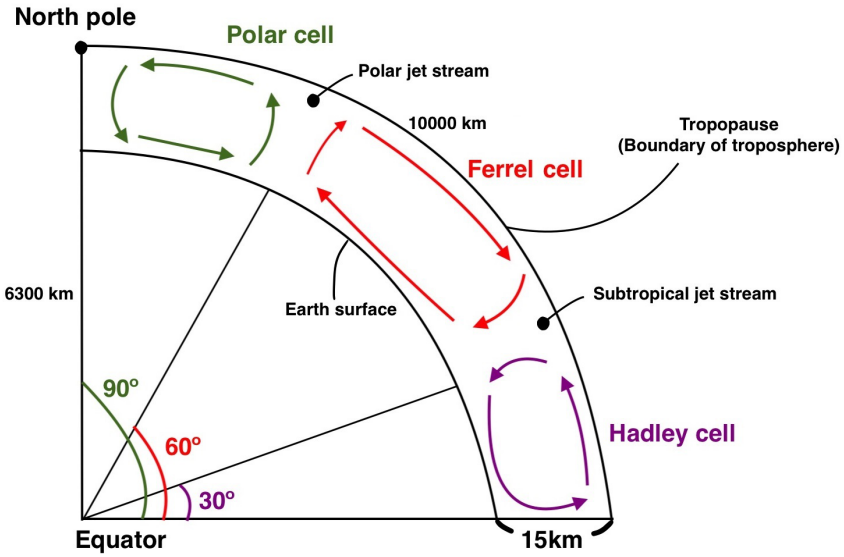

Figure 2.3: Air movement within the troposphere (5–15 km altitude), organized into three large circulation cells per hemisphere.

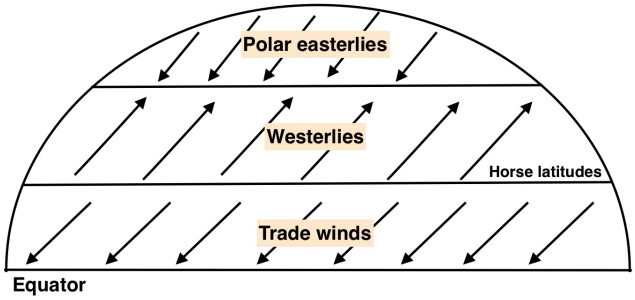

Figure 2.4: The Coriolis effect diverts winds to the right in the northern hemisphere and to the left in the southern hemisphere.

- centrifugal force; and
- friction.

2.3.1 Pressure gradient

To understand how pressure differences drive wind, consider a simple control volume: a cylindrical slice of air with length L [m] and cross-sectional area A [m^2].

The volume of this slice is:

$$\text{Volume} = L \cdot A,$$

and its mass m [kg] is:

$$m = \rho\, L\, A,$$

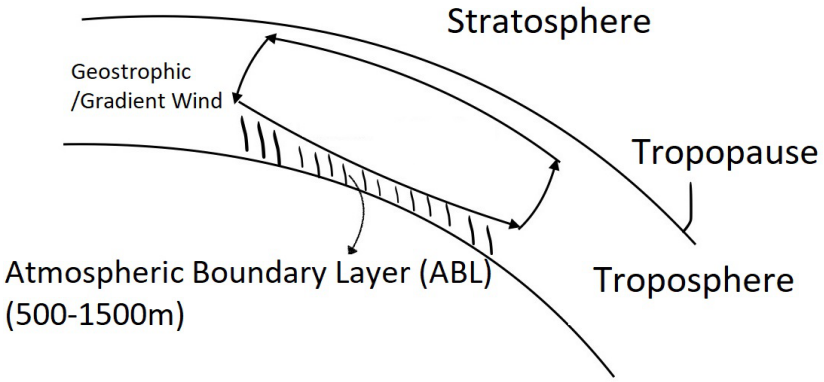

Figure 2.5: Strong wind shear in the Atmospheric Boundary Layer (ABL): magnitude and direction change with altitude, with ground friction having a major influence.

where ρ [kg m^{-3}] is the air density.

Figure 2.6: A cylindrical control volume used to illustrate the effect of a pressure gradient.

Pressure in the atmosphere varies in both space and time, and is denoted $P(x,t)$ [Pa]. Recall that:

$$1 \text{ Pa} = 1 \text{ N/m}^2 \quad \text{and} \quad 1 \text{ millibar} = 1 \text{ hectopascal} = 100 \text{ Pa}.$$

The standard atmospheric pressure at sea level is about 101.325 kPa.

Because pressure differs across the two ends of our control volume, there is a **net force** on the air:

$$F = \big(\text{force on the left side}\big) - \big(\text{force on the right side}\big).$$

Expressing this mathematically:

$$\begin{aligned} F &= A\,P(x_0) - A\,P(x_0 + L) && (2.1)\\ &\approx A\,P(x_0) - A\left[P(x_0) + \frac{\partial P}{\partial x}(x_0)\,L\right] && (2.2)\\ &= -A\,\frac{\partial P}{\partial x}(x_0)\,L. && (2.3) \end{aligned}$$

This simplified expression shows that a pressure gradient creates a force directed from high pressure toward low pressure.

From Newton's second law, the acceleration a [m s^{-2}] of the air mass is:

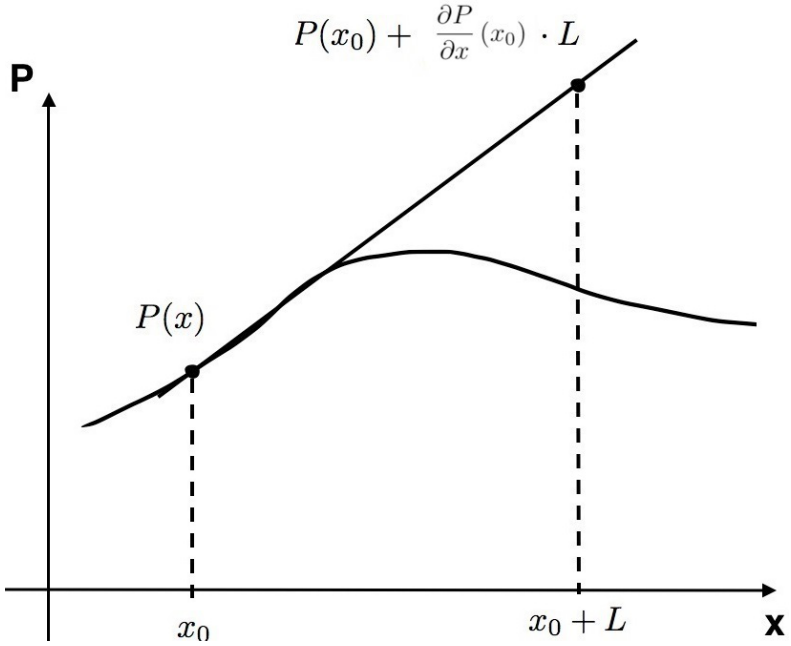

Figure 2.7: Pressure varies across space and time, creating differences that drive the motion of air.

$$a = \frac{F}{m} = \frac{-A\frac{\partial P}{\partial x}L}{\rho L A} = -\frac{1}{\rho}\frac{\partial P}{\partial x}. \tag{2.4}$$

This final equation shows that the acceleration of air is **directly proportional** to the pressure gradient and **inversely proportional** to air density: the steeper the pressure difference, the stronger the resulting motion of the air.

2.3.2 Coriolis force

The Coriolis force arises from the rotation of the Earth.

Consider a point on the surface of the Earth in Freiburg. This point is moving eastward because of the Earth's rotation. Now consider another point much closer to the North Pole: it too is moving east, but because it is closer to the Earth's axis of rotation, it moves eastward more slowly than Freiburg.

Now imagine air moving from the North Pole toward the south. As it moves farther south, the ground below is moving eastward faster and faster. From the air's perspective, the ground "slides away" underneath it. When viewed from the ground's frame of reference, it appears as though the wind is curving or accelerating to the right (Figure 2.8). This phenomenon is called the **Coriolis Effect**.

This rightward acceleration applies to air moving in all horizontal directions in the Northern Hemisphere. In the Southern Hemisphere, the acceleration is to the left.

The Coriolis effect can be described as either a **virtual force** or as an **acceleration**. At the North Pole, it is given by:

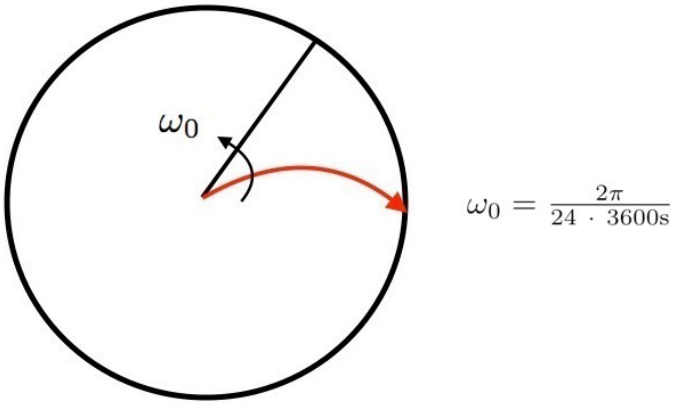

Figure 2.8: As viewed from above the North Pole, with the Earth's rotation ω_0, an air current traveling southward appears to curve to the right.

$$F_{\text{Coriolis}} = 2m\omega_0 V_{\text{GEO}} \tag{2.5}$$

If we divide this Coriolis force F_{Coriolis} [N] by the mass, we get a specific-force f_{Coriolis} [$\text{m}\,\text{s}^{-2}$] which is just an acceleration:

$$f_{\text{Coriolis}} = a_{\text{Coriolis}} = 2\omega_0 V_{\text{GEO}} \tag{2.6}$$

where:

- V_{GEO} [$\text{m}\,\text{s}^{-1}$] is the geostrophic wind velocity,
- ω_0 [$\text{rad}\,\text{s}^{-1}$] is the Earth's angular rotation speed,
- F_{Coriolis} [N] is the Coriolis force,
- f_{Coriolis} [N] is the Coriolis force-per-unit-mass, and
- a_{Coriolis} [$\text{m}\,\text{s}^{-2}$] is the resulting Coriolis acceleration.

On a flat rotating body, the above would suffice. But, the Earth is a sphere. So, the Coriolis effect depends on the latitude φ. There is **no Coriolis force at the equator** ($\sin\varphi = 0$). Accounting for latitude, the acceleration becomes:

$$a_{\text{Coriolis}} = 2\omega_0 \sin\varphi V_{\text{GEO}} = f_{\text{Coriolis}} \tag{2.7}$$

Effect of pressure gradient and Coriolis force

Geostrophic wind represents the balance between the pressure gradient force and the Coriolis effect.

In a simple case with straight isobars, for example running east–west as shown in Figure 2.9, the pressure gradient pushes the air northward, while the Coriolis force deflects the air southward. The result is that the wind flows parallel to the isobars, where the two accelerations are in balance.

Note: the geostrophic wind velocity V_{GEO} is proportional to the pressure gradient but flows parallel to the isobars.

In a geostrophic balance, the Coriolis force would exactly balance out the pressure gradient:

$$\underbrace{-\frac{\partial p}{\partial x}\frac{1}{\rho}}_{\text{pressure gradient}} = \underbrace{2\sin\varphi\omega_0 V_{\mathrm{GEO}}}_{\text{Coriolis effect}} \quad \Leftrightarrow \quad V_{\mathrm{GEO}} = \left(\frac{1}{2\rho\omega_0\sin\varphi}\right)\left(-\frac{\partial p}{\partial x}\right) \tag{2.8}$$

where ρ [kg m^{-3}] is air density and $\frac{\partial P}{\partial x}$ [Pa m^{-1}] is the horizontal pressure gradient.

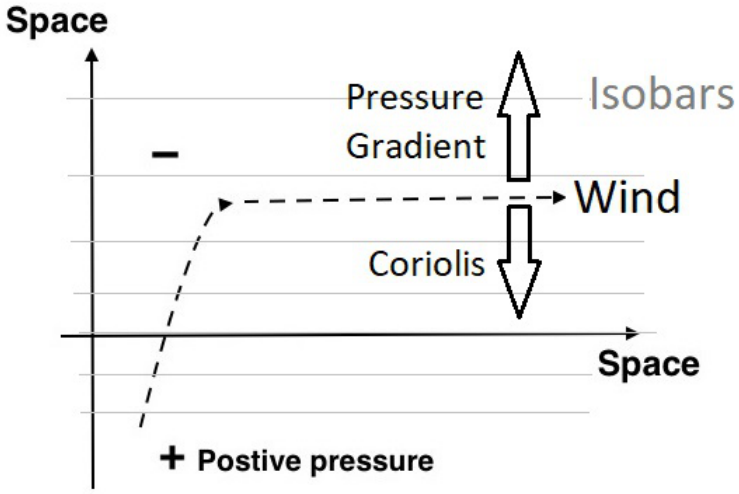

Figure 2.9: Geostrophic wind flows parallel to isobars: the pressure gradient force (towards low pressure) is balanced by the Coriolis effect (opposite direction).

Weather maps often show isobars - lines of constant pressure. The concept of geostrophic wind explains why, in many real cases, the wind direction follows the isobars instead of cutting straight across them (Figure 2.10).

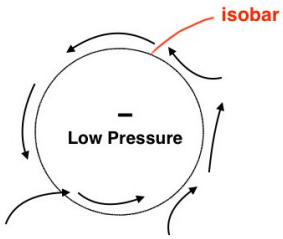

Figure 2.10: Weather maps depict isobars; geostrophic wind tends to flow parallel to these lines.

2.3.3 Centrifugal acceleration

Geostrophic wind considers the pressure gradient and the Coriolis force. However, when the isobars are curved — which is almost always the case — there is a third effect that

influences the wind: the **centrifugal force**, which arises whenever an object travels along a circular path.

A refinement of the geostrophic wind V_{GEO} is called the **gradient wind**, denoted V_G. Figure 2.11 illustrates a situation where there is a circular isobar and the wind is traveling along the isobar.

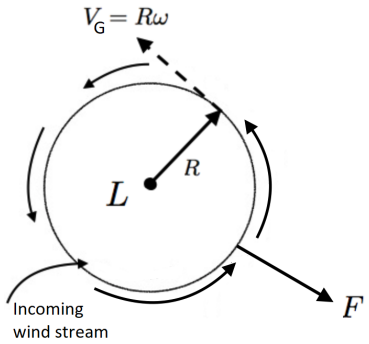

Figure 2.11: The gradient wind: wind flowing along curved isobars experiences centrifugal acceleration in addition to Coriolis and pressure-gradient forces.

Any rotating motion - with an angular speed ω [rad s^{-1}] at a radial distance R [m] from the center of rotation - has a centripetal acceleration a [m s^{-2}]. Since the angular speed ω could also be written in terms of the tangential speed $v = \omega R$ [m s^{-1}], we can write the centripetal acceleration a in different ways:

$$a_{\text{ctrpl}} = \omega^2 R = \frac{v^2}{R} = \omega v$$

And, since this acceleration represents the actual path of the rotating object, we know that the resultant (net) force acting on the object must be:

$$\mathbf{F}_{\text{ctrpl}} = m a_{\text{ctrpl}}(-\hat{\mathbf{r}}), \tag{2.9}$$

where m [kg] is the mass of the object, and $(-\hat{\mathbf{r}})$ is a vector pointing radially inwards towards the center of rotation. If we're talking in a specific sense, then the resultant (net) force per unit mass $\mathbf{f}_{\text{ctrpl}}$ [m s^{-2}] of the rotating object must be:

$$\mathbf{f}_{\text{ctrpl}} = \frac{\mathbf{F}_{\text{ctrpl}}}{m} = a_{\text{ctrpl}}(-\hat{\mathbf{r}}) = \frac{v^2}{R}(-\hat{\mathbf{r}}). \tag{2.10}$$

Now, we saw in the previous section a geostrophic wind (from the previous section) that is moving along an isobar when the pressure gradient is horizontal. But, on a globe, we're very likely to have curved isobars, circling around regions of high pressure, and also around regions of low pressure. Either type of pressure (with corresponding direction of rotation), the basic fact of saying that an air masses is 'circling around' something, implies that the resultant (net) force acting on the air mass must match the centripetal force given in (2.10). And this means that the sum of the pressure gradient and the Coriolis force acting on our air-mass must be equal (in the vector sense) to our centripetal force.

So, the defining characteristic of the gradient wind V_{G} [m s^{-1}] is that:

$$\mathbf{f}_{\text{ctrpl}} = \mathbf{f}_p + \mathbf{f}_{\text{Coriolis}}. \tag{2.11}$$

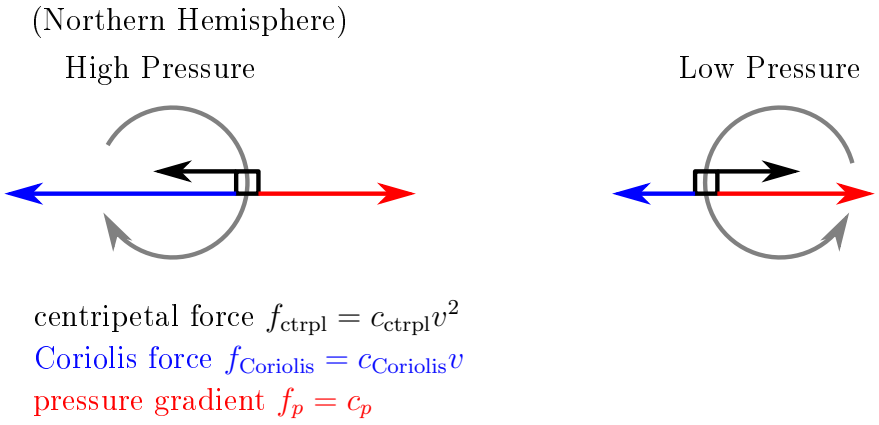

Figure 2.12: The force balance acting on the fluid elements in a gradient wind must lead to a resultant (net) force acting radially inwards. (The shown vectors are not-to-scale.)

The centripetal force is proportional to V_{G}^2:

$$f_{\text{ctrpl}} \propto V_{\text{G}}^2, \quad f_{\text{ctrpl}} = c_{\text{ctrpl}} V_{\text{G}}^2 \text{ with } c_{\text{ctrpl}} = \frac{1}{R}. \tag{2.12}$$

The specific Coriolis force (2.5) happens to be proportional to the velocity V_{G}:

$$f_{\text{Coriolis}} \propto V_{\text{G}}, \quad f_{\text{Coriolis}} = c_{\text{Coriolis}} \text{ with } c_{\text{Coriolis}} = 2 \sin \varphi \omega_0. \tag{2.13}$$

The pressure gradient is a constant:

$$f_p = c_p \text{ with } c_p = \frac{\partial p}{\partial x} \frac{1}{\rho}, \tag{2.14}$$

where we've dropped the negative sign in order to make determining the direction of the force easier.

Let's consider what this looks like in the northern hemisphere, in Fig. 2.12. Here, we've imagined a high pressure and a low pressure center in some line. In the northern hemisphere, the Coriolis force pushes the flow around these centers in the clockwise and anticlockwise directions, respectively. As we've already mentioned, the Coriolis force pushes the air mass to the right (in the northern hemisphere) of it's path, the pressure gradient pushes the air mass from high pressure to low pressure, and the resultant (net) centripetal force must be radially towards the center-of-pressure.

So, let's treat these two centers in order.

Low pressure center Around the low pressure center, (2.11) becomes:

$$f_{\text{ctrpl}} = f_p - f_{\text{Coriolis}} \quad \Rightarrow \quad c_{\text{ctrpl}} V_{\text{G}}^2 + c_{\text{Coriolis}} V_{\text{G}} - c_p = 0. \tag{2.15}$$

By the quadratic formula, this means that:

$$V_{\text{G}} = \frac{-c_{\text{Coriolis}} \pm \sqrt{c_{\text{Coriolis}}^2 + 4 c_{\text{ctrpl}} c_p}}{2 c_{\text{ctrpl}}} \tag{2.16}$$

When both terms are the same sign, the final velocity ends up negative. So, we will choose the '+' option:

$$V_{\mathrm{G}} = \frac{-c_{\mathrm{Coriolis}} + \sqrt{c_{\mathrm{Coriolis}}^2 + 4c_{\mathrm{ctrpl}}c_p}}{2c_{\mathrm{ctrpl}}} = R\sqrt{\frac{\partial p}{\partial x}\frac{1}{\rho R} + \omega_0^2 \sin^2(\varphi)} - R\omega_0 \sin(\varphi) \quad (2.17)$$

High pressure center Around the high pressure center, (2.11) becomes:

$$f_{\mathrm{ctrpl}} = f_{\mathrm{Coriolis}} - f_p \quad \Rightarrow \quad c_{\mathrm{ctrpl}}V_{\mathrm{G}}^2 - c_{\mathrm{Coriolis}}V_{\mathrm{G}} + c_p = 0. \quad (2.18)$$

By the quadratic formula, this means that:

$$V_{\mathrm{G}} = \frac{c_{\mathrm{Coriolis}} \pm \sqrt{c_{\mathrm{Coriolis}}^2 - 4c_{\mathrm{ctrpl}}c_p}}{2c_{\mathrm{ctrpl}}} \quad (2.19)$$

If both signs are positive, the speeds found are far too large. So, we'll chose the '-' option:

$$V_{\mathrm{G}} = \frac{c_{\mathrm{Coriolis}} - \sqrt{c_{\mathrm{Coriolis}}^2 - 4c_{\mathrm{ctrpl}}c_p}}{2c_{\mathrm{ctrpl}}} = -R\sqrt{-\frac{\partial p}{\partial x}\frac{1}{\rho R} + \omega_0^2 \sin^2(\varphi)} + R\omega_0 \sin(\varphi). \quad (2.20)$$

Combined It turns out, that if we define a sign s, which takes values depending on whether it's a high-pressure or low-pressure center being rotated,

$$s = \begin{cases} +1 & \text{if high pressure} \\ -1 & \text{if low pressure,} \end{cases} \quad (2.21)$$

then we have a defining equation:

$$sf_{\mathrm{ctrpl}} = f_p - f_{\mathrm{Coriolis}} \quad \Rightarrow \quad sc_{\mathrm{ctrpl}}V_{\mathrm{G}}^2 + c_{\mathrm{Coriolis}}V_{\mathrm{G}} - c_p = 0. \quad (2.22)$$

Then we can combine (2.17) and (2.20) into one expression:

$$\begin{aligned} V_{\mathrm{G}} &= \frac{-c_{\mathrm{Coriolis}} + \sqrt{c_{\mathrm{Coriolis}}^2 + 4c_{\mathrm{ctrpl}}c_p s}}{2c_{\mathrm{ctrpl}}s} \\ &= s\left(R\sqrt{\frac{\partial p}{\partial x}\frac{s}{\rho R} + \omega_0^2 \sin^2(\varphi)} - R\omega_0 \sin(\varphi)\right). \end{aligned} \quad (2.23)$$

Example Let's follow[2] an example.

Suppose the pressure gradient $\frac{\partial p}{\partial x}$ is:

$$\frac{\partial p}{\partial x} = \frac{\Delta p}{\Delta x} = \frac{1 \cdot 10^3 \mathrm{N\,m^{-2}}}{1 \cdot 10^6 \mathrm{m}} = 1 \cdot 10^{-3} \mathrm{N\,m^{-3}}, \quad (2.24)$$

[2]from Fovell, Robert. 'Some gradient wind examples' in 'ATM 210: Atmospheric Structure, Thermodynamics, and Circulation' (Fall, 2023). State Uni. of New York at Albany. `https://www.atmos.albany.edu/facstaff/rfovell/ATM210/ATM210_gradient_wind.pdf`.

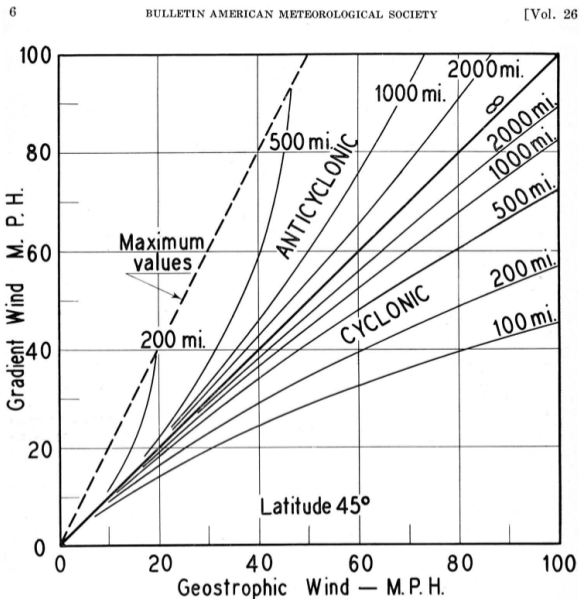

Figure 2.13: Whether the geostrophic wind or the gradient wind is faster, depends on the radius of curvature and the direction of the flow. Figure from: Kendall, G. R., "A Slide Rule for Computing Gradient Winds". Bulletin American Meteorological Society. Vol 26. Jan, 1945.

and the air density is $1\mathrm{kg\,m^{-3}}$ so that the pressure coefficient $c_p = 1 \cdot 10^{-3}\mathrm{N\,kg^{-1}}$. Also, at 43 deg. North, the Coriolis proportionality factor $c_{\mathrm{Coriolis}} \approx 1 \cdot 10^{-4}\mathrm{Hz}$.

Then, a fluid element rotating about a low pressure center $s = +1$ at a radius of $R = 1 \cdot 10^{6}\mathrm{m}$, will have a centripetal-force proportionality factor $c_{\mathrm{ctrpl}} = 1 \cdot 10^{-6}\mathrm{m^{-1}}$. This gives a gradient wind of:

$$
\begin{aligned}
V_{\mathrm{G}} &= \frac{-c_{\mathrm{Coriolis}} + \sqrt{c_{\mathrm{Coriolis}}^2 + 4c_{\mathrm{ctrpl}}c_p s}}{2c_{\mathrm{ctrpl}}s} \\
&= \frac{-10^{-4} + \sqrt{(10^{-4})^2 + (4)(10^{-6})(10^{-3})(+1)}}{2(10^{-6})(+1)} \\
&= -50 + 5 \cdot 10^{5}\sqrt{10^{-8} + 4(10^{-9})} \\
&= -50 + 5 \cdot 10^{5}\sqrt{1.4 \cdot 10^{-8}} \\
&= -50 + 5 \cdot 10^{5}(1.1832 \cdot 10^{-4}) \\
&= 9.1608\mathrm{m\,s^{-1}}
\end{aligned}
\tag{2.25}
$$

And, what happens if it's a high-pressure center? Then, the only thing we have to do, is

to switch the sign of $s = -1$.

$$\begin{aligned} V_{\mathrm{G}} &= \frac{-c_{\mathrm{Coriolis}} + \sqrt{c_{\mathrm{Coriolis}}^2 + 4c_{\mathrm{ctrpl}}c_p s}}{2c_{\mathrm{ctrpl}}s} \\ &= \frac{-10^{-4} + \sqrt{(10^{-4})^2 + (4)(10^{-6})(10^{-3})(-1)}}{2(10^{-6})(-1)} \\ &= 50 - 5 \cdot 10^5 \sqrt{10^{-8} - 4(10^{-9})} \\ &= 50 - 5 \cdot 10^5 \sqrt{6 \cdot 10^{-9}} \\ &= 50 - 5 \cdot 10^5 (7.7459 \cdot 10^{-5}) \\ &= 11.2702 \mathrm{m\,s^{-1}} \end{aligned} \tag{2.26}$$

(2.27)

(The other $\pm$ alternatives give, respectively, -109$\mathrm{m\,s^{-1}}$ and 88$\mathrm{m\,s^{-1}}$, which seem definitively implausible.)

We could, in this example, figure out what the geostrophic wind V_{GEO} [$\mathrm{m\,s^{-1}}$] would be, by setting the radius to infinity ($R = \infty$), or the centripetal coefficient to zero ($c_{\mathrm{ctrpl}} = 0$):

$$c_{\mathrm{Coriolis}} V_{\mathrm{GEO}} - c_p = 0, \quad \Rightarrow \quad V_{\mathrm{GEO}} = \frac{c_p}{c_{\mathrm{Coriolis}}} = \frac{\partial p}{\partial x} \frac{\csc \phi}{2\rho\omega_0} = 10 \mathrm{m\,s^{-1}} \tag{2.28}$$

Since $R = \infty$ is the case when the geostrophic wind and the gradient wind are the same, the example demonstrates the following trend: when the flows rotate anticlockwise (low pressure in the northern hemisphere, high pressure in the southern hemisphere, also labelled as 'cyclonic') the geostrophic wind $V_{\mathrm{GEO}} > V_{\mathrm{G}}$. The opposite is true for flows rotating clockwise!

Assessing the importance of centrifugal force. To evaluate when the centrifugal term matters, we compare the Coriolis term $2 \sin\varphi\, \omega_0\, V_G$ with the centrifugal term $\frac{V_G^2}{R}$ by computing their ratio:

$$\frac{\text{Coriolis}}{\text{Centrifugal}} = \frac{2\,\omega_0\, \sin\varphi\, R}{V_G}.$$

For typical values:

$$\varphi = 50^\circ \Rightarrow \sin\varphi \approx 0.75, \quad V_G \approx 50 \text{ km/h}, \quad R \approx 500 \text{ km},$$

the ratio becomes:

$$\frac{\text{Coriolis}}{\text{Centrifugal}} \approx \frac{2 \times 0.75 \times 2\pi \times 500 \text{ km}}{24 \times 50 \text{ km}} \approx 4.$$

Thus, in this scenario, the centrifugal term contributes about one-quarter of the Coriolis force. Under strong circular wind conditions, this contribution is significant and cannot be neglected.

2.3.4 Friction

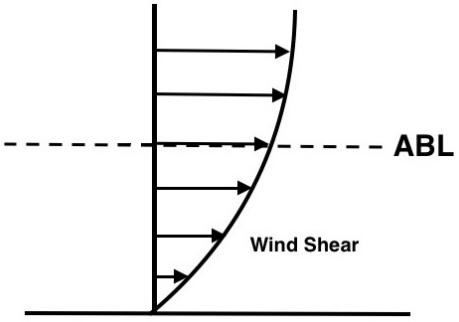

Figure 2.14: In the Atmospheric Boundary Layer (ABL), friction slows down the wind. At the Earth's surface, wind speed goes to zero.

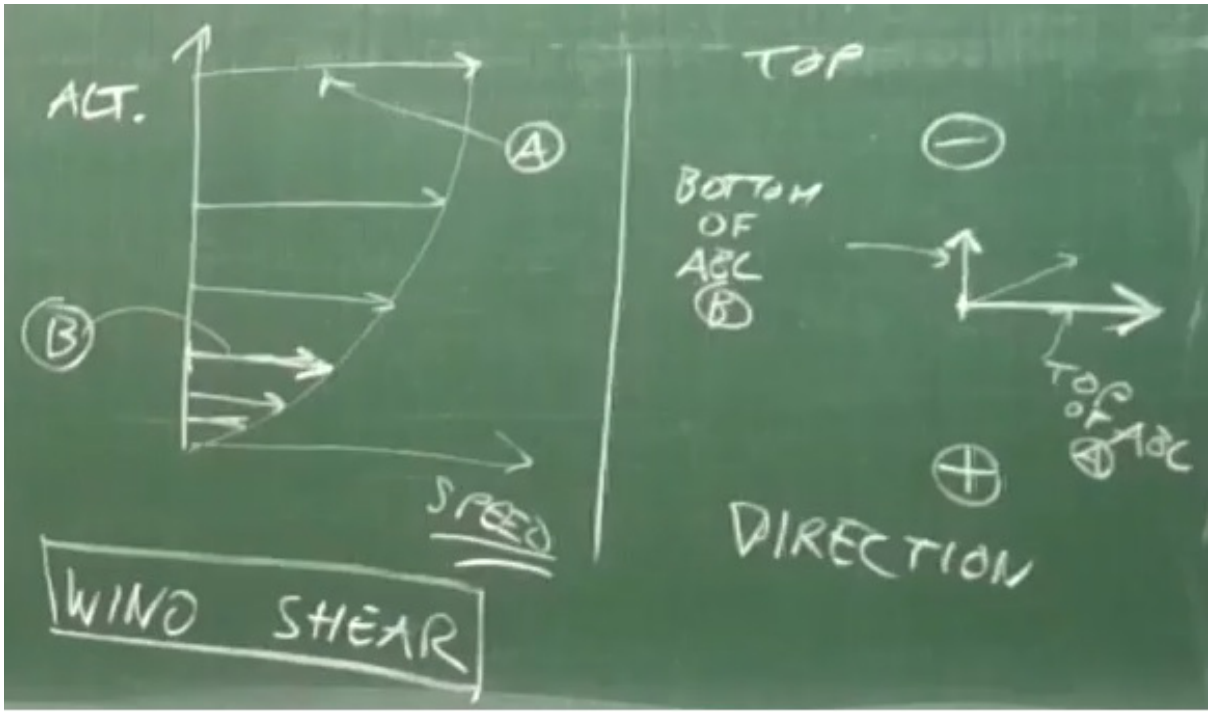

Figure 2.15: The logarithmic wind profile in the ABL: wind speed increases with height according to surface roughness.

Friction is complex and depends on the surface properties of the Earth, but it generally slows down the air — and this effect is confined to the Atmospheric Boundary Layer (ABL)[3]. This slowing of air also reduces the Coriolis and centrifugal forces. As a result, very low-altitude winds tend to align more directly with the direction of the pressure gradient. At the Earth's surface, the wind speed drops to zero (Figure 2.12).

The change in wind speed with altitude is called **wind shear**. A common way to describe the long-term, time-averaged wind shear is with a logarithmic profile (Figure 2.13):

[3]The Atmospheric Boundary Layer (ABL) is the thin part of the atmosphere closest to the ground where friction effects are significant.

$$V(z) = V_0 \frac{\log\left(\frac{Z}{Z_r}\right)}{\log\left(\frac{Z_0}{Z_r}\right)} \tag{2.29}$$

where:

- $V(z)$ [$\mathrm{m\,s^{-1}}$] is the wind speed at height z,
- V_0 [$\mathrm{m\,s^{-1}}$] is the wind speed at reference height Z_0,
- Z_r [m] is the "roughness length" (a few millimeters for flat ground).

2.4 Stable and unstable atmospheric stratification

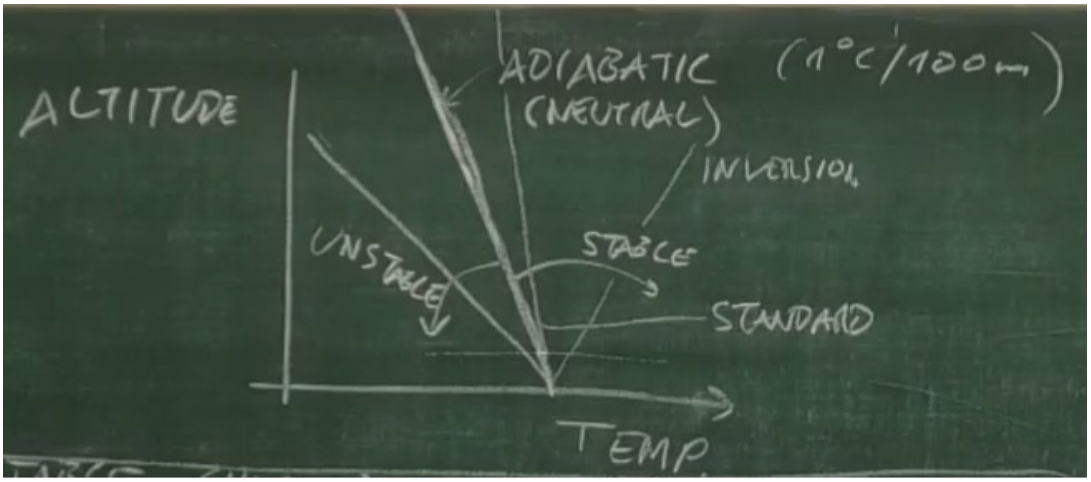

Figure 2.16: Stable and unstable atmospheric stratification: how the temperature gradient affects rising air.

A hot parcel of air becomes lighter than the surrounding air and begins to rise. However, as this air rises, it expands due to lower pressure and therefore cools. This cooling follows the **dry adiabatic lapse rate**, which is about 1°C per 100 m – meaning that rising air cools by roughly 1°C for every 100 m it rises in altitude due to its own expansion.

If the surrounding (ambient) air cools more slowly than 1°C per 100 m, the atmosphere is considered **stable**: the rising air will become cooler than its surroundings and stop rising. If the ambient air cools faster than 1°C per 100 m, the atmosphere is considered **unstable**: the rising air remains warmer than its surroundings and continues to rise.

The **standard atmospheric lapse rate** is about 0.66°C per 100 m, which corresponds to a generally stable stratification. Even more stable is an **inversion**, where the air actually becomes hotter with height.

Generally, the wind shear is stronger under stable conditions. "Stronger" means a larger change in wind speed over a change in altitude, often with a thinner Atmospheric Boundary Layer (ABL). Under stable conditions, there is less mixing between air layers. Therefore, for a given high-altitude wind speed, there is less momentum transferred downward within the flow than under neutral conditions (i.e. when the atmospheric lapse rate equals the dry adiabatic lapse rate).

dist.	"Normal" or Gaussian	Weibull	Rayleigh
accepts	$U \in \mathbb{R}$	$U \in [0, \infty)$	$U \in [0, \infty)$
1st param	mean $\bar{U}$ $[\mathrm{m\,s^{-1}}]$	scale λ $[\mathrm{m\,s^{-1}}]$	scale s $[\mathrm{m\,s^{-1}}]$
2nd param	variance σ_u $[\mathrm{m\,s^{-1}}]$	shape k [-]	–
$f(U)$	$\frac{1}{\sqrt{2\pi\sigma_u^2}} e^{\left(-\frac{(U-\bar{U})^2}{2\sigma_u^2}\right)}$	$\frac{k}{\lambda}\left(\frac{U}{\lambda}\right)^{k-1} e^{\left(-\left(\frac{U}{\lambda}\right)^k\right)}$	$\frac{U}{s^2} e^{\left(-\frac{U^2}{2s^2}\right)}$
$F(U)$	$\frac{1}{2}\left(1 + \mathrm{erf}\left(\frac{U-\bar{U}}{\sigma_u\sqrt{2}}\right)\right)$	$1 - e^{\left(-(U/\lambda)^{k-1}\right)}$	$1 - e^{\left(-\frac{U^2}{2s^2}\right)}$
mean	$\bar{U}$	$\lambda\Gamma\left(1 + \frac{1}{k}\right)$	$s\sqrt{\frac{\pi}{2}}$
variance	σ_u^2	$\lambda^2\left(\Gamma\left(1 + \frac{2}{k}\right) - \left(\Gamma\left(1 + \frac{1}{k}\right)\right)^2\right)$	$\frac{4-\pi}{2}s^2$
notes	typically used to describe measurement errors and gusts	typically used to model long-term averaged wind speeds at sites	a special case of Weibull distribution, with $k = 2$ and $\lambda = s\sqrt{2}$. It corresponds to the PDF of the vector magnitude of a two-dimensional Gaussian distribution

Table 2.1: Typical distributions for wind data, where erf() is the error function and $\Gamma(x) = \int_0^\infty e^{-t}t^{x-1}\mathrm{d}t$ is the Gamma function. Some useful values are $\Gamma(n) = (n-1)!$, $\Gamma(1) = 1$, $\Gamma(2) = 1$, etc.

2.5 Statistics of wind

At any given site, wind speed and direction vary with time. If we consider only the wind speed, we can plot time series data similar to Figure 2.15. From such data, we can compute quantities like the mean wind speed $\bar{U}$ and the variance σ_u^2 using hourly averages over a year.

From the same data we can construct a histogram (see Figure 2.17a), which shows how often each wind speed occurs. Different statistical distributions can be used to describe $f(U)$, the probability density function (PDF) of wind speeds. Closely related is its integral, $F(U)$, the cumulative distribution function (CDF).

The PDF satisfies the normalization condition:

$$\int_0^\infty f(U)\ \mathrm{d}U = 1 \tag{2.30}$$

The CDF is defined as:

$$F(U) = \int_0^U f(U)\ \mathrm{d}U, \tag{2.31}$$

meaning that the PDF can also be obtained as the derivative of the CDF:

$$f(U) = \frac{\mathrm{d}}{\mathrm{d}U}F(U). \tag{2.32}$$

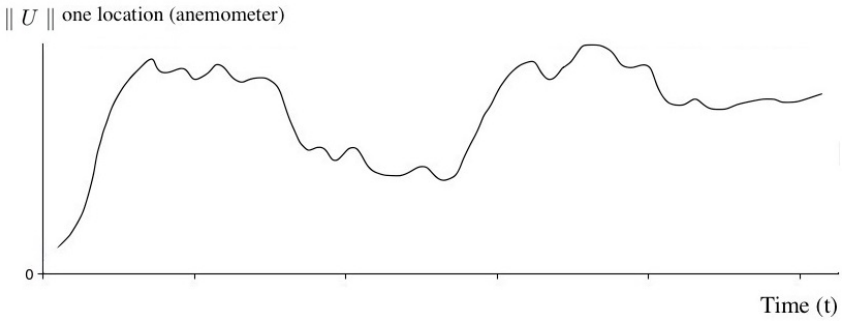

(a) Hourly average wind speeds over one year.

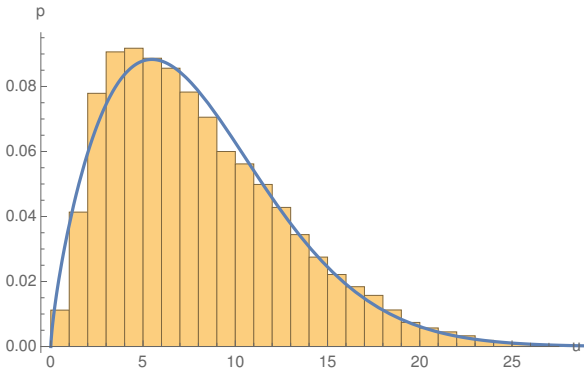

(b) Histogram of wind speeds over all time.

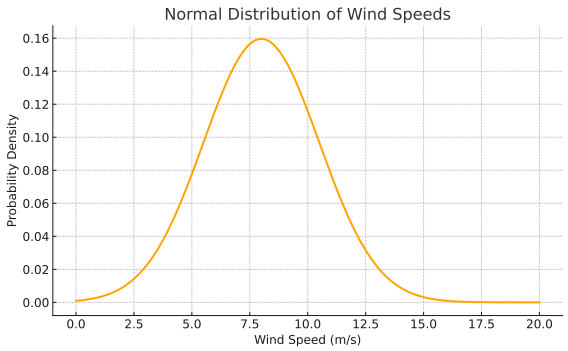

(c) Example of a Gaussian (Normal) probability density function (PDF) for wind speeds.

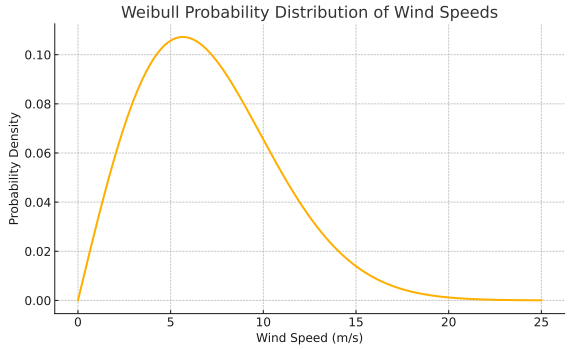

(d) Example of a Weibull probability density function (PDF) for wind speeds.

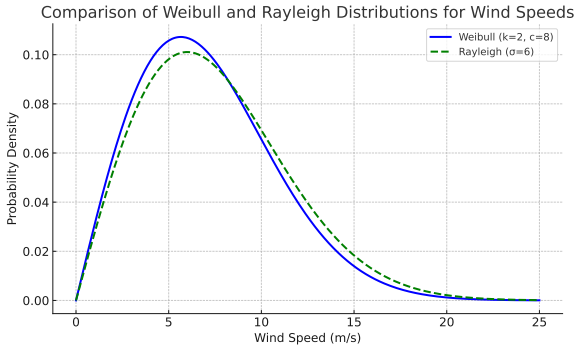

(e) Example of a Rayleigh probability density function (PDF), which is a special case of the Weibull distribution.

Figure 2.17: The wind measurements taken over a long period of time can be plotted in a histogram, and the occurance vs wind speeds can be used to fit a probability distribution function.

The mean wind speed $\bar{U}$ and the variance σ_u^2 of the probability density function $f(U)$ are defined as:

$$\bar{U} = \int_0^\infty U\ f(U)\ \mathrm{d}U \tag{2.33}$$

$$\sigma_u^2 = \int_0^\infty (U - \bar{U})^2\ f(U)\ \mathrm{d}U \tag{2.34}$$

$$= \left(\int_0^\infty U^2\ fU\ \mathrm{d}U \right) - \bar{U}^2. \tag{2.35}$$

There are a couple of types of distributions that are typically used to describe wind speeds:

- the Gaussian distribution;
- the Weibull distribution; and
- the Rayleigh distribution.

The most important information about these distributions is included in Table 2.1.

2.5.1 How to determine 'What is the average power per year?' from a wind speed probability density function

Question: What is the average power output of a wind turbine over a year?

To determine this, we combine two pieces of information:

- The **power curve** of the turbine, $P(U)$, which shows how much power the turbine produces at each wind speed U.
- The **wind speed PDF**, $f(U)$, which shows how often each wind speed occurs at the site.

Answer:

The average power output $\bar{P}$ [W] over a year is obtained by integrating the turbine's power curve weighted by the wind speed probability density function:

$$\bar{P} = \int_0^\infty P(U) f(U)\ \mathrm{d}U \tag{2.36}$$

In other words, the contribution of each wind speed to the annual energy production is its occurrence probability multiplied by the power the turbine generates at that speed. Summing (integrating) these contributions across all wind speeds yields the annual average power.

2.6 Spectral properties of wind

2.6.1 Power Spectral Density

When a Fourier series is taken of wind speed data, the **power spectral density** $S(f)$ is obtained. The power spectral density describes how the variance of wind speed is

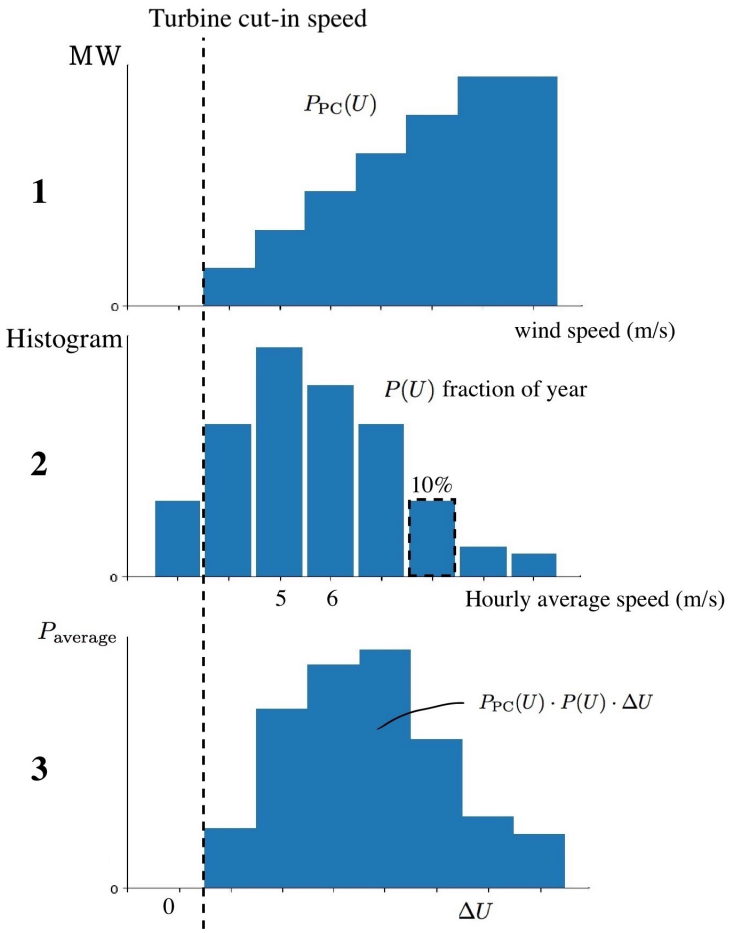

Figure 2.18: Combining a turbine power curve with the site's wind speed distribution allows calculation of the average annual power output.

distributed across different frequencies.

Turbulence is most relevant at time scales shorter than about 10 minutes. The **turbulence intensity** in a 10-minute window is defined as:

$$I = \frac{\sigma_u}{U},$$

where U is the 10-minute mean wind speed $[\mathrm{m\,s^{-1}}]$ and σ_u is the standard deviation of the wind speed (e.g., computed from 1-second samples).

For a dataset of N samples U_i, the mean and variance are computed as:

$$U = \frac{1}{N}\sum_{i=1}^{N} U_i \tag{2.37}$$

$$\sigma_u^2 = \frac{1}{N-1}\sum_{i=1}^{N}(U_i - U)^2 \tag{2.38}$$

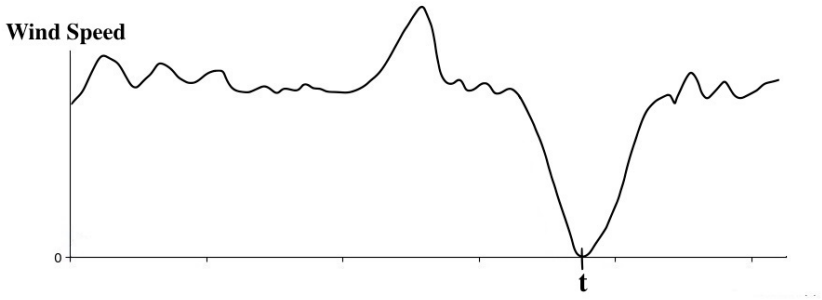

Figure 2.19: Autocorrelation and spectral analysis concepts for wind data.

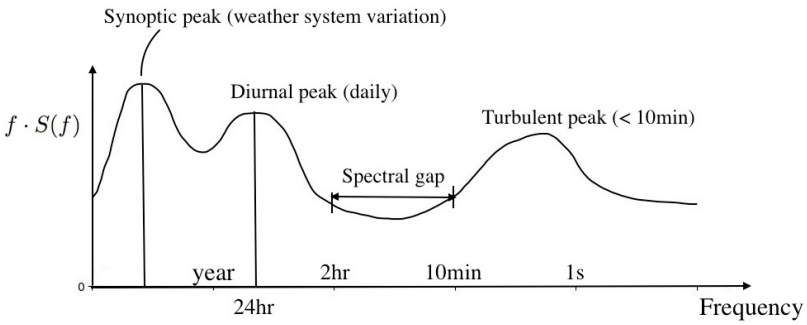

Figure 2.20: Example of a wind speed power spectral density $S(f)$ from a Fourier transform.

2.6.2 Autocorrelation

Another important quantity is the **autocorrelation function** $r(t)$, which helps characterize repeating patterns, such as periodic wind fluctuations.

For discrete time steps, the autocorrelation at lag time $t = k\Delta t$ is computed as:

$$r(k\Delta t) = \frac{1}{\sigma_u^2(N-k)} \sum_{i=1}^{N-k} (U_i - U)(U_{i+k} - U), \tag{2.39}$$

where:

- Δt is the sampling time,
- k is the lag number,
- $k\Delta t$ is the lag time.

Between these discrete lag values, $r(t)$ can be interpolated to provide a continuous autocorrelation function for all $t > 0$.

Figure 2.22 shows a typical autocorrelation function: wind speeds are strongly autocorrelated at very short lag times and progressively less correlated at longer lag times. This is expected because wind conditions one second ago strongly influence the current wind, while wind from a day ago has very little impact.

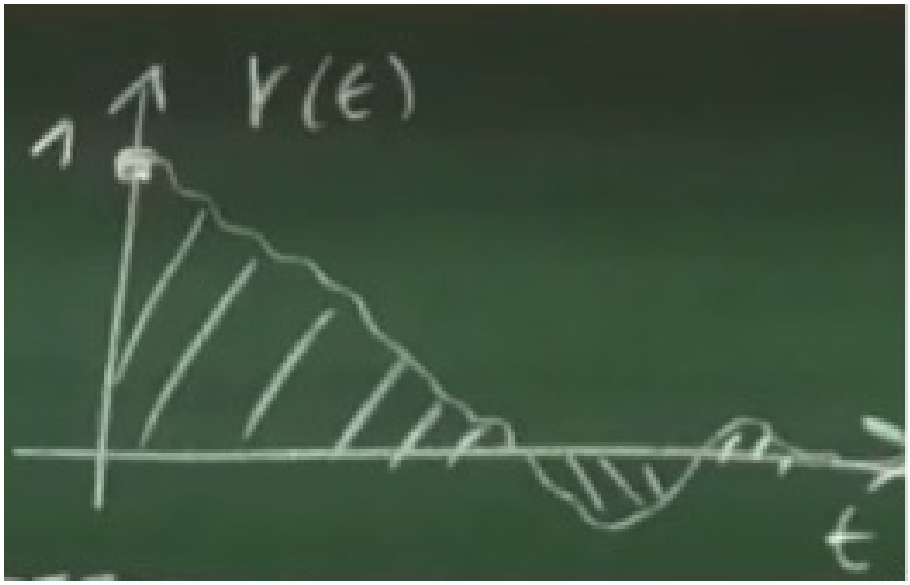

Figure 2.21: Typical autocorrelation function for wind speed: high autocorrelation at short lags, decaying at longer lags.

An important quantity derived from $r(t)$ is the **integral time scale** T, defined as:

$$T = \int_0^\infty r(t)\, dt. \tag{2.40}$$

Related to it is the **integral length scale** L, which links turbulence to a physical length:

$$L = U \cdot T \approx \text{size of turbulent eddies or interruptions.}$$

Note: The Fourier transform of the autocorrelation function equals (up to scaling factors) the **power spectral density (PSD)**.

Chapter 3

Aerodynamics of Wind Turbines

3.1 Wakes

Like a boat passing through water and leaving a wake, a wind turbine also disturbs the flow of air blowing across it. The air downstream of the rotor is slower and more turbulent, forming what is called the **wake**.

Figure 3.1: Photo of wakes forming behind turbines in a wind park. Source: Vattenfall.

The wake expands and mixes with surrounding air as it moves downstream. This phenomenon is crucial for wind farm planning, because turbines positioned downstream in another turbine's wake will experience reduced wind speed and increased turbulence, leading to lower power production and higher mechanical stresses.

In this chapter we're going to meet two non-dimensional values (the axial induction factor a [-] and the tangential induction factor a' [-]) that describe the change in the flow field.

These values are functions of the radial position at which they're located, and we care about them for three reasons:

1. The turbine harvests power, conceptually, by pulling kinetic energy out of the wind, with a describing the amount removed. More practically, the turbine harvests power by transmitting the aerodynamic torque applied by the flow to the blades (which depends on a') down a shaft into a generator. So, without understanding how these processes work, we won't be able to determine how much power the system produces.

2. We will later (see Chapter 4) talk about some of the structural aspects of wind turbine design. But, that process will need an as-yet-unknown load-distribution along the beam-like elements of the turbine, including along the length of the blades. But, to find that load-distribution, we need to know what the flow is at radial-position along the blades (a and a') and what the corresponding forces are.

3. Not all of the blade-shape is determined by stuctural reasons, some of it is determined by aerodynamic arguments. It turns out, that some of the work we do to address the previous questions, will give us insight into these aerodynamic considerations.

3.2 Actuator Disc Model and Betz' Limit (Momentum Theory)

The wind slows down as it approaches the turbine, at the turbine rotor itself, and even further downstream. Figure 3.2 shows a side view of a wind turbine and the surrounding flow field. A **stream tube** is defined as a tube whose boundaries are parallel to the local fluid velocity.

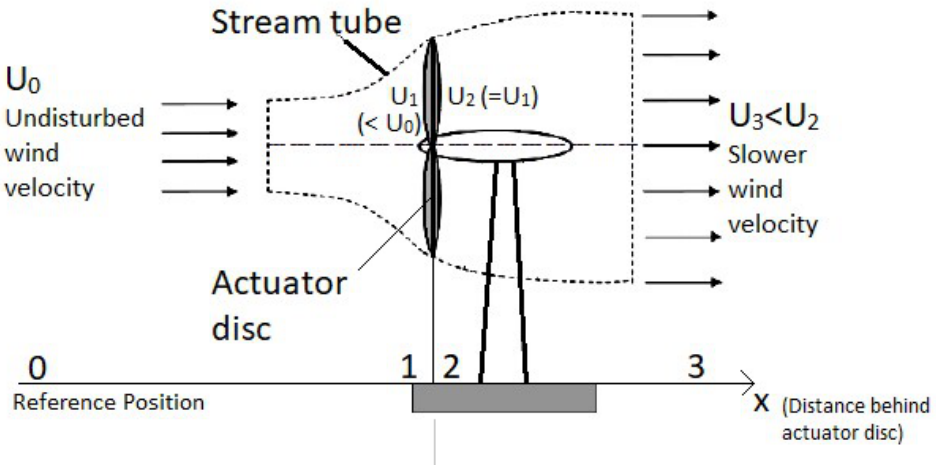

Figure 3.2: Side view of a wind turbine and its stream tube. Position 0 is infinitely far upstream of position 1; position 3 is infinitely far downstream of position 2.

First guess (not achievable): The power in the air that would flow through the actuator disc area if the turbine were not there would be:

$$P_{\text{air}} = \frac{1}{2}\rho A u_0^3,$$

where P_{air} is the theoretical power of the undisturbed wind, ρ is the air density [kg/m^3] (which we will assume is constant), A is the area of the actuator disc [m^2], and u_0 is the undisturbed upstream wind speed [m/s].

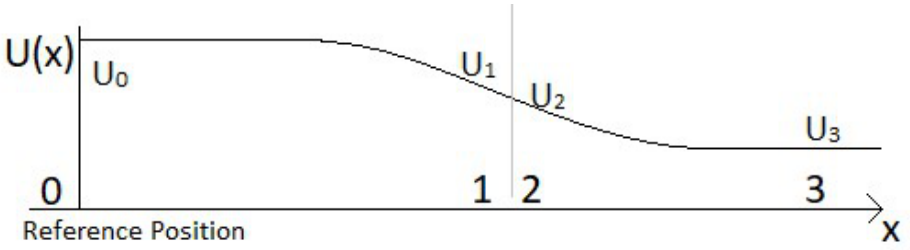

Figure 3.3: Axial wind velocity slows down as it approaches the turbine and is slowed further as it passes through the rotor disk.

We define four positions along the wind direction x and the corresponding wind speeds $u(x)$:

- x_0: far upwind of the turbine ($u(x_0) = u_0$),
- x_1: just before the turbine ($u(x_1) = u_1$),
- x_2: just after the turbine ($u(x_2) = u_2$),
- x_3: very far downstream of the turbine ($u(x_3) = u_3$).

Note: We assume the stream tube does not interact with surrounding air outside of the tube, but that - still somehow - the pressure within the flow recovers to its freestream value infinitely far downstream of the actuator at x_3. That is: $p_3 = p_0$.

The inflow through the actuator disc equals the outflow, and the cross-sectional area of the stream tube at the rotor plane equals the rotor area A. Then, the mass flow through the turbine can be determined:

$$\dot{m}_1 = \rho A u_1, \quad \dot{m}_2 = \rho A u_2 \tag{3.1}$$

Since the density and the area are the same, conservation of mass ($\dot{m} = \dot{m}_1 = \dot{m}_2$) means that the speed has to be continuous across the rotor:

$$u_1 = u_2.$$

Thrust of the turbine

The thrust can be expressed in two equivalent ways. Either, from the pressure drop across the disc:

$$T = A(p_1 - p_2) \tag{3.2}$$

or from the change of momentum:

$$T = \dot{m}(u_0 - u_3) \tag{3.3}$$

Notice that the pressure has to drop over the actuator (as opposed to rise), because energy is being pulled out of the flow.

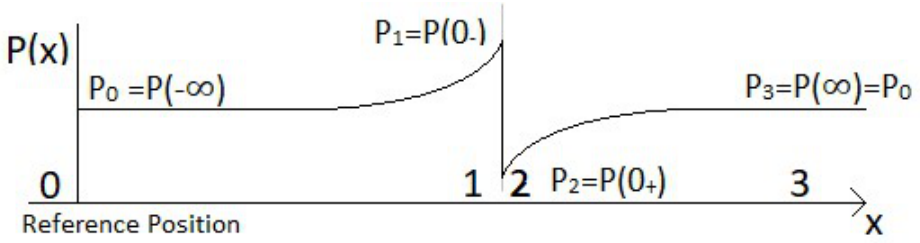

Figure 3.4: Pressure builds up as the wind approaches the wind turbine, and drops after passing through the turbine.

Power extraction

Similiarly, we can find two ways to express the instantaneous power. First, from the thrust:

$$P = Tu_1 \tag{3.4}$$

or from the change of kinetic energy of the air:

$$P = \dot{m}\frac{1}{2}\left(u_0^2 - u_3^2\right) \tag{3.5}$$

Governing equations

Remember, that we have $u_1 = u_2$ and $p_3 = p_0$ and 'known' values u_0 and p_0. The things we don't know are: u_1, p_1, and p_2.

Luckily, we can assemble a number of relationships from above.

From (3.2) and (3.3), we have a thrust equation:

$$T = A(p_1 - p_2) = \dot{m}(u_0 - u_3). \tag{3.6}$$

By a similar token as (3.6), we can relate (3.4) and (3.5) to give a power equation:

$$P = Tu_1 = \dot{m}(u_0 - u_3)u_1 = \dot{m}\frac{1}{2}\left(u_0^2 - u_3^2\right). \tag{3.7}$$

Bernoulli's principle (valid in regions where no energy is extracted, where the flow is adiabatic, inviscid, incompressible, and with a negligible altitude difference) says that:

$$p(x) + \frac{1}{2}\rho u(x)^2 = \text{constant}.$$

If we apply Bernoulli before the actuator, we get:

$$p_0 + \frac{1}{2}\rho u_0^2 = p_1 + \frac{1}{2}\rho u_1^2 \tag{3.8}$$

and, after the actuator:

$$p_3 + \frac{1}{2}\rho u_3^2 = p_2 + \frac{1}{2}\rho u_2^2. \tag{3.9}$$

Average speed

I propose to you that the flow crossing the annulus has a speed u_1 exactly average of the far-upstream and far-downstream speeds u_0 and u_3.

We have two different ways to demonstrate this.

First, from (3.7), we could notice that:

$$\dot{m}(u_0 - u_3)u_1 = \dot{m}\frac{1}{2}\left(u_0^2 - u_3^2\right) \quad \Rightarrow \quad (u_0 - u_3)u_1 = \frac{1}{2}(u_0 - u_3)(u_0 + u_3) \quad \Rightarrow \quad u_1 = \frac{1}{2}(u_0 + u_3). \tag{3.10}$$

Alternatively, we can subtracting the Bernoulli pressure equations from each other, and substitute in the known pressure and speed relations ($p_3 = p_0$, $u_1 = u_2$):

$$\begin{aligned} p_0 + \frac{1}{2}\rho u_0^2 - p_3 - \frac{1}{2}\rho u_3^2 &= p_1 + \frac{1}{2}\rho u_1^2 - p_2 - \frac{1}{2}\rho u_2^2 \\ \frac{1}{2}\rho(u_0^2 - u_3^2) &= p_1 - p_2 \end{aligned} \tag{3.11}$$

Applying this pressure difference into the thrust equation (3.6)

$$A\frac{1}{2}\rho(u_0^2 - u_3^2) = \dot{m}(u_0 - u_3) \quad \Rightarrow \quad A\rho\frac{1}{2}(u_0 + u_3)(u_0 - u_3) = \dot{m}(u_0 - u_3) \quad \Rightarrow \quad A\rho\frac{1}{2}(u_0 + u_3) = \dot{m} = \rho A u_1 \quad \Rightarrow \quad u_1 = \frac{1}{2}(u_0 + u_3). \tag{3.12}$$

Whichever derivation we like, we can further define a helpful value a [-], the axial induction factor, as the nondimesional, axial-direction speed loss at the annulus:

$$u_1 = (1 - a)u_0 \quad \Leftrightarrow \quad a = \frac{u_0 - u_1}{u_0}, \tag{3.13}$$

and use this induction factor a to help us say something about the far downstream speed u_3. Then, starting with the $u_1 = (u_0 + u_3)/2$ relation:

$$(1 - a)u_0 = \frac{1}{2}(u_0 + u_3) \quad \Rightarrow \quad u_3 = (1 - 2a)u_0. \tag{3.14}$$

Which means that, as we step from position 0 to position 1 to position 3, we're each time losing the same amount of flow speed.

Power and thrust as a function of the induction factor a

Let's recall that that power which was (not-acheivably) offered by the wind was $(1/2)\rho A u_0^3$.

Now, if we return to the power relationship of (3.4):

$$\begin{aligned} P &= \dot{m}(u_0 - u_3)u_1 \\ &= \rho A u_1^2(u_0 - u_3) \\ &= \rho A(1 - a)^2 u_0^2(u_0 - (1 - 2a)u_0) \\ &= \rho A u_0^3(1 - a)^2(2a), \end{aligned} \tag{3.15}$$

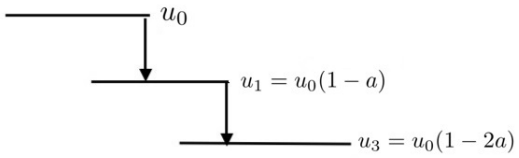

Figure 3.5: Velocities defined for the actuator disc: upstream u_0, at the disk u_1, and far downstream u_3. The axial induction factor a relates them.

and divide this value by the amount of power which was (not-achievably) in the wind, we get a non-dimensional power coefficient C_P [-].

That is:

$$C_P(a) = \frac{P}{\frac{1}{2}\rho A u_0^3} = \frac{\rho A u_0^3 (1-a)^2 (2a)}{\frac{1}{2}\rho A u_0^3} = 4a(1-a)^2. \tag{3.16}$$

So, we can describe how much power can be harvested, proportionally, from the wind with this power coefficient. This means that we can compare between different systems, designs, operating modes, etc. with this nondimensional power coefficient C_P.

$$P = C_P \left(\frac{1}{2}\rho A u_0^3\right) = 4a(1-a)^2 \left(\frac{1}{2}\rho A u_0^3\right). \tag{3.17}$$

We can do a similar thing with the thrust -

$$\begin{aligned} T &= \dot{m}(u_0 - u_3) \\ &= \rho A u_1 (u_0 - u_3) \\ &= \rho A u_0 (1-a)(u_0 - u_0(1-2a)) \\ &= \rho A u_0^2 (1-a)(1-1+2a) \\ &= \rho A u_0^2 2a(1-a) \end{aligned} \tag{3.18}$$

- dividing the thrust we can actually achieve considering our induction factor by the product of the dynamic pressure at the actuator and the area of the actuator, to create a thrust coefficient C_T [-] that we can compare.

$$C_T(a) = \frac{T}{\frac{1}{2}\rho u_0^2 A} = \frac{\rho A u_0^2 2a(1-a)}{\frac{1}{2}\rho u_0^2 A} = 4a(1-a). \tag{3.19}$$

Where telling someone a system's thrust coefficient effectively tells them what the instantaneous thrust is, under the environmental conditions.

$$T = C_T \left(\frac{1}{2}\rho u_0^2 A\right) = 4a(1-a) \left(\frac{1}{2}\rho u_0^2 A\right) \tag{3.20}$$

You can see that the two nondimensional coefficients are related:

$$C_P(a) = (1-a) C_T(a). \tag{3.21}$$

which happens to be consistent with the relationship we'd expect from Eq. (3.4).

Maximize power extraction

The goal is to find the value of the axial induction factor a that maximizes the power coefficient $C_P(a)$.

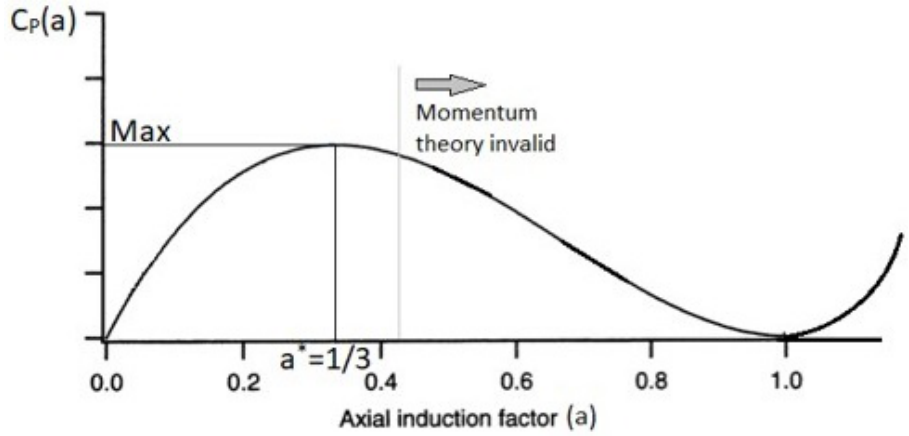

Figure 3.6: Power coefficient C_P as a function of induction factor a. The maximum occurs at the Betz limit.

We differentiate the power coefficient:

$$\frac{dC_P}{da} = 2(1-a)\cdot 4a + (1-a)^2 \cdot 4.$$

Setting the derivative to zero:

$$\frac{dC_P}{da} = 0 \quad \Leftrightarrow \quad 2a = 1-a \quad \Rightarrow \quad a^* = \frac{1}{3}.$$

This value $a^* = \frac{1}{3}$ is the **optimal induction factor**.

Substituting a^* into $C_P(a)$:

$$C_P(a^*) = \left(\frac{2}{3}\right)^2 \cdot 4 \cdot \frac{1}{3} = \frac{16}{27} \approx 0.59.$$

This upper limit is known as the **Betz limit** — meaning that, at most, about 59% of the kinetic energy in the wind can be extracted by an ideal wind turbine.

Because $C_T(a) = 4a(1-a)$, the thrust coefficient at the optimal induction factor is:

$$C_T(a^*) = 4 \cdot \frac{1}{3}\left(1 - \frac{1}{3}\right) = \frac{8}{9}.$$

For comparison, if we substitute $a = \frac{1}{2}$ into $C_T(a)$ we get:

$$C_T\left(\frac{1}{2}\right) = 4 \cdot \frac{1}{2}\left(1 - \frac{1}{2}\right) = 1.$$

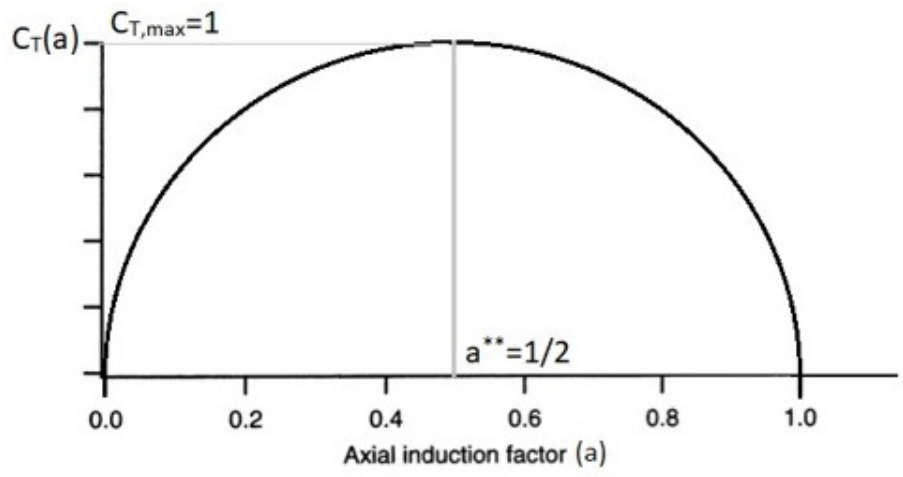

Figure 3.7: The Betz limit: theoretical maximum efficiency for an ideal wind turbine.

3.3 Wake Rotation & Rotor Disc Theory

Remember our approach in the previous section: we found the power-due-to-thrust and set this equal to the power-due-to-changing-the-flow's-momentum. We can do this in the tangential direction as well as in the axial direction.

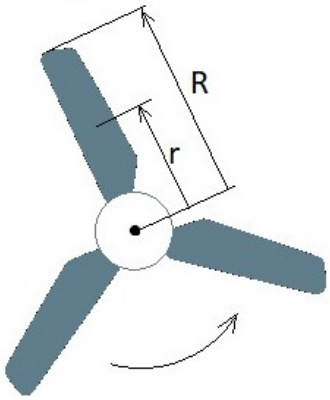

Figure 3.8: Blade tip speed and speed at radius r for a rotor spinning with angular velocity Ω.

That is, we don't just know the power from (3.17), we also know that the power should be the rate of change of angular momentum ($\dot{m}(L_2 - L_0)$) times the angular speed Ω [rad s^{-1}]. Here L is the angular momentum [kg m^2 s^{-1}] of the flow.

Now, far upstream of the turbine, the angular velocity ω_0 has to be whatever the angular velocity would have been if the turbine'd never been built or turned on. So:

$$\omega_0 = 0. \tag{3.22}$$

When we determine how much angular velocity the actuator adds ($\omega_2 - \omega_0 = \omega_2$), we will decide that this angular velocity will be added half on the upstream-side of the actuator at position 1 and the other half on the downstream-side of the actuator at position 2:

$$\omega_2 = 2\omega_1. \tag{3.23}$$

After this, the inviscid (friction-less flow) model assumes that the angular momentum stays constant in the flow forever. So:

$$\omega_3 = \omega_2 \tag{3.24}$$

This is sketched in Figures 3.9 and 3.10, as well as philosophically motivated in Figure ??.

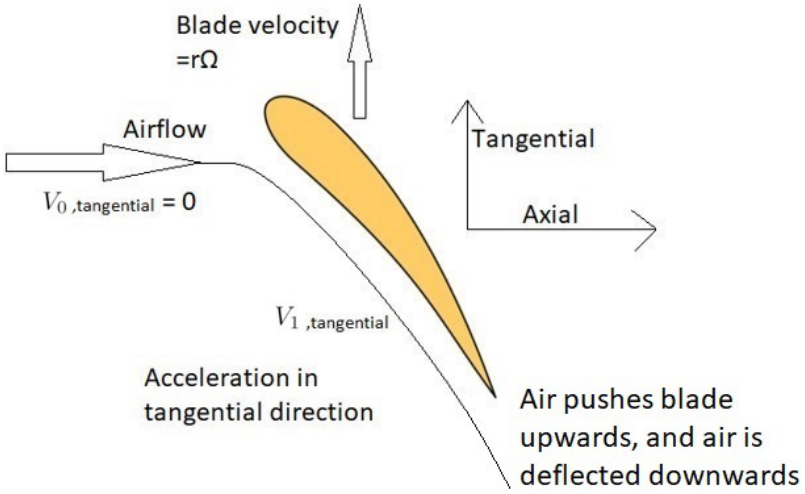

Figure 3.9: Tangential velocity induction: downstream air rotates opposite to the blade's direction of rotation.

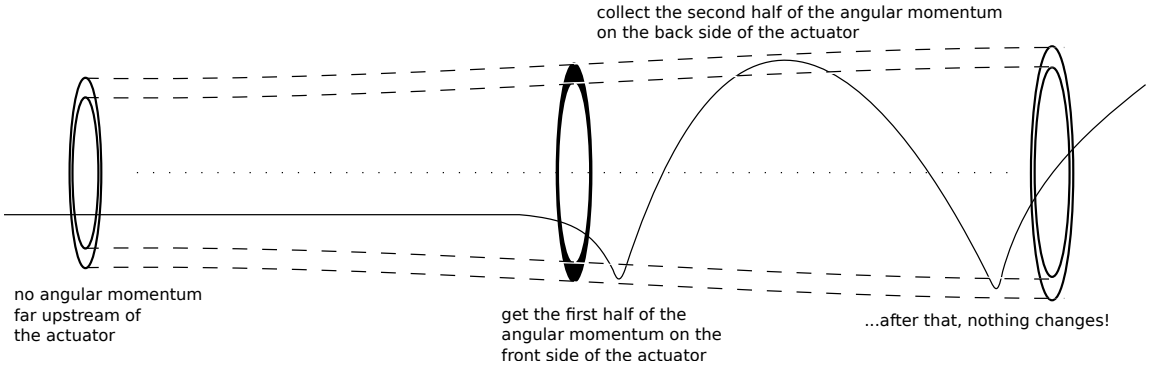

Figure 3.10: The actuator adds angular momentum to the flow: half of the ultimate value at the upstream side of the actuator and the other half immediately afterwards, at the downstream side. After this, the inviscid model assumes that the angular momentum stays indefinitely.

Either way, if we define some helpful tangential induction factor a' as the change in flow speed in the indicated direction divided by the main velocity in that direction, this gives:

$$a' = \frac{\omega_1}{\Omega} = \frac{\omega_2}{2\Omega} \quad \Leftrightarrow \quad \omega_2 = 2a'\Omega \tag{3.25}$$

Here, $\Omega = \frac{2\pi}{T}$ is the angular velocity of the rotor [rad/s], where T is the period of one rotation.

Now, let's consider just one thin annular slice of the actuator disk (an actuator annulus), at radius r from the center of the disk. If the annulus has a thickness $\mathrm{d}r$, then the area of the annulus is $\mathrm{d}A = 2\pi r \mathrm{d}r$. (You'll notice that integrating $\int_0^R 2\pi r \mathrm{d}r = \pi R^2$.)

The torque applied by the annulus to the flow must be equal to the change in angular momentum.

(Remember, also, that the moment of inertia I [kg m^2] of a thin circular loop of radius r and mass m is $I = mr^2$.)

So, since the fluid didn't have any angular momentum before position 1, the torque on the infinitessimal annulus must be:

$$\mathrm{d}Q(r) = \mathrm{d}\dot{m} r^2 \omega_2 = \rho u_1 (\mathrm{d}A) r^2 \omega_2. \tag{3.26}$$

Substitute in $u_1 = (1-a)u_0$ and $\omega_2 = 2a'\Omega$:

$$\mathrm{d}Q(r) = \rho(1-a)u_0(2a'\Omega)r^2(\mathrm{d}A) \tag{3.27}$$

And since power is torque times angular speed, the power harvested by our thin actuator annulus is:

$$\mathrm{d}P(r) = \Omega \mathrm{d}Q = 2a'(1-a)\rho u_0 \Omega^2 r^2 \mathrm{d}A. \tag{3.28}$$

But, remember, we already know how much power our system is supposed to be harvesting: we found it in (3.17). Recall:

$$\mathrm{d}P = 2a(1-a)^2 \rho u_0^3 \mathrm{d}A. \tag{3.29}$$

So, in rotor disk theory, we're going to set these two estimates of the power are equal.

$$\begin{aligned} 2a'(1-a)\rho u_0 \Omega^2 r^2 \mathrm{d}A &= 2a(1-a)^2 \rho u_0^3 \mathrm{d}A \\ a'\Omega^2 r^2 &= a(1-a)u_0^2 \\ a' &= a(1-a)\left(\frac{u_0}{\Omega r}\right)^2 \end{aligned} \tag{3.30}$$

But wait... Haven't we seen this ratio $\Omega r/u_0$ somewhere before?

Yes, this is the local tip speed ratio $\lambda_r = \Omega r/u_0$ [-] that we used in (1.9)!

$$a' = a(1-a)\lambda_r^{-2} \quad \Leftrightarrow \quad a(1-a) = a'\lambda_r^2. \tag{3.31}$$

And returning to our definition of the tangential induction factor (3.25)

$$\omega_2(r) = 2a(1-a)\frac{u_0^2}{\Omega r^2}, \tag{3.32}$$

which means that if the axial induction factor stays (roughly) similar at all radial positions, then our wake's angular velocity is proprtional to $1/r^2$. Considering that the radius can become quite small near the hub, this means that the wake should be rotated substantially more near the hub than near the blade tips.

3.4 Blade Element Momentum Theory (BEM)

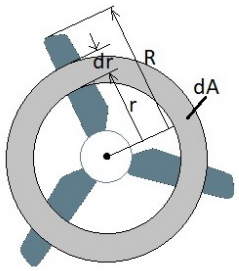

Figure 3.11: Rotor divided into annular elements for blade element momentum theory.

The blade element momentum (BEM) theory combines actuator disc momentum theory with two-dimensional airfoil aerodynamics to predict turbine performance.

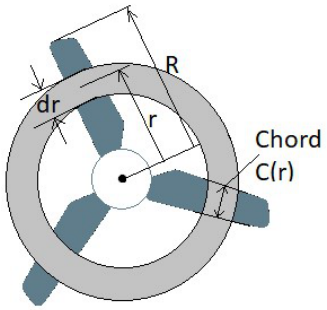

Figure 3.12: Each annulus of the rotor is treated like a small actuator disk.

Geometry and Speeds

Before anything else, we should remind outselves that the axial and tangential induction both vary with radius:

$$a = a(r), \qquad a' = a'(r).$$

At a given element, we define:

- $\beta(r)$: the pitch angle at radius r,
- α: the angle of attack,
- $\phi = \alpha + \beta$: the flow angle.

The effective wind speed at the element is:

$$W = u_\infty \sqrt{(1-a)^2 + \lambda_r^2 (1+a')^2}, \tag{3.33}$$

where $\lambda_r = \frac{r\Omega}{u_\infty}$ is the local speed ratio.

Element Forces

The area of a thin slice of a blade $\mathrm{d}A_\mathrm{B}$ [m^2] is:

$$\mathrm{d}A_\mathrm{B} = c(r)\mathrm{d}r, \tag{3.34}$$

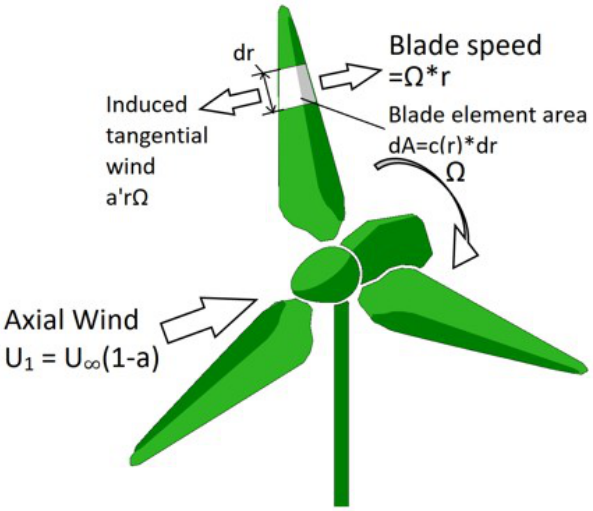

Figure 3.13: Blade element geometry: annular section at radius r.

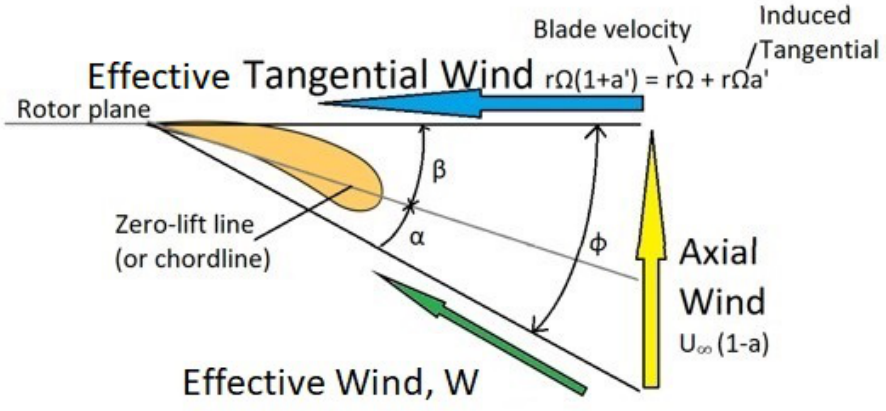

Figure 3.14: Blade element top view showing pitch angle β, angle of attack α, and flow angle ϕ.

where c is the profile's chord-length [m].

This thin slice is effectively a 2D airfoil sliced out of a much-longer wing. That means that we have lift and drag force contributions $\mathrm{d}L$ [$\mathrm{N\,m^{-1}}$] and $\mathrm{d}D$ [$\mathrm{N\,m^{-1}}$], as well as the nondimensional 2D lift and drag coefficients $c_\ell(\alpha)$ and $c_\mathrm{d}(\alpha)$.

$$\mathrm{d}L = c_\ell \frac{1}{2}\rho W^2 \mathrm{d}A_\mathrm{B}, \quad \mathrm{d}D = c_\mathrm{d} \frac{1}{2}\rho W^2 \mathrm{d}A_\mathrm{B}. \tag{3.35}$$

The directions that these force components are oriented depend on the local flow angle $\phi(r)$:

$$\sin\phi = \frac{(1-a)u_\infty}{W}, \quad \cos\phi = \frac{r\Omega(1+a')}{W}. \tag{3.36}$$

This gives an angle of attack α [rad]:

$$\alpha = \phi - \beta, \tag{3.37}$$

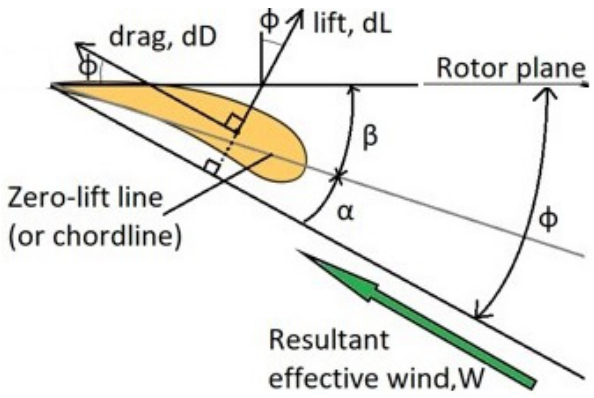

Figure 3.15: Lift and drag on a blade element.

with the blade pitch angle β [rad].

We can resolve the forces into axial and tangential components over all blades: an axial force $\mathrm{d}F_\mathrm{A}$ [$\mathrm{N\,m^{-1}}$]:

$$\mathrm{d}F_\mathrm{A} = B(\mathrm{d}L\cos\phi + \mathrm{d}D\sin\phi). \tag{3.38}$$

and a tangential force:

$$\mathrm{d}F_\mathrm{T} = B(\mathrm{d}L\sin\phi - \mathrm{d}D\cos\phi). \tag{3.39}$$

Momentum Balance

The same axial and tangential forces can be written from momentum theory.

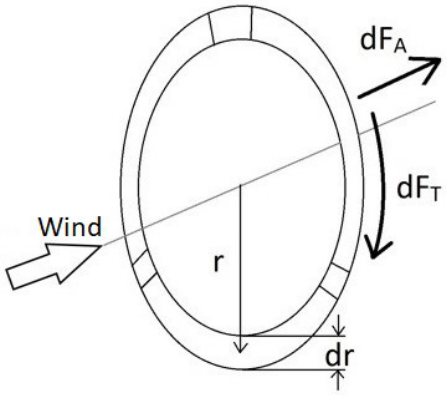

Figure 3.16: The axial and tangential force, imposed by the annulus.

Recall that we said in (3.3), that the thrust is the product of the mass flow rate and the difference in speed between the far downstream and the far upstream. Remember, also, that we'd determined in the Betz analysis (3.14) that the far-downstream flow speed is $(1-2a)u_\infty$. That means:

$$\begin{aligned} \mathrm{d}F_\mathrm{A} &= \mathrm{d}\dot{m}u_\infty(1-(1-2a)) = \mathrm{d}\dot{m}u_\infty(2a) \\ &= \rho\,(2\pi r\mathrm{d}r)\,u_\infty(1-a)(2au_\infty) \\ &= \frac{1}{2}\rho u_\infty^2\,(2\pi r\mathrm{d}r)\,(4a(1-a)). \end{aligned} \tag{3.40}$$

The tangential force is exactly the same, it just depends on the tangential speed after the actuator disk (which we'd previously called $\omega_2 r$) and relies on the fact that the upstream

tangential speed is zero. Refering back to (3.25), we have:

$$\begin{aligned} \mathrm{d}F_\mathrm{T} &= \mathrm{d}\dot{m}(2a'\Omega r) \\ &= \rho\,(2\pi r\mathrm{d}r)\,u_\infty(1-a)(2a'\Omega r) \\ &= \frac{1}{2}\rho u_\infty(r\Omega)\,(2\pi r\mathrm{d}r)\,(4a'(1-a)) \end{aligned} \tag{3.41}$$

If we now set the two axial force equations (3.38) and (3.40) equal, and then set the two tangential force equations (3.39) and (3.41) equal, we obtain two equations for the unknowns (a and a'), which have to be solved numerically.

Setting the force from the blades' perspective equal to the force from the annulus' perspective

From Eq. 3.38 and Eq. 3.40:

$$\frac{1}{2}\rho W^2 Bc(c_\ell\cos\phi + c_\mathrm{d}\sin\phi)\mathrm{d}r = \frac{1}{2}\rho u_\infty^2(2\pi r\mathrm{d}r)(4a(1-a)) \tag{3.42}$$

From Eq. 3.39 and Eq. 3.41:

$$\frac{1}{2}\rho W^2 Bc(c_\ell\sin\phi - c_\mathrm{d}\cos\phi)\mathrm{d}r = \frac{1}{2}\rho u_\infty r\Omega(2\pi r\mathrm{d}r)(4a'(1-a)) \tag{3.43}$$

Using nondimensional parameters to simplify

We're already met the local speed ratio λ_r. The other nondimensional parameter that might end up being useful here is the local 'solidity' a radius r. This is defined as:

$$\sigma_r = \frac{Bc(r)}{2\pi r}, \tag{3.44}$$

which means that as we follow the circumpherence of an annulus, we compare the 'amount of blade' we 'walk over' to the total path length. Here:

- B [-] is the number of blades,
- $c(r)$ [m] is the chord length at radius r [m].

The overall rotor solidity is the total blade planform area divided by the rotor disc area:

$$\sigma = \frac{B\int_0^R c(r)dr}{\pi R^2}. \tag{3.45}$$

So, returning to (3.42) and (3.43), we can substitute in this local solidity $\sigma_r = \frac{Bc}{2\pi r}$ and express terms using the local speed ratio $\lambda_r = \frac{r\Omega}{U_\infty}$.

The effective wind speed simplifies to:

$$W = \sqrt{U_\infty^2(1-a)^2 + U_\infty^2\lambda_r^2(1+a')^2} = U_\infty\sqrt{(1-a)^2 + \lambda_r^2(1+a')^2} \tag{3.46}$$

with:

$$\sin\phi = \frac{u_\infty(1-a)}{W} = \frac{1-a}{\sqrt{(1-a)^2+\lambda_r^2(1+a')^2}},$$
$$\cos\phi = \frac{\lambda_r u_\infty(1+a')}{W} = \frac{\lambda_r(1+a')}{\sqrt{(1-a)^2+\lambda_r^2(1+a')^2}}.$$

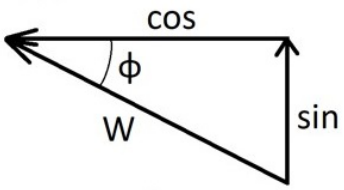

Figure 3.17: Trigonometric relations in the velocity triange.

Starting from (3.42) and plugging in the above non-dimensional parameters gives:

$$\frac{1}{2}\rho W^2\sigma_r(2\pi r)\left(c_\ell\left(\frac{\lambda_r u_\infty(1+a')}{W}\right)+c_{\mathrm{d}}\left(\frac{u_\infty(1-a)}{W}\right)\right)\mathrm{d}r = \frac{1}{2}\rho u_\infty^2(2\pi r\mathrm{d}r)(4a(1-a)). \tag{3.47}$$

If we divide each side by $\pi r\rho u_\infty^2(\mathrm{d}r)$ and simplify, we get:

$$\sigma_r\sqrt{(a-1)^2+(a'+1)^2\lambda_r^2}(-ac_{\mathrm{d}}+(a'+1)c_\ell\lambda_r+c_{\mathrm{d}}) = 4(1-a)a. \tag{3.48}$$

Doing the same thing from (3.43), gives first:

$$\pi(\mathrm{d}r)r\rho\sigma_r u_\infty^2\sqrt{(a-1)^2+(a'+1)^2\lambda_r^2}((1-a)c_\ell-(a'+1)c_{\mathrm{d}}\lambda_r) = 4\pi(1-a)a'(\mathrm{d}r)\lambda_r r\rho u_\infty^2, \tag{3.49}$$

which divides and simplifies to:

$$\frac{1}{\lambda_r}\left(\sigma_r\sqrt{(a-1)^2+(a'+1)^2\lambda_r^2}((1-a)c_\ell-(a'+1)c_{\mathrm{d}}\lambda_r)\right) = 4(1-a)a'. \tag{3.50}$$

Solving via quadratic formula!

Dividing (3.48) by (3.50), gives:

$$\lambda_r\cdot\frac{c_l\lambda_r(1+a')+c_d(1-a)}{c_l(1-a)-c_d\lambda_r(1+a')} = \frac{a}{a'} \tag{3.51}$$

Now, let's multiply both sides by the denominators, move everything to one side of the equality, and collect the terms:

$$\begin{aligned} -a^2c_\ell+a(c_\ell-c_{\mathrm{d}}\lambda_r)-a'\lambda_r\left((a'+1)\,c_\ell\lambda_r+c_{\mathrm{d}}\right) &= 0 \\ (a')^2c_\ell\lambda_r^2-a'\left(-c_{\mathrm{d}}\lambda_r-c_\ell\lambda_r^2\right)+a^2c_\ell-a(c_\ell-c_{\mathrm{d}}\lambda_r) &= 0, \end{aligned} \tag{3.52}$$

which happens to be the quadratic relationship $H_2(a')^2 + H_1 a' + H_0 = 0$ if

$$H_2 = c_\ell \lambda_r^2, \quad H_1 = c_\mathrm{d}\lambda_r + c_\ell \lambda_r^2, \quad H_0 = a^2 c_\ell - a(c_\ell - c_\mathrm{d}\lambda_r). \tag{3.53}$$

This means that:

$$\begin{aligned} a' &= \frac{-H_1 \pm \sqrt{H_1^2 - 4H_0 H_2}}{2H_2} \\ &= \frac{-c_\mathrm{d}\lambda_r - c_\ell\lambda_r^2 \pm \sqrt{(c_\mathrm{d}\lambda_r + c_\ell\lambda_r^2)^2 + 4ac_\ell\lambda_r^2((1-a)c_\ell - c_\mathrm{d}\lambda_r)}}{2c_\ell\lambda_r^2} \end{aligned} \tag{3.54}$$

(and, the $\pm$ sign has to be a positive sign to keep the value of a' reasonable.)

So, we're left with:

$$a' = \frac{-c_\mathrm{d}\lambda_r - c_\ell\lambda_r^2 + \sqrt{(c_\mathrm{d}\lambda_r + c_\ell\lambda_r^2)^2 + 4ac_\ell\lambda_r^2((1-a)c_\ell - c_\mathrm{d}\lambda_r)}}{2c_\ell\lambda_r^2} \tag{3.55}$$

Special case when $c_\mathrm{d} = 0$

$$a' = -\frac{1}{2} + \sqrt{\frac{1}{4} + \frac{a(1-a)}{\lambda_r^2}} \tag{3.56}$$

$$= -\frac{1}{2} + \frac{1}{2}\sqrt{1 + \frac{4a(1-a)}{\lambda_r^2}} \tag{3.57}$$

$$= -\frac{1}{2} + \frac{1}{2}\left[1 + \frac{1}{2}\frac{4a(1-a)}{\lambda_r^2} + O\left(\lambda_r^{-4}\right)\right] \tag{3.58}$$

$$= \frac{a(1-a)}{\lambda_r^2} + O\left(\lambda_r^{-4}\right) \tag{3.59}$$

Recalling that by Taylor series:

$$\sqrt{1+x} = 1 + \frac{1}{2}x + O(x^2).$$

So, it turns out that - for vanishing drag coefficients and small values of λ_r^{-4}, we get the same result as we found in rotor-disk theory

$$a' = \frac{a(1-a)}{\lambda_r^2}.$$

BEM example

Let us now assume a few typical values: $\lambda_r \in [1, 7]$ and $B = 3$. For $\lambda_R = 7$, we assume the induction factor $a = \frac{1}{3}$ for all r (extracting maximum power according to Betz' limit).

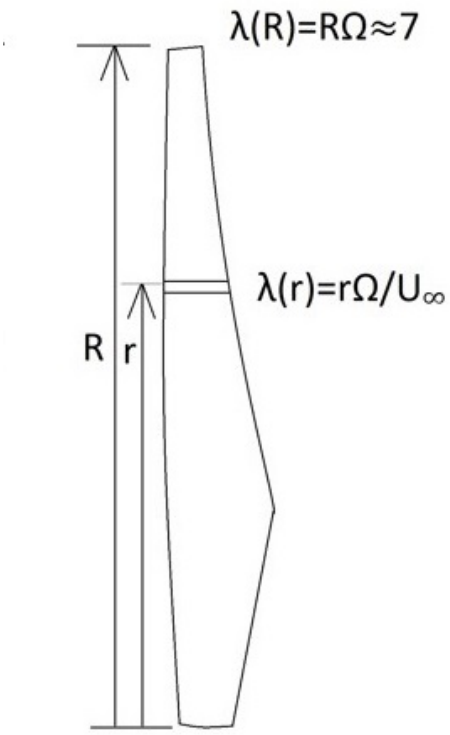

Figure 3.18: Considering one particular slice of the blade...

Assume that the 2D lift and drag coefficients of each radial airfoil section can be chosen as:

$$c_l = 1 \qquad c_d = 0.01$$

The tangential induction factor a' is approximated as:

$$a' \approx \frac{a(1-a)}{\lambda_r^2}$$

Substituting $a = \frac{1}{3}$ gives:

$$a' \approx \frac{\frac{1}{3} \cdot \frac{2}{3}}{\lambda_r^2} = \frac{2}{9}\frac{1}{\lambda_r^2}$$

Local solidity σ_r From Eq. (3.48) we have:

$$\sigma_r = \frac{4a(1-a)}{c_l \lambda_r (1+a') + c_d(1-a)} \cdot \frac{1}{\sqrt{\lambda_r^2(1+a')^2 + (1-a)^2}}$$

With $a = \frac{1}{3}$ we simplify:

$$4a(1-a) = 4 \cdot \frac{1}{3} \cdot \frac{2}{3} = \frac{8}{9}$$

Given that $c_d \ll c_l$ and $a' \ll 1$ for large λ_r, we approximate:

$$c_d(1-a) \approx 0, \qquad (1+a') \approx 1$$

Thus the local solidity simplifies to:

$$\sigma_r \approx \frac{8}{9}\frac{1}{\lambda_r^2}$$

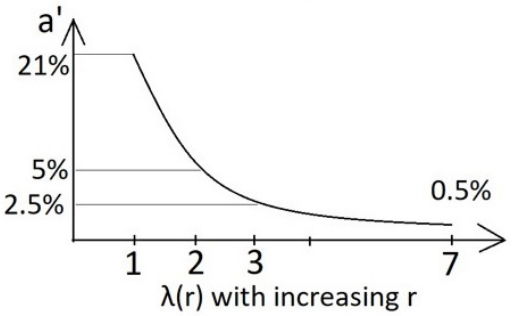

Figure 3.19: Relationship between local speed ratio λ_r and tangential induction factor a', showing that a' decreases rapidly as λ_r increases.

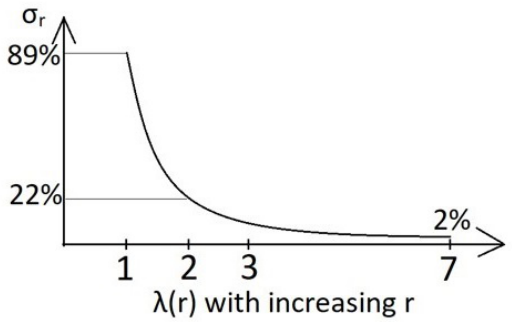

Figure 3.20: Local solidity σ_r as a function of λ_r, demonstrating the $1/\lambda_r^2$ dependency derived above.

What does this mean for chord length c? Since we have derived that:

$$\sigma_r = \frac{8}{9}\frac{1}{\lambda_r^2}$$

and we know the definition of local solidity:

$$\sigma_r = \frac{B\,c(r)}{2\pi r}$$

we can solve for the chord length $c(r)$:

$$c(r) = \frac{2\pi r}{B}\sigma_r$$

Substituting $\sigma_r = \frac{8}{9}\frac{1}{\lambda_r^2}$:

$$c(r) = \frac{2\pi r}{B} \cdot \frac{8}{9}\frac{1}{\lambda_r^2}$$

Recall that the local tip speed ratio is:

$$\lambda_r = \frac{r}{R}\lambda_R$$

where $\mu = \frac{r}{R}$ is the nondimensional radius fraction. Substituting $\lambda_r = \mu\lambda_R$:

$$c(r) = \frac{2\pi r}{B} \cdot \frac{8}{9}\frac{1}{(\mu\lambda_R)^2}$$

Simplify:

$$c(r) = \frac{2\pi R}{B\,\lambda_R^2} \cdot \frac{8}{9} \cdot \frac{1}{\mu}$$

This shows that the chord length is inversely proportional to μ (the radial fraction).

We substitute $\lambda_R = 7$ and simplify further. Using $\frac{8}{9}\frac{1}{\lambda_R^2} \approx 2\%$:

$$c(r) \approx \frac{2\pi R}{B} \cdot 2\% \cdot \frac{1}{\mu} \approx \frac{4\%\,R}{\mu}$$

This shows that the chord length is roughly $4\,\%$ of the radius divided by the nondimensional radius μ.

In our specific example, with $R = 50\,\mathrm{m}$, $B = 3$ blades, and $\lambda_R = 7$:

$$c(R) = 2\,\mathrm{m} \quad \text{and} \quad c(10\,\mathrm{m}) = 10\,\mathrm{m}.$$

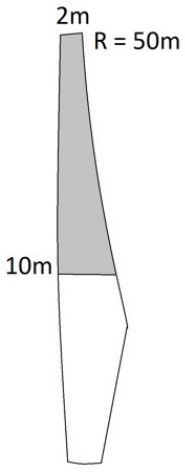

Figure 3.21: Resulting chord length distribution $c(r)$ along the blade radius, illustrating the $1/\mu$ dependency and showing wider chords near the hub.

The most important equation to remember

Assumptions The following simplifying assumptions are made for the optimal chord derivation:

$$\left.\begin{cases} \lambda_r = \frac{r}{R} \cdot \lambda \gg 1 \\ \\ \frac{C_L}{C_D} \gg 1 \end{cases}\right\} \text{Assumptions}$$

This includes:

- the **local tip speed ratio** λ_r is large. This means the blades are operating at a high enough speed that cross-flow dominates, and the inflow angle is small.
- Drag is neglected (high C_L/C_D).
- Axial momentum balance holds.
- Steady flow conditions.

Axial momentum balance The force on the blade area -

$$F_B = \frac{1}{2}\rho\, A_B \underbrace{(\lambda_r U_\infty)^2}_{W^2} C_L$$

- equals the thrust on the annulus:

$$F_A = \rho A_A U_\infty (1-a)\,(2a\,U_\infty) = \frac{1}{2}\rho A_A U_\infty^2 \underbrace{4a(1-a)}_{C_T(a)}$$

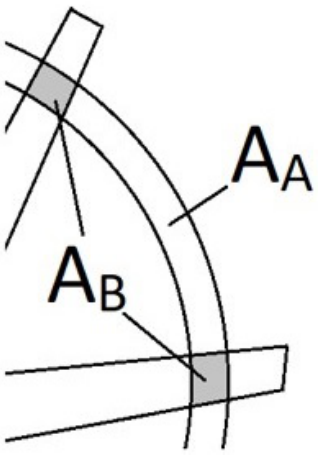

Figure 3.22: A conceptual sketch: the aerodynamic forces must equal the annulus thrust.

Local solidity The local solidity is defined as:

$$\sigma_r = \frac{A_B}{A_A} = \frac{B\,c(r)}{2\pi r}$$

Optimal chord By equating the blade lift force to the annular thrust, we obtain:

$$\frac{1}{2}\rho U_\infty^2 A_B C_L \lambda_r^2 = \frac{1}{2}\rho U_\infty^2 A_A 4a(1-a)$$

This simplifies to:

$$\sigma_r C_L = \frac{4a(1-a)}{\lambda_r^2}$$

For the Betz-optimal induction factor $a = \frac{1}{3}$:

$$\sigma_r C_L = \frac{8}{9}\frac{1}{\lambda_r^2}$$

Thus:

$$\frac{B\,c(r)}{2\pi r} C_L(r) = \frac{8}{9}\frac{1}{\lambda_r^2}$$

$$c(r) = \frac{1}{B\,C_L(r)}\frac{2\pi R^2}{9\lambda^2}\frac{8}{r}$$

Or more neatly:

$$c(r) \propto \frac{1}{r}$$

This shows that, for a fixed C_L (and under the stated assumptions), the **optimal chord is inversely proportional to radius**.

Figure 3.23: The outer portions of the inverse-radius rule seem give a close-to-linear taper.

Practical blade design

In practice, **linear taper** is often used (see Figure 3.23), meaning that the chord length is treated as an affine function of the radius, which avoids the excessive chord growth that the theoretical $c(r) \propto 1/r$ law would predict very close to the hub.

To compensate for the lower solidity in the inner part of the blade, the angle of attack can be increased to raise $C_L(r)$ accordingly. Here the extra drag in the inner part of the blade is considered less critical.

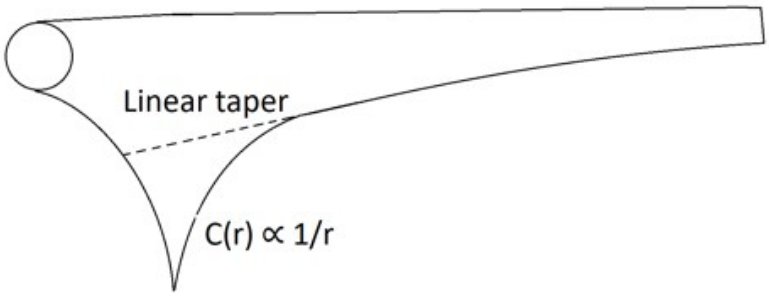

Figure 3.24: Linear taper approximation for chord length, avoiding excessive chord growth near the hub.

Pitch, twist, and the flow angle

The flow angle ϕ [rad] is the angle between the effective velocity W and the blade's path (ie, the tangential direction). This means that it ranges from $\phi = 0$ (if momentum keeps the rotor turning while a gust momentarily drops the wind speed to zero or the rotor is turning infinitely fast) to $\phi = 90\text{deg}$ (while the rotor is not turning or at the blade root). This angle is the angle that we use, when we try to figure out how to project the lift and drag forces into the axial and tangential directions.

With a range of $\phi \in (0, 90)$, we notice that this range is too large for the chord-line to always lay along the tangential direction: because that would make the angle of attack α too large, and the blades would stall.

(The angle of attack, remember, is the angle between the chord-line and the tangential direction, and is one of the main inputs that determine the 2D lift and drag coefficients $c_\ell(\alpha)$ and $c_\text{d}(\alpha)$. It's very important for finding the optimal c_ℓ/c_d value.)

So, we're going to use two different ways to reduce the angle of attack:

- by **pitching** the blade by an angle β [rad]. 'Pitching' is the deliberately controlled rotation of the entire blade around the blade's socket in the hub. In almost all cases, the same β is applied to all of the blades at the same time.
- by **twisting** the blade when we construct it. That is, the twist angle $\theta(r)$ [rad] doesn't have to be, and usually isn't, constant over the whole blade length. But, of course, since it's literally fiber-glassed into the blade, it can't be changed once the turbine is operational.

When we substract the combined pitch and twist angles β and $\theta(r)$ from the flow angle ϕ, whatever angle is left is the angle of attack α. You can see this in Figure 3.25:

$$\phi = \alpha + \beta + \theta(r) \quad \Leftrightarrow \quad \alpha = \phi - \beta - \theta(r)$$

Remember that from the definitions of the trigonometic functions, we know that:

$$\sin\phi = \frac{u_\infty(1-a)}{W} = \frac{1-a}{\sqrt{(1-a)^2 + \lambda_r^2(1+a')^2}} = \frac{1-a}{\lambda_r(1+a')}\sqrt{1 + \frac{(1-a)^2}{\lambda_r^2(1+a')^2}}$$

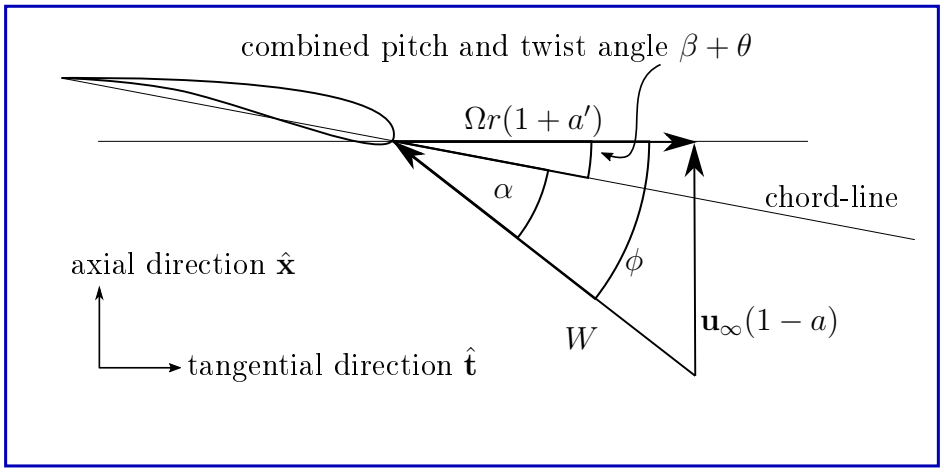

Figure 3.25: Definition of the flow angle ϕ, twist θ, and angle of attack α.

If we now assume that $(1 - a)^2 \ll \lambda^2(r/R)^2(1 + a')^2$, then the thing inside the square root drops away. That is:

$$\sin\phi \approx \frac{1 - a}{\lambda_r(1 + a')}$$

By the small-angle approximation:

$$\phi \approx \frac{1 - a}{\lambda_r(1 + a')}$$

so in the case of Betz-optimal induction factor $a = \frac{1}{3}$ (from axial momentum theory) and a small tangential induction function $a' \to 0$, this give:

$$\phi \approx \frac{2}{3}\frac{R}{\lambda r}$$

This would argue that, towards the blade tips (where our simplifying assumption $(1 - a)^2 \ll \lambda^2(r/R)^2(1 + a')^2$ is most likely to hold) the flow angle ϕ must be inversely proportional to the radius. (See Figure 3.26).

So, if we know what angle of attack will give us the desired c_ℓ/c_d value, then we can achieve this by pitching and twisting the blade.

The power harvesting factor ζ

The power harvesting factor, denoted as ζ, is defined as the ratio between the power actually harvested by the blade and the total power available in the wind passing through the blade area. This can be written mathematically as

$$\zeta = \frac{P}{\frac{1}{2}\rho A_B U_0^3},$$

where P is the mechanical power extracted by the rotor, ρ is the air density, A_B is the blade area, and U_0 is the free-stream wind speed.

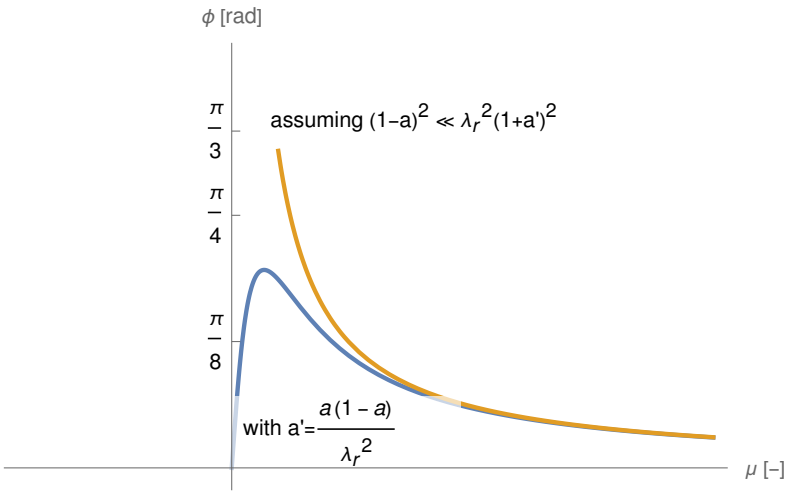

Figure 3.26: Flow angle ϕ under Betz optimal $a = \frac{1}{3}$ and the corresponding zero-drag BEM $a' = a(1-a)/(\lambda\mu)^2$ value (blue) fits quite nicely with the approximation of $\phi \approx (2/(3\lambda\mu))$ on the outer part of the blade. Shown at $\lambda = 7$.

Because the solidity and aerodynamic loading vary along the radius of the blade, ζ can be considered as a function of radius. We therefore define a local power harvesting factor, $\zeta(r)$, which can be expressed in terms of the local power coefficient C_P and the local solidity σ_r:

$$\zeta(r) = \frac{C_P}{\sigma_r}.$$

Neglecting blade drag and other aerodynamic losses, the power coefficient can be written in terms of the axial induction factor a as

$$C_P(a) = 4a(1-a)^2.$$

From earlier momentum balance derivations, we know that the local solidity, lift coefficient, and local tip-speed ratio are related by

$$\sigma_r C_L \lambda_r^2 = 4a(1-a),$$

which can be rearranged to isolate the local solidity:

$$\sigma_r = \frac{4a(1-a)}{C_L \lambda_r^2}.$$

Substituting this expression for σ_r into the definition of ζ gives

$$\zeta = \frac{4a(1-a)^2}{\frac{4a(1-a)}{C_L \lambda_r^2}}.$$

After simplifying, the result becomes

$$\zeta = (1 - a)\, C_L \lambda_r^2.$$

This equation shows that the power harvesting factor increases with both the lift coefficient and the square of the local tip-speed ratio, but decreases as the axial induction factor a approaches one.

At the Betz-optimal induction factor, $a = \frac{1}{3}$, the expression simplifies further:

$$\zeta = \frac{2}{3} C_L \lambda_r^2.$$

This optimal case provides a clear scaling law: the power harvesting factor grows proportionally to C_L and to λ_r^2, the square of the local tip-speed ratio.

Examples

- **Case A – outer blade element (tip):** For $\lambda_r^2 \approx 7$ and $C_L \approx 1$, we get:

$$\zeta \approx \frac{2}{3} \times 1 \times 7 \approx 4.7$$

- **Case B – half radius:** For a smaller λ_r^2 (about half of Case A's value), $\zeta \approx 8$.

At a position halfway along the blade radius, where the local tip-speed ratio is lower, the value of ζ is substantially reduced, showing how the harvesting factor diminishes quickly as one moves inwards toward the hub.

Chapter 4

Mechanics & Dynamics of Wind Turbines

4.1 Loads and Forces

Wind turbines experience a variety of loads from different sources. These include:

- **Aerodynamic loads**, which arise from lift and drag forces acting on the blades.
- **Gravity**, which produces constant weight forces on all structural components.
- **Inertial loads**, which include both gyroscopic effects from yawing and pitching motions and centrifugal forces from rotation.
- **Electromechanical loads**, such as the torque generated by the electrical generator.
- **Operational loads**, coming from actuators including brakes, the yaw system, and blade pitch mechanisms.

The loads acting on the turbine can be classified by type:

- **Steady loads**, which are static or rotational and do not fluctuate significantly over time.
- **Cyclic loads**, which occur as harmonics of the rotation frequency:
  - **1P**: loads occurring once per revolution.
  - **3P**: loads occurring three times per revolution.
  - **B.P**: the blade passing frequency, which occurs B times per revolution where B is the number of blades.
- **Resonant loads**, which are associated with vibrations of the tower and blades.
- **Transient loads**, which arise during events such as start-up, shut-down, or yaw maneuvers.
- **Stochastic loads**, which result from the random and turbulent nature of the wind.

4.2 Steady loads in normal operation

When a wind turbine operates at constant speed and power, it is subject to steady loads that do not fluctuate significantly with time. Two important steady loads are the aerodynamic thrust on the rotor and the gravitational load from the nacelle.

The aerodynamic thrust force F_T [N] can be estimated from the mechanical power P [W] produced by the turbine and the free-stream wind speed U_∞ [$\mathrm{m\,s^{-1}}$] as

$$F_T \approx \frac{2P}{3U_\infty}.$$

The gravitational force F_G [N] acting on the nacelle is given by

$$F_G = m_N g,$$

where m_N [kg] is the mass of the nacelle and g [$\mathrm{m\,s^{-2}}$] is the gravitational acceleration.

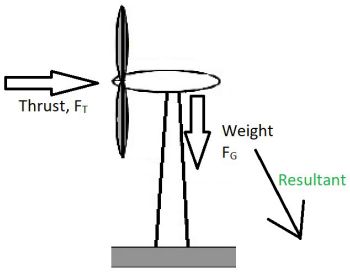

Figure 4.1: Illustration of steady loads on a wind turbine, showing aerodynamic thrust F_T acting on the rotor and gravitational force F_G from the nacelle mass.

As an example, consider a turbine producing $P = 6\,\mathrm{MW}$ at a wind speed of $U_\infty = 9\,\mathrm{m\,s^{-1}}$, with a nacelle mass of $m_N = 360\,\mathrm{t}$.

The thrust force is calculated as:

$$F_T \approx \frac{2 \times 6\,\mathrm{MW}}{3 \times 9\,\mathrm{m\,s^{-1}}} = 1\,\mathrm{MN}.$$

The gravitational force on the nacelle is:

$$F_G = 360\,\mathrm{t} \times 9.81\,\mathrm{m\,s^{-2}} = 3.6\,\mathrm{MN}.$$

4.3 Stress and strain

When a material is subjected to tension, it experiences both stress and strain. Figure 4.2 illustrates a material sample under tension.

Stress, denoted by σ [Pa], is defined as the internal force F [N] acting per unit cross-sectional area A [$\mathrm{m^2}$]:

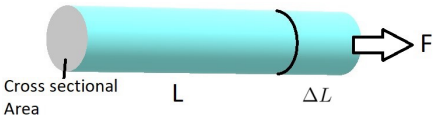

Figure 4.2: A material sample under tension, showing the applied force F and elongation ΔL.

$$\sigma = \frac{F}{A}.$$

Strain, denoted by ε [–], is the relative elongation of the material, calculated as the change in length ΔL [m] divided by the original length L [m]:

$$\varepsilon = \frac{\Delta L}{L}.$$

Figure 4.3 shows a typical stress–strain curve.

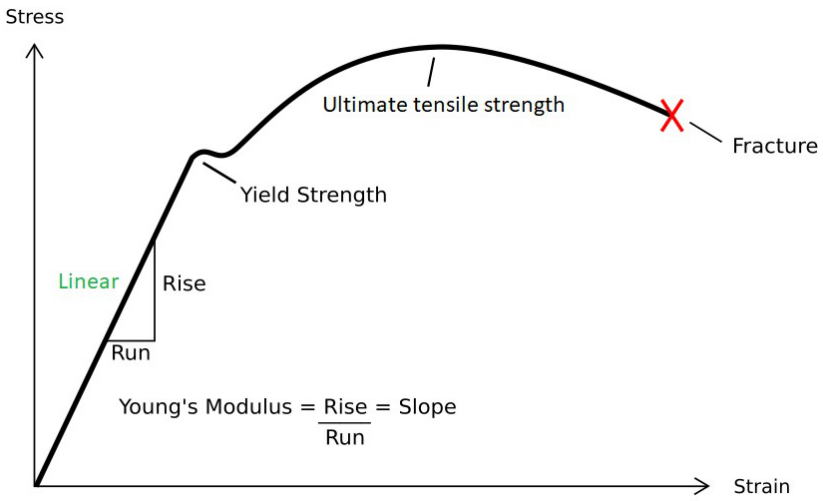

Figure 4.3: A stress–strain curve showing the elastic region, yield point, and plastic deformation region.

For example, consider a steel material with a Young's modulus $E = 200\,\text{GPa}$, a yield strength $Y = 250\,\text{MPa}$, and an ultimate tensile strength $U = 500\,\text{MPa}$.

At which strain does steel start to deform plastically/permanently? Hooke's law relates stress and strain in the elastic range:

$$\sigma_Y = E\,\varepsilon_Y,$$

where σ_Y [Pa] is the stress at the yield point and ε_Y [–] is the corresponding strain. Since at yielding $\sigma_Y = Y$, we can solve for the strain:

$$\varepsilon_Y = \frac{Y}{E}.$$

This equation shows that the yield strain is simply the yield strength divided by Young's modulus.

When does a beam start to deform? Figure 4.4 illustrates the geometry of a bent beam. The strain at the outermost fiber can be expressed in terms of curvature:

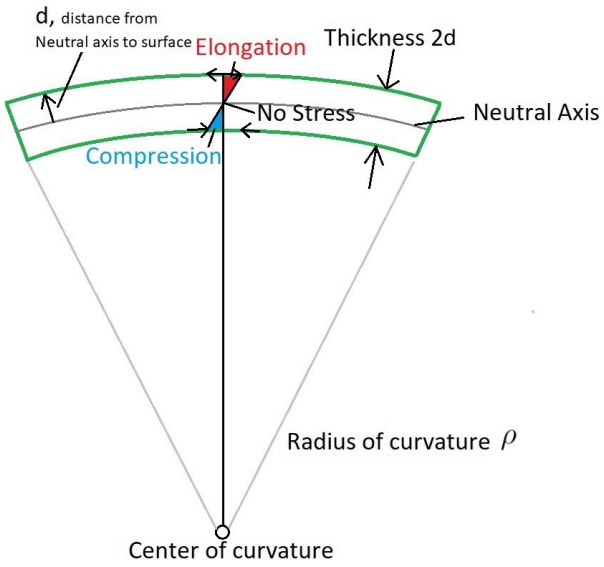

Figure 4.4: Relationship between strain ε and beam curvature, with outer fibers at a distance d from the neutral axis and radius of curvature ρ.

$$\varepsilon_Y = \frac{d}{\rho},$$

where d [m] is the distance from the neutral axis to the outermost fiber, and ρ [m] is the radius of curvature of the bent beam.

4.4 (Static) beam bending (Euler-Bernoulli theory)

Hooke's law Hooke's law relates stress, strain, and the stiffness of a material. It is written as

$$\sigma = E\,\varepsilon,$$

where σ [Pa] is the stress, E [Pa] is the Young's modulus of the material, and ε [–] is the strain (deformation).

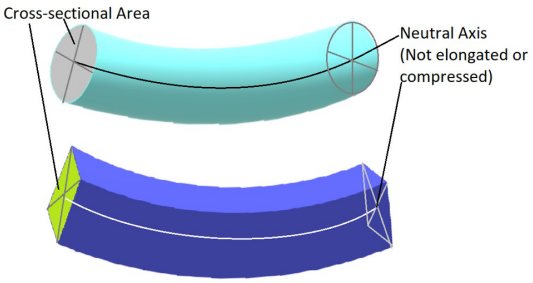

Figure 4.5: Conceptual illustration of bending beam's cross-section

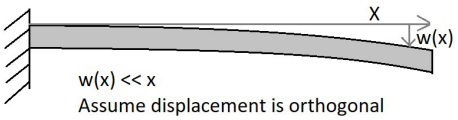

Figure 4.6: Schematic showing displacement of a bending beam

Strain In a bent beam, the strain ε [–] at a distance z [m] from the neutral axis is related to the radius of curvature ρ [m] by

$$\varepsilon = \frac{z}{\rho}.$$

Because curvature is defined as the reciprocal of the radius, we can also write

$$\frac{1}{\rho} = \frac{d^2w(x)}{dx^2},$$

where $w(x)$ [m] is the beam deflection as a function of position x [m]. Substituting this curvature relation into the strain expression gives

$$\varepsilon = z\,\frac{d^2w(x)}{dx^2}.$$

Bending moment The bending moment $M(x)$ [N m] along the beam can be calculated by integrating the stress distribution:

$$M(x) = \int_{-d}^{d} z\,\sigma(z)\,dA,$$

where d [m] is the half-depth of the beam cross section and dA [m^2] is an infinitesimal cross-sectional area.

Substituting $\sigma(z) = Ez\frac{d^2w(x)}{dx^2}$ into the integral yields:

$$M(x) = \int_{-d}^{d} z\,E\,z\left(\frac{d^2w(x)}{dx^2}\right)dA.$$

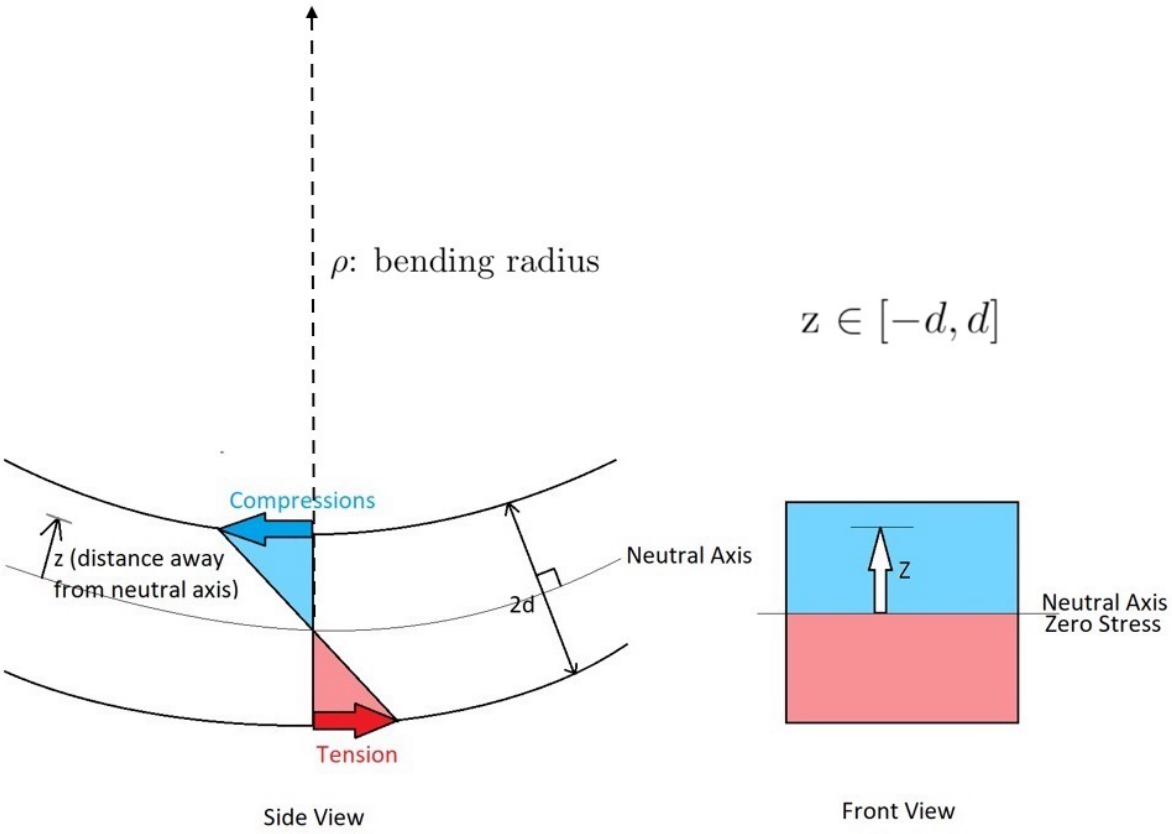

Figure 4.7: Illustration of strain variation across the cross section of a beam.

The terms E and $\frac{d^2w(x)}{dx^2}$ are constant over the cross section and can be taken outside the integral:

$$M(x) = E\,\frac{d^2w(x)}{dx^2}\int_{-d}^{d} z^2 dA.$$

The integral

$$\int_{-d}^{d} z^2 dA$$

is defined as the second moment of area I [m^4]. Thus we can write:

$$M(x) = E\,I\,\frac{d^2w(x)}{dx^2}.$$

Alternatively, using the curvature notation $\frac{1}{\rho}$, this relationship is often written as:

$$M = E\,I\,\frac{1}{\rho}.$$

Static beam equation (Euler–Bernoulli) The Euler–Bernoulli beam equation connects the applied load to beam deflection:

$$\frac{d^2}{dx^2}\left[E(x)I(x)\frac{d^2w(x)}{dx^2}\right] = q(x),$$

where $q(x)$ [$\mathrm{N\,m^{-1}}$] is the distributed load along the beam.

The related definitions are:

- The shear force $Q(x)$ [N] is the first derivative of the bending moment:

$$Q(x) = \frac{dM(x)}{dx}.$$

- The distributed load $q(x)$ [$\mathrm{N\,m^{-1}}$] is the derivative of the shear force:

$$q(x) = \frac{dQ(x)}{dx}.$$

4.4.1 Examples

Let's try this on two examples:

- a cantilevered beam with an end load, and
- a cantilevered beam with constant loading.

Cantilever beam with end load

Consider a cantilever beam with a point load applied at its free end. Figure 4.8 illustrates the setup.

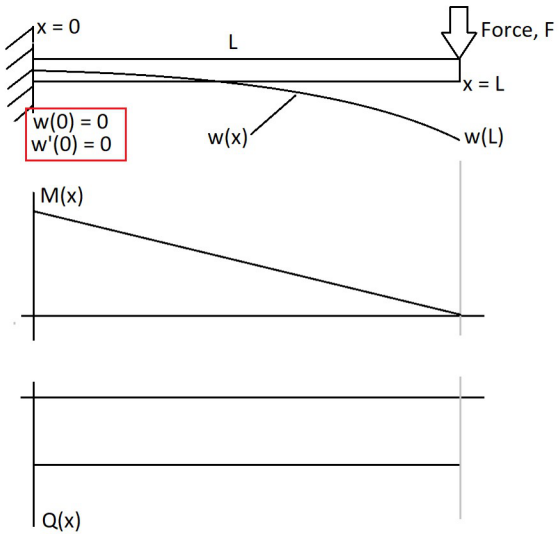

Figure 4.8: Cantilever beam with a force F applied at its free end, length L, and fixed boundary on the left side.

The bending moment $M(x)$ [N m] along the beam is given by

$$M(x) = E\,I\,\frac{d^2w(x)}{dx^2} = F(L-x),$$

where E [Pa] is the Young's modulus of the beam material, I [m^4] is the second moment of area, $w(x)$ [m] is the deflection at position x [m], F [N] is the applied force, and L [m] is the beam length.

The shear force $Q(x)$ [N] is the derivative of the bending moment:

$$Q(x) = \frac{dM(x)}{dx} = -F.$$

Because $Q(x)$ is constant, the derivative of $Q(x)$ with respect to x is zero:

$$\frac{dQ(x)}{dx} = 0.$$

This reflects the fact that there is no distributed load on the beam ($q(x) = 0$) and gravity of the beam itself is neglected.

Since E and I are constant and there is no distributed load, the Euler–Bernoulli equation simplifies to:

$$EI\,\frac{d^2w(x)}{dx^2} = F(L-x).$$

Integrating twice with respect to x yields the deflection:

$$w(x) = \frac{F}{6EI}\left(Lx^2 - \frac{x^3}{3} + c_0 + c_1 x\right),$$

where c_0 and c_1 are integration constants determined by boundary conditions. For a cantilever beam with the root clamped at $x = 0$, both deflection and slope are zero at that point, which sets $c_0 = 0$ and $c_1 = 0$.

Substituting these values simplifies the deflection to:

$$w(x) = \frac{F}{6EI}x^2\,(3L - x)\,.$$

At the free end ($x = L$), the displacement becomes:

$$w(L) = \frac{FL^3}{3EI}.$$

This final expression can be interpreted as a spring relationship:

$$\underbrace{w(L)}_{\text{displacement}} = \frac{FL^3}{3EI} = \underbrace{F}_{\text{force}} \cdot \underbrace{\frac{L^3}{3\,E\,I}}_{\text{spring constant}}$$

where the **effective spring constant** k is:

$$k = \frac{3EI}{L^3}.$$

Cantilever beam with constant loading

Now consider a cantilever beam of length L [m] with a constant distributed load q [N m^{-1}]. Figure 4.9 illustrates this loading case.

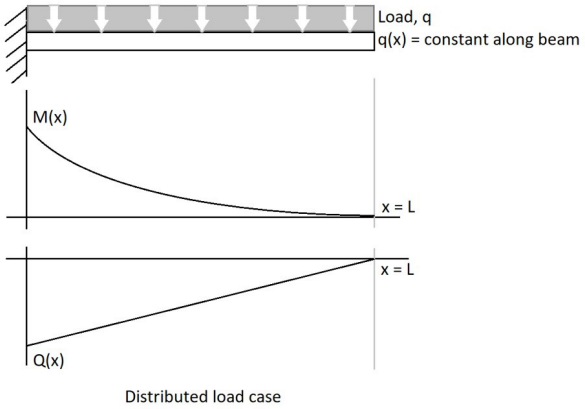

Figure 4.9: Cantilever beam with a constant distributed load q.

With constant Young's modulus E [Pa] and second moment of area I [m^4], the Euler–Bernoulli beam equation becomes:

$$q = EI\,\frac{d^4w(x)}{dx^4}.$$

Integrating four times with respect to x gives the general deflection:

$$w(x) = \frac{q}{24EI}x^4 + c_3x^3 + c_2x^2 + c_1x + c_0,$$

where c_0, c_1, c_2, and c_3 are integration constants to be determined by boundary conditions.

Let's step-quickly to the side, and list the derivatives of $w(x)$:

$$\frac{\mathrm{d}^0w}{\mathrm{d}x^0} = w(x) \tag{4.1}$$

$$\frac{\mathrm{d}^1w}{\mathrm{d}x^1} = \frac{q\left(3c_3x^2 + 2c_2x + c_1 + \frac{x^3}{6}\right)}{EI} \tag{4.2}$$

$$\frac{\mathrm{d}^2w}{\mathrm{d}x^2} = \frac{q\left(x\left(12c_3 + x\right) + 4c_2\right)}{2EI} \tag{4.3}$$

$$\frac{\mathrm{d}^3w}{\mathrm{d}x^3} = \frac{q\left(6c_3 + x\right)}{EI} \tag{4.4}$$

Boundary conditions If you have a cantilevered beam clamped at $x = 0$, then the clamped side should be undeflected (i.e., 'clamped'), and it should not be moving:

$$w(0) = 0 \quad \Rightarrow \quad c_0 = 0,$$

$$\frac{dw}{dx}(0) = 0 \quad \Rightarrow \quad c_1 = 0.$$

The bending moment $M(x)$ [N m] is related to the curvature:

$$M(x) = EI\,\frac{d^2w(x)}{dx^2} = \frac{1}{2}q\left(x\left(12c_3 + x\right) + 4c_2\right).$$

And the shear force $Q(x)$ [N] is the derivative of the moment:

$$Q(x) = \frac{dM(x)}{dx} = q\left(6c_3 + x\right).$$

At the free end ($x = L$), the moment and shear force must vanish, because there's no force acting past that end:

$$M(L) = 0 \quad \Rightarrow \quad q\left(6c_3L + 2c_2 + \frac{L^2}{2}\right) = 0 \tag{4.5}$$

$$Q(L) = 0 \quad \Rightarrow \quad q\left(6c_3 + L\right) = 0 \tag{4.6}$$

Determining constants This means, we have four independent equations with four variables $[c_0, c_1, c_2, c_3]$:

$$\frac{c_0 q}{EI} = 0 \tag{4.7}$$

$$\frac{c_1 q}{EI} = 0 \tag{4.8}$$

$$q\left(6c_3L + 2c_2 + \frac{L^2}{2}\right) = 0 \tag{4.9}$$

$$q\left(6c_3 + L\right) = 0. \tag{4.10}$$

Since E and I are positive real values, they aren't zero! So, we can solve (4.7), (4.8), (4.10) right away, and then plug the solved c_3 into (4.9):

$$c_0 = 0, \quad c_1 = 0, \quad c_3 = -\frac{L}{6}, \quad \Rightarrow \quad q\left(2c_2 - \frac{L^2}{2}\right) = 0 \tag{4.11}$$

$$\hookrightarrow c_2 = \frac{L^2}{4}. \tag{4.12}$$

We can plug these constants back into the forms we defined for the deflection, the moment, and the shear force:

$$w(x) = \frac{q}{24EI}x^4 + c_3x^3 + c_2x^2 + c_1x + c_0 = \frac{qx^2\left(6L^2 - 4Lx + x^2\right)}{24EI} \tag{4.13}$$

$$M(x) = EI\,\frac{d^2w(x)}{dx^2} = EI\left(\frac{q\left(x\left(12c_3 + x\right) + 4c_2\right)}{2EI}\right) = q\left(\frac{L^2}{2} - Lx + \frac{x^2}{2}\right) \tag{4.14}$$

$$= \frac{1}{2}q(L-x)^2$$

$$Q(x) = \frac{dM(x)}{dx} = q\left(6c_3 + x\right) = q(x - L) \tag{4.15}$$

These expressions describe the internal forces and deflections in a cantilever beam under a constant distributed load, and are shown (in nondimensionalized form) in Figure 4.10.

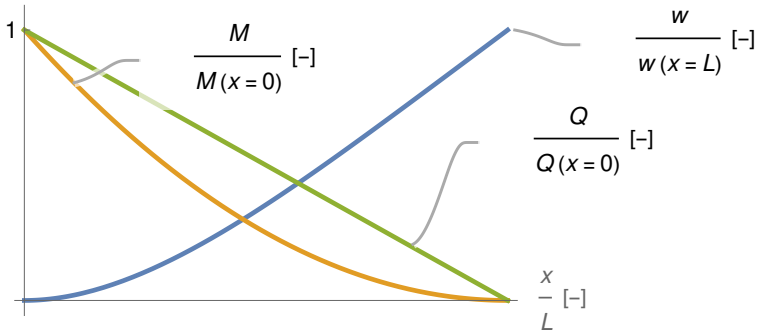

Figure 4.10: The deflection, moment, and shear-force distribution for the cantilever beam with a constant distributed load q.

4.4.2 Moment at the blade root

The maximum bending moment at the blade root can be derived using the Euler–Bernoulli beam equation:

$$\frac{d^2}{dx^2}\left[E(x)I(x)\frac{d^2w(x)}{dx^2}\right] = q(x), \tag{4.16}$$

where $E(x)$ [Pa] is the Young's modulus of the blade material, $I(x)$ [m^4] is the second moment of area, $w(x)$ [m] is the blade deflection as a function of the spanwise coordinate x [m], and $q(x)$ [$\mathrm{N\,m^{-1}}$] is the distributed load.

In this context: - The bending moment $M(x)$ [N m] is defined by

$$M(x) = E(x)I(x)\frac{d^2w(x)}{dx^2}.$$

- The shear force $Q(x)$ [N] is the derivative of the moment:

$$Q(x) = \frac{dM(x)}{dx}.$$

Maximum strain The maximum strain in the blade, $\varepsilon_{\max}$ [–], is related to the blade curvature:

$$\varepsilon_{\max} = \frac{d}{\rho},$$

where d [m] is the distance from the neutral axis to the outermost fiber and ρ [m] is the local radius of curvature.

Using the curvature form of the Euler–Bernoulli relation, this strain can be written in terms of the bending moment:

$$\varepsilon_{\max} = \frac{d(0)M(0)}{I(0)E(0)}, \tag{4.17}$$

where $M(0)$ [N m] is the bending moment at the blade root, $I(0)$ [m^4] is the second moment of area at the root, and $E(0)$ [Pa] is the Young's modulus at the root.

Maximum bending moment Rearranging Equation (4.17) to solve for the maximum moment that the blade can support gives:

$$M_{\max} = \varepsilon_{\max}\frac{IY}{d}, \tag{4.18}$$

where Y [Pa] is the yield strength of the blade material.

Equation (4.18) shows that the maximum bending moment scales with the material's yield strain and stiffness, and with the geometry of the blade root cross-section (via the second moment of area I and the distance to the outer fiber d).

4.4.3 Loads at blade root (in flapwise direction)

For a blade in an ideal design, the distributed load $q(r)$ [N m^{-1}] can be obtained from the thrust of the corresponding annulus (see Figure 4.11).

The differential force dF [N] on the annulus is given by:

$$dF = 4a(1-a)\,\frac{1}{2}\rho U_\infty^2\, 2\pi r\, dr, \tag{4.19a}$$

$$= C_T(a)\,\frac{1}{2}\rho U_\infty^2\, 2\pi r\, dr, \tag{4.19b}$$

where a [–] is the axial induction factor, ρ [kg m^{-3}] is the air density, U_∞ [m s^{-1}] is the free-stream wind speed, r [m] is the local radius, dr [m] is the annulus width, and $C_T(a)$ [–] is the thrust coefficient.

Since this load is shared between B blades, the distributed load per blade is:

$$q(r) = \frac{C_T(a)}{B}\,\frac{1}{2}\rho U_\infty^2\, 2\pi r. \tag{4.20}$$

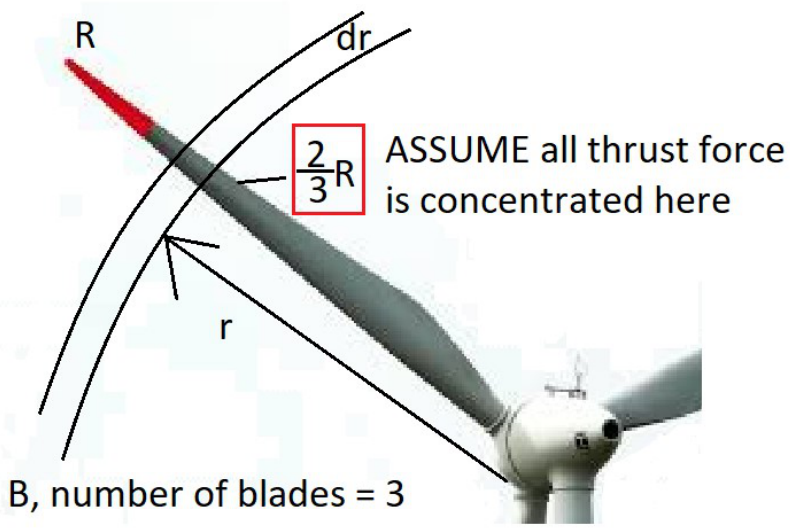

Figure 4.11: Force distribution on an annular section of the rotor blade.

Bending moment at the blade root The bending moment $M(0)$ [N m] at the blade root is computed by integrating $q(r)r$ from $r = 0$ to the rotor radius R:

$$M(0) = \int_0^R q(r)\, r\, dr, \tag{4.21a}$$

$$= \frac{1}{B} C_T(a)\, \frac{1}{2}\rho U_\infty^2\, 2\pi \int_0^R r^2 dr, \tag{4.21b}$$

$$= \frac{1}{B} C_T(a)\, \frac{1}{2}\rho U_\infty^2\, \pi R^3\, \frac{2}{3}, \tag{4.21c}$$

$$= \frac{1}{B}\, \frac{2}{3} R\, C_T(a)\, \frac{1}{2}\rho U_\infty^2\, (\pi R^2). \tag{4.21d}$$

The term (πR^2) represents the swept area of the rotor disk, and the force acting on it is the total thrust F_T [N].

$$\underbrace{F_T}_{\text{total force on actuator disk}} = C_T(a)\frac{1}{2}\rho U_\infty^2(\pi R^2).$$

Thus, the bending moment at the blade root can be interpreted simply as:

$$M(0) = \frac{2}{3} R\, \frac{F_T}{B}.$$

Approximate thrust The thrust force F_T can also be approximated from the mechanical power P [W] and the wind speed U_∞:

$$F_T \approx \frac{P}{(1-a)U_\infty}. \tag{4.22}$$

Example For a turbine producing 6 MW at a wind speed $U_\infty = 9\,\mathrm{m\,s^{-1}}$ with rotor radius $R = 75\,\mathrm{m}$ and $F_T \approx 1\,\mathrm{MN}$, the blade root bending moment is:

$$M(0) = \frac{2}{3} R \frac{F_T}{B} \approx 50\,\mathrm{m} \times \frac{1\,\mathrm{MN}}{3} \approx 16\,\mathrm{MN\,m}.$$

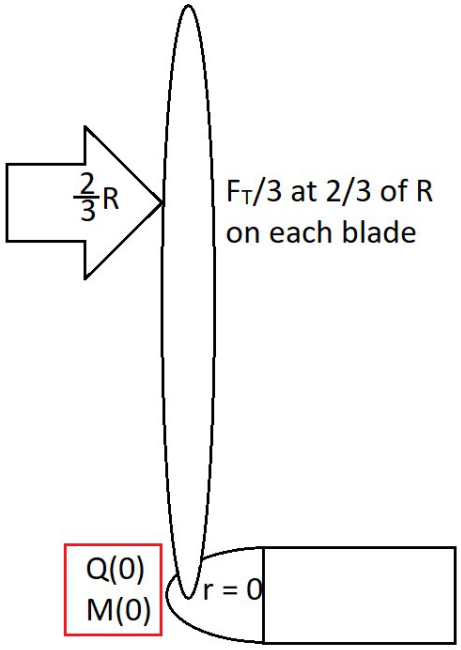

Figure 4.12: Illustration of total thrust F_T and blade root bending moment $M(0)$.

Maximum bending stress at the blade root Consider the annular cross-section of the blade root shown in Figure 4.13, with outer radius r_2 [m] and wall thickness b [m]. The second moment of area I [m^4] is:

$$I = \frac{\pi}{4} r_2^4 - \frac{\pi}{4} r_1^4 \approx \pi r_2^3 b,$$

assuming the inner radius $r_1 = r_2 - b$ and that $b \ll r_2$.

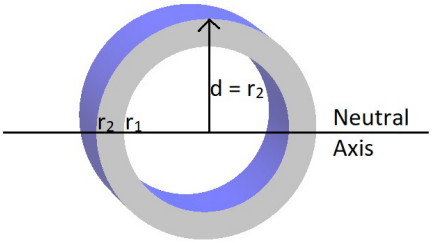

Figure 4.13: Cross-section of the blade root, showing outer radius r_2 and shell thickness b.

The maximum bending stress $\sigma_{\max}$ [Pa] is given by:

$$\sigma_{\max} = \frac{r_2 M(0)}{I} = \frac{M(0)}{\pi r_2^2 b}.$$

Example thickness calculation If $r_2 = 1\,\mathrm{m}$, $\sigma_{\max} = 250\,\mathrm{MPa}$, and $M(0) = 5\,\mathrm{MN\,m}$, the required shell thickness b is:

$$b = \frac{M(0)}{\pi r_2^2 \sigma_{\max}} = \frac{5\,\mathrm{MN\,m}}{\pi(1)^2 \times 250\,\mathrm{MPa}} \approx 0.02\,\mathrm{m} = 2\,\mathrm{cm}.$$

4.5 Oscillations & eigenmodes

4.5.1 Intro: spring–mass–damper system

The dynamics of a wind turbine blade, tower, or drivetrain component can often be approximated by the classical spring–mass–damper model. The governing differential equation is:

$$m\ddot{x} + \beta\dot{x} + kx = F(t), \tag{4.23}$$

where x [m] is the displacement, m [kg] is the mass, $F(t)$ [N] is the external force, k [$\mathrm{N\,m^{-1}}$] is the spring constant, and β [$\mathrm{N\,s\,m^{-1}}$] is the viscous (linear) damping coefficient.

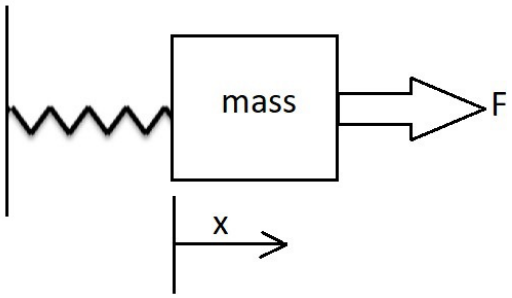

Figure 4.14: The spring–mass–damper model: a mass m connected to a spring with stiffness k and a damper with damping coefficient β, subject to external force $F(t)$.

Harmonic forcing Assume a harmonic external force of the form:

$$F(t) = F_0 e^{j\omega t},$$

where F_0 [N] is the force amplitude and ω [$\mathrm{rad\,s^{-1}}$] is the forcing frequency. In design, we consider the real part of the solution.

We assume a solution of the form:

$$x(t) = x_0 e^{j\omega t}, \quad x_0 \in \mathbb{C}, \tag{4.24}$$

where x_0 [m] is a complex amplitude.

Differentiating this assumed solution gives:

$$\dot{x}(t) = (j\omega) x_0 e^{j\omega t}, \tag{4.25}$$
$$\ddot{x}(t) = -\omega^2 x_0 e^{j\omega t}. \tag{4.26}$$

Substituting Equations (4.24)–(4.26) into Equation (4.23):

$$-m\omega^2 x_0 e^{j\omega t} + \beta j\omega x_0 e^{j\omega t} + k x_0 e^{j\omega t} = F_0 e^{j\omega t}. \tag{4.27}$$

Canceling $e^{j\omega t}$ throughout, we get:

$$x_0 \underbrace{(k - m\omega^2)}_{\text{real}} + x_0 \underbrace{(j\beta\omega)}_{\text{imaginary}} = F_0. \tag{4.28}$$

The magnitude of x_0 is given by:

$$|x_0| = \frac{F_0}{\sqrt{(k - m\omega^2)^2 + (\beta\omega)^2}}, \tag{4.29}$$

where the denominator combines the real stiffness term $(k - m\omega^2)$ and the imaginary damping term $(\beta\omega)$.

Natural frequency The maximum response $|x_0|$ occurs approximately at the natural (resonant) eigenfrequency ω_{NR}:

$$k - m\omega_{NR}^2 = 0 \quad \Leftrightarrow \quad \omega_{NR} = \sqrt{\frac{k}{m}}. \tag{4.30}$$

How much can F_0 be amplified? The spring force is:

$$F_{0,\text{spring}} = kx.$$

At steady state, its amplitude is:

$$|F_{0,\text{spring}}| = k|x_0| = \frac{F_0}{\sqrt{\left(1 - \left(\frac{\omega}{\omega_{NR}}\right)^2\right)^2 + \left(\frac{\beta\omega}{k}\right)^2}}, \tag{4.31}$$

which shows how the spring force depends on frequency.

At resonance ($\omega = \omega_{NR}$), the expression simplifies to:

$$\frac{|F_{0,\text{spring}}|}{F_0} = \frac{k}{\beta\,\omega_{NR}}, \tag{4.32}$$

which indicates that the amplification factor is inversely proportional to the damping coefficient.

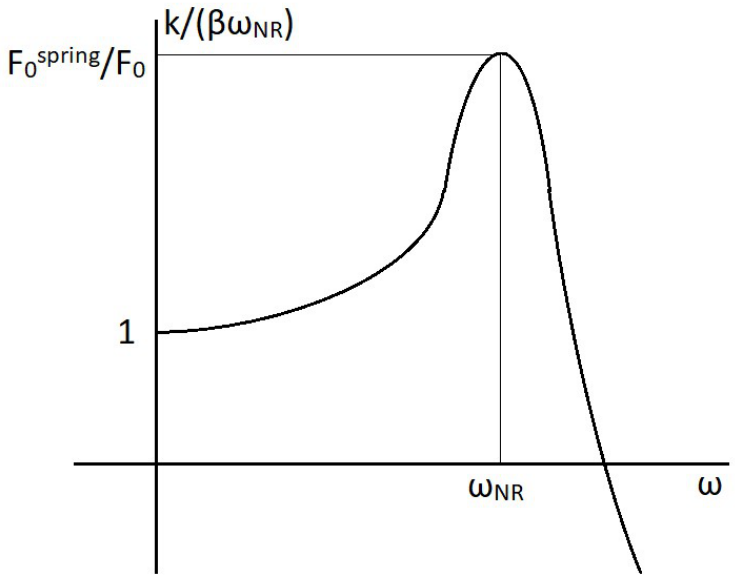

Figure 4.15: Bode diagram showing amplification of the spring force relative to applied force F_0 as a function of frequency. Amplification factors can reach 5–10 if damping β is low, so resonance should typically be avoided.

At very low forcing frequencies, the spring force equals the applied force, meaning static analysis is sufficient (as discussed in Section 4.3).

4.5.2 Eigenmodes

For spring–mass–damper systems with more than one degree of freedom, the displacement is described by a vector $\mathbf{w}(t) \in \mathbb{R}^n$. The equation of motion becomes:

$$\mathbf{M}\ddot{\mathbf{w}} + \mathbf{D}\dot{\mathbf{w}} + \mathbf{K}\mathbf{w} = \mathbf{F}(t), \tag{4.33}$$

where $\mathbf{M}$ [kg] is the mass matrix ($n \times n$), $\mathbf{D}$ [$\mathrm{N\,s\,m^{-1}}$] is the damping matrix, $\mathbf{K}$ [$\mathrm{N\,m^{-1}}$] is the stiffness matrix ($n \times n$), and $\mathbf{F}(t)$ [N] is the external force vector.

If damping is neglected ($\mathbf{D} = 0$), the natural resonance modes must satisfy the condition that the solution takes the form:

$$\mathbf{w}(t) = \bar{\mathbf{w}} e^{j\omega t}, \tag{4.34}$$

where $\bar{\mathbf{w}} \in \mathbb{R}^n$ is the mode shape vector and ω [$\mathrm{rad\,s^{-1}}$] is the angular frequency.

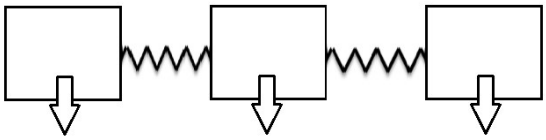

Figure 4.16: Multi–degree of freedom spring–mass–damper system. The displacement is described by vector $\mathbf{w}(t)$.

Substituting Equation (4.34) into the equation of motion (4.33) with $\mathbf{D} = 0$ gives:

$$\mathbf{M}\ddot{\mathbf{w}} + \mathbf{K}\mathbf{w} = 0. \tag{4.35}$$

This leads to the algebraic condition:

$$-\omega^2\mathbf{M}\bar{\mathbf{w}} + \mathbf{K}\bar{\mathbf{w}} = 0 \quad \Leftrightarrow \quad (\mathbf{M}^{-1}\mathbf{K} - \omega^2\mathbf{I})\bar{\mathbf{w}} = 0. \tag{4.36}$$

This is an eigenvalue problem for the matrix $\mathbf{M}^{-1}\mathbf{K} \in \mathbb{R}^{n\times n}$. There are n eigenvalues, each with an associated eigenvector $\bar{\mathbf{w}}$ (the *eigenmode*). Because both $\mathbf{M}$ and $\mathbf{K}$ are positive definite, the eigenvalues of $\mathbf{M}^{-1}\mathbf{K}$ are real and positive.

In practice, we are often most interested in the eigenmode with the lowest eigenfrequency, because this mode typically dominates the system's dynamic response.

4.5.3 Rayleigh's method

Assume we have a good guess of an eigenmode vector $\bar{\mathbf{w}} \in \mathbb{R}^n$. To find the corresponding eigenfrequency ω^2 [$\mathrm{rad}^2\,\mathrm{s}^{-2}$], we start with the eigenvalue equation:

$$\mathbf{K}\bar{\mathbf{w}} = \omega^2\mathbf{M}\bar{\mathbf{w}}, \tag{4.37}$$

where $\mathbf{K}$ [$\mathrm{N\,m}^{-1}$] is the stiffness matrix and $\mathbf{M}$ [kg] is the mass matrix.

Equation (4.37) is overdetermined if $\bar{\mathbf{w}}$ is fixed. To proceed, we multiply Equation (4.37) on the left by $\frac{1}{2}\bar{\mathbf{w}}^T$:

$$\underbrace{\frac{1}{2}\bar{\mathbf{w}}^T\mathbf{K}\bar{\mathbf{w}}}_{\text{elastic/potential energy at max. displacement}} = \underbrace{\omega^2\frac{1}{2}\bar{\mathbf{w}}^T\mathbf{M}\bar{\mathbf{w}}}_{\text{kinetic energy at max. speed}}, \tag{4.38}$$

Notice, this becomes an expression of energy conservation, one that we can rearrange to give us the natural frequency ω:

$$\omega = \sqrt{\frac{\bar{\mathbf{w}}^T\mathbf{K}\bar{\mathbf{w}}}{\bar{\mathbf{w}}^T\mathbf{M}\bar{\mathbf{w}}}} := f(\bar{\mathbf{w}}). \tag{4.39}$$

If the guess of $\bar{\mathbf{w}}$ is good, this method can give a surprisingly accurate estimation of ω. (To check, one can insert ω and $\bar{\mathbf{w}}$ into Equation (4.37).)

What is the error of Rayleigh's method? Assume ω_0 [rad s^{-1}] and $\mathbf{w}_0 \in \mathbb{R}^n$ are the true eigenpair, i.e., they satisfy:

$$\mathbf{K}\mathbf{w}_0 = \omega_0^2 \mathbf{M}\mathbf{w}_0. \tag{4.40}$$

Let our guess be $\bar{\mathbf{w}} = \mathbf{w}_0 + \Delta\mathbf{w}$, where $\Delta\mathbf{w}$ is the error in the guess. Substituting this into the Rayleigh quotient:

$$\underbrace{f(\bar{\mathbf{w}})}_{:=\omega^2} = \underbrace{f(\mathbf{w}_0)}_{=\omega_0^2} + \nabla f(\mathbf{w}_0)^T \Delta\mathbf{w} + \mathcal{O}(\|\Delta\mathbf{w}\|^2), \tag{4.41}$$

where the gradient is:

$$\nabla f(\mathbf{w}_0) = \frac{\left(\frac{1}{2}\mathbf{w}_0^T \mathbf{M}\mathbf{w}_0\right)\mathbf{K}\mathbf{w}_0 - \left(\frac{1}{2}\mathbf{w}_0^T \mathbf{K}\mathbf{w}_0\right)\mathbf{M}\mathbf{w}_0}{\left(\frac{1}{2}\mathbf{w}_0^T \mathbf{M}\mathbf{w}_0\right)^2}, \tag{4.42a}$$

$$= \frac{\mathbf{K}\mathbf{w}_0 - \omega_0^2 \mathbf{M}\mathbf{w}_0}{\frac{1}{2}\mathbf{w}_0^T \mathbf{M}\mathbf{w}_0}. \tag{4.42b}$$

Since $\mathbf{w}_0$ satisfies Equation (4.40), the numerator in (4.42b) vanishes, and we see that the error in Rayleigh's method is second-order:

$$\omega^2 = \omega_0^2 + \mathcal{O}(\|\Delta\mathbf{w}\|^2). \tag{4.43}$$

We're going to try out Rayleigh's method on some examples -

- a simple pendulum, and
- a two-mass system

- before moving on to wind energy system components in Sections 4.5.4 and 4.5.5

A simple pendulum

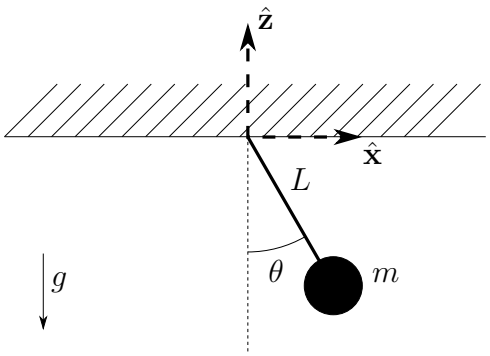

Figure 4.17: A very simple test problem to see how Rayleigh's method finds natural frequencies, imagines a simple pendulum.

We already know that the natural frequency of a simple pendulum - a mass m [kg] hanging from the end of a massless, frictionless, rigid string-or-rod of length L [m], under the acceleration of gravity g [$\mathrm{m\,s^{-2}}$] - will be $\omega = \sqrt{g/L}$. So, now let's use Rayleigh's method to get the same result[1].

The harmonic displacement here, is the angle θ [rad] between the pendulum and the vertical-line-of-symmetry:

$$\theta(t) = \theta_{\max} \sin(\omega t), \tag{4.44}$$

where we're pretending not to know the angular speed and natural frequency ω [$\mathrm{rad\,s^{-1}}$] so that we can try to find it again.

Then, the amplitude $\theta_{\max}$ is the literally the maximum displacement of the pendulum: $\theta_{U,\max} = \theta_{\max}$. This gives the potential energy of the system as

$$U(t) = mgL(1 - \cos(\theta)) = mgL\left(\frac{\theta^2}{2} - \frac{\theta^4}{24} + \frac{\theta^6}{720} + O(\theta^8)\right), \tag{4.45}$$

using a series expansion.

Now, assuming θ is small enough that the contribution of it's higher-order power terms doesn't overwhelm the expansion ($\theta^4 \ll 12\theta^2$), we can find the potential energy at maximum displacement $U_{\max}$ [J] as:

$$U_{\max} \approx mgL\frac{\theta_{\max}^2}{2}. \tag{4.46}$$

The maximum kinetic energy $T_{\max}$ [J] occurs at the bottom of the swing when $\cos\theta_{T,\max} = \cos\theta(\omega t_{T,\max}) = 1$. Since the kinetic energy depends on the angular speed of the pendulum ($\dot{\theta}$), we'll differentiate first:

$$\begin{aligned} \dot{\theta}(t) = \theta_{\max}\omega\cos(\omega t), \quad &\Rightarrow \quad T(t) = \frac{1}{2}m(L\theta_{\max}\omega\cos(\omega t))^2, \\ &\Rightarrow \quad T_{\max} = \frac{1}{2}m(L\theta_{\max})^2\omega^2 \end{aligned} \tag{4.47}$$

So, when we set the maximum kinetic energy equal to the maximum potential energy, we get:

$$T_{\max} = U_{\max} \quad \Rightarrow \quad \frac{1}{2}m(L\theta_{\max})^2\omega^2 = mgL\frac{\theta_{\max}^2}{2}. \tag{4.48}$$

When we cancel terms, we find a natural frequency that matches our expectations.

$$L\omega^2 = g \quad \Rightarrow \quad \omega = \sqrt{\frac{g}{L}} \tag{4.49}$$

[1] this follows the example given in Irvine, T. "Rayleigh's Method", Revision D. `https://citeseerx.ist.psu.edu/document?repid=rep1&type=pdf&doi=9ce169da44f898d8688599a4a1c946e0f59b1b74`

Two-mass system

Now, let's take a slightly more complicated example. Consider a simple system with two masses m_1 [kg] and m_2 [kg], and two springs with stiffness k_1 [$\mathrm{N\,m^{-1}}$] and k_2 [$\mathrm{N\,m^{-1}}$]. The equations of motion are:

$$m_2\ddot{x}_2 + k_2(x_2 - x_1) = 0,$$

$$m_1\ddot{x}_1 + k_1x_1 - k_2(x_2 - x_1) = 0,$$

where x_1 [m] and x_2 [m] are displacements.

Define the displacement vector:

$$\mathbf{w} = \begin{bmatrix} x_1 \\ x_2 \end{bmatrix} \in \mathbb{R}^2.$$

The system can be written in matrix form:

$$\underbrace{\begin{bmatrix} m_1 & 0 \\ 0 & m_2 \end{bmatrix}}_{\mathbf{M} \in \mathbb{R}^{2\times 2}} \ddot{\mathbf{w}} + \underbrace{\begin{bmatrix} (k_1 + k_2) & -k_2 \\ -k_2 & k_2 \end{bmatrix}}_{\mathbf{K} \in \mathbb{R}^{2\times 2}} \mathbf{w} = 0. \tag{4.50}$$

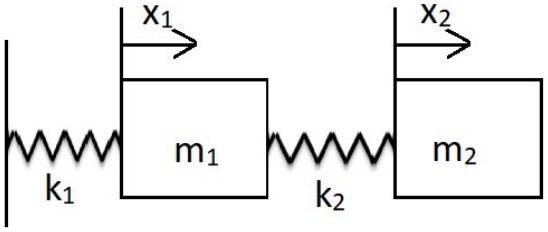

Figure 4.18: Two-mass, two-spring system for Rayleigh's method Example 1.

Now, let's assume $m_2 \gg m_1$ and $k_1 \approx k_2$. An approximate eigenvector guess is:

$$\bar{\mathbf{w}} = \begin{bmatrix} 1 \\ 2 \end{bmatrix}, \qquad \mathbf{w}(t) = \begin{bmatrix} e^{j\omega t} \\ 2e^{j\omega t} \end{bmatrix}.$$

The kinetic energy is:

$$E_{\text{kin}} = \frac{1}{2}\bar{\mathbf{w}}^T\mathbf{M}\bar{\mathbf{w}}\,\omega^2 A_0^2 = \frac{1}{2}(m_1 + 4m_2)\omega^2 A_0^2, \tag{4.51}$$

and the potential energy is:

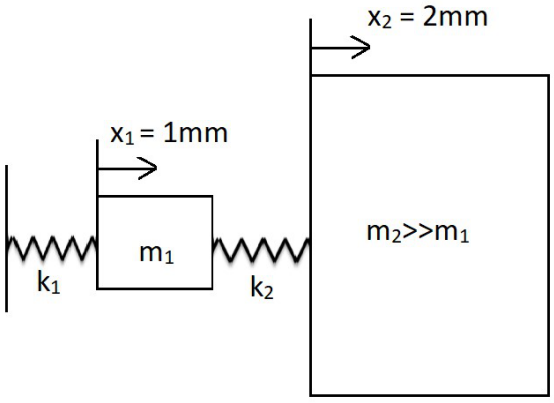

Figure 4.19: Approximate eigenvector for Example 2, showing relative displacements of the two masses.

$$E_{\text{pot}} = \frac{1}{2}\bar{\mathbf{w}}^T\mathbf{K}\bar{\mathbf{w}}A_0^2, \tag{4.52a}$$

$$= \frac{1}{2}A_0^2\begin{bmatrix}1 & 2\end{bmatrix}\begin{bmatrix}(k_1+k_2) & -k_2\\ -k_2 & k_2\end{bmatrix}\begin{bmatrix}1\\2\end{bmatrix}, \tag{4.52b}$$

$$= \frac{1}{2}A_0^2(k_1 - k_2 + 2k_2), \tag{4.52c}$$

$$= \frac{1}{2}A_0^2(k_1 + k_2). \tag{4.52d}$$

From Rayleigh's quotient, the squared natural frequency is:

$$\omega^2 = \frac{k_1+k_2}{m_1+4m_2} \approx \frac{k_1+k_2}{4}\cdot\frac{1}{m_2} \approx \frac{k_1}{2}\cdot\frac{1}{m_2}. \tag{4.53}$$

4.5.4 Dynamic beam equation

Of course, if we want to use Rayleigh's method for the long beamlike components of the wind turbine, we'll need some way to estimate the "potential energy at maximum displacement" and "kinetic energy at maximum speed" terms.

For this purpose, we look at the equation that Euler–Bernoulli and Lagrange derived for a beam, known as the **Dynamic Beam Equation**. Unlike the static case, this formulation includes time dependence, which is why it is referred to as the "dynamic" beam equation:

$$\frac{\partial^2}{\partial x^2}\left[E(x)I(x)\frac{\partial^2 w}{\partial x^2}\right] = q(x,t) - \mu(x)\frac{\partial^2 w}{\partial t^2}, \tag{4.54}$$

where: - $\mu(x)$ [$\mathrm{kg\,m^{-1}}$] is the mass density per unit length, - $q(x,t)$ [$\mathrm{N\,m^{-1}}$] is the distributed load along the beam, and - $w(x,t)$ [m] is the time-varying deflection of the beam (assuming no damping).

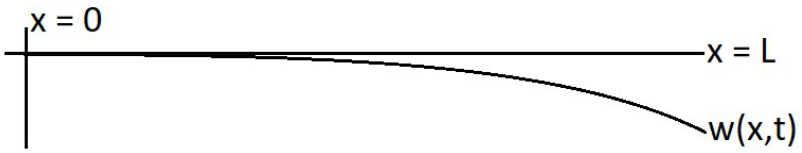

Figure 4.20: The dynamic beam equation describes a beam with spatially variable stiffness $E(x)I(x)$, mass density $\mu(x)$, and a time-varying deflection $w(x,t)$.

Note that Equation (4.54) is a **linear partial differential equation**. After spatial discretization, it becomes:

$$\mathbf{Kw} = -\mathbf{M}\ddot{\mathbf{w}},$$

where $\mathbf{K}$ is the stiffness matrix and $\mathbf{M}$ is the mass matrix.

The result of the dynamic beam equation, is that we can find the energies of beam-like components (the tower and blades) that we will next apply into Rayleigh's method. That is, the kinetic energy of the beam is given by:

$$E_{\text{kin}} = \frac{1}{2}\int_0^L \mu(x)\left(\frac{\partial w}{\partial t}\right)^2 dx, \tag{4.55}$$

and the elastic (strain) energy is:

$$E_{\text{ela}} = \frac{1}{2}\int_0^L E(x)I(x)\left(\frac{\partial^2 w}{\partial x^2}\right)^2 dx, \tag{4.56}$$

where L [m] is the beam length, $E(x)$ [Pa] is Young's modulus, and $I(x)$ [m^4] is the second moment of area.

4.5.5 Rayleigh's method applied to a wind turbine tower

Let's make a more wind-energy specific example of Rayleigh's method, than we'd previously given. Specifically, let's consider the tall slender beam topped with a point-mass that we call the "tower".

Both the tower and the nacelle have significant mass. For example, the MHI–Vestas V164 (9.5 MW) has a heavy nacelle mounted on top of a tall flexible tower (see Figure 4.21).

Because of the large mass imbalance, the eigenmodes of the tower must be computed for a very unequal mass distribution. Remember that we looked at a demonstration example for this sort of situation in the "two-mass" example, and - there - we had to guess at the eigenmodes. Here, we happen to be able to make decent guesses about what the main eigenmodes look like, because the tower is so beam-like and beams have very typical ways of deforming. The lowest two eigenmodes look approximately as shown in Figure 4.22.

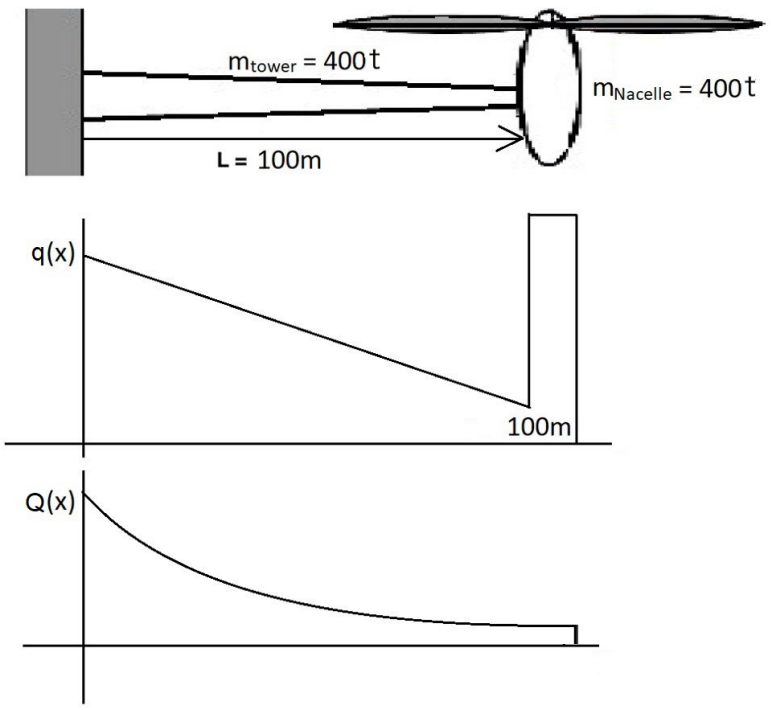

Figure 4.21: Example of a heavy nacelle on a tall flexible tower: MHI–Vestas V164 (9.5 MW).

Determine the kinetic and potential energies The kinetic energy of the tower is:

$$E_{\text{kin}} = \frac{1}{2}\int_0^L \mu(x)\left(\frac{\partial w(x,t)}{\partial t}\right)^2 dx, \tag{4.57}$$

and the elastic (potential) energy is:

(a) Lowest eigenmode of the tower.

(b) Second-lowest eigenmode of the tower.

Figure 4.22: Eigenmodes of tower deformation. Notice that these shapes look like increasing fractions of a sinusoid.

$$E_{\text{ela}} = \frac{1}{2}\int_0^L E(x)I(x)\left(\frac{\partial^2 w(x,t)}{\partial x^2}\right)^2 dx, \tag{4.58}$$

where: - $\mu(x)$ [kg m^{-1}] is the mass per unit length of the tower, - $E(x)$ [Pa] is Young's modulus, - $I(x)$ [m^4] is the second moment of area, - and $w(x,t)$ [m] is the time-dependent displacement.

After assuming a particular displacement (eigen)mode Assume for this example that the displacement is approximated by:

$$w(x,t) = \bar{w}(x)e^{j\omega t}, \qquad \bar{w}(x) = A_0\frac{x^2}{L^2},$$

for a rough approximation of the lowest eigenmode. Assume constant mass density $\mu(x)$, Young's modulus $E(x)$, and moment of inertia $I(x)$ along the tower.

Applying the energy equations derived with dynamic beam theory, we write the kinetic energy as:

$$E_{\text{kin}} = \omega^2\left(\frac{1}{2}\int_0^L \frac{m_{\text{tower}}}{L}A_0^2\frac{x^4}{L^4}dx + \frac{1}{2}m_{\text{nacelle}}A_0^2\right), \tag{4.59a}$$

$$= \omega^2 A_0^2\left(\frac{m_{\text{tower}}}{2L^5}\int_0^L x^4 dx + \frac{m_{\text{nacelle}}}{2}\right), \tag{4.59b}$$

$$= \omega^2 A_0^2\left(\frac{m_{\text{tower}}}{5} + m_{\text{nacelle}}\right), \tag{4.59c}$$

where m_{tower} [kg] is the total mass of the tower and m_{nacelle} [kg] is the mass of the nacelle.

The elastic energy is:

$$E_{\text{ela}} = \frac{1}{2}\int_0^L EI\left(\frac{\partial^2}{\partial x^2}\left(A_0\frac{x^2}{L^2}\right)\right)^2 dx, \tag{4.60a}$$

$$= \frac{1}{2}\int_0^L EI\left(\frac{2A_0}{L^2}\right)^2 dx, \tag{4.60b}$$

$$= \frac{1}{2}A_0^2\frac{4EI}{L^4}L, \tag{4.60c}$$

where E [Pa] and I [m^4] are assumed constant.

Eigenfrequency estimate Now, equating $E_{\text{kin}} = E_{\text{ela}}$ yields an expression for the square of the eigenfrequency:

$$\omega^2\left(\frac{m_{\text{tower}}}{5} + m_{\text{nacelle}}\right) = \frac{4EI}{L^3}. \tag{4.61}$$

This result provides an estimate for the tower's lowest eigenfrequency using Rayleigh's method, given the tower mass, nacelle mass, stiffness, and geometry.

4.6 Site and weight of wind turbines

This section provides examples of the size and weight of modern wind turbines.

Example 1: Vestas V90 (1.8 MW)

- Tower height: 120 m
- Blade length: $R = 45$ m
- Nacelle weight: 75 t
- Weight of 3 blades: 40 t
- Total nacelle + blades: 115 t
- Tower weight: 152 t

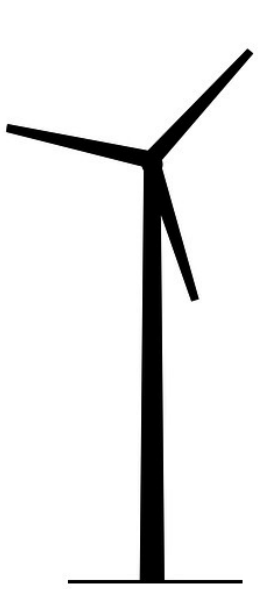

Figure 4.23: Example weights and dimensions of a Vestas V90 1.8 MW wind turbine.

Example 2: MHI–Vestas V164 (9.5 MW)

- Tower height: 105 m
- Blade length: $R = 82$ m
- Nacelle weight: 390 t
- Weight of 3 blades: 105 t (approximately 150 t total including hub)
- Tower weight: 400 t
- Base diameter: 6.5 m

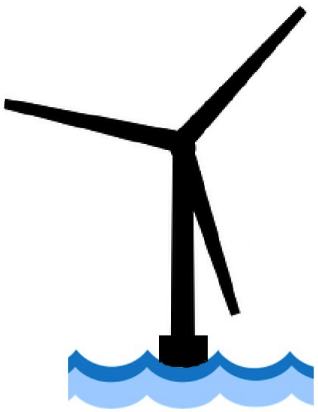

Figure 4.24: Example weights and dimensions of an MHI–Vestas V164 9.5 MW wind turbine.

4.6.1 Stiff & soft towers

The tower's dynamic behavior is strongly influenced by its lowest excitation frequencies.

Lowest excitation frequencies Two key excitation frequencies come from the rotor:

- **1P**: the rotor rotation frequency, which can cause excitation due to blade asymmetries.
- **B.P**: the blade passing frequency, where B is the number of blades.

Given the rotor radius R [m] and wind speed U_∞ [$\mathrm{m\,s^{-1}}$], and with the tip speed ratio defined as

$$\lambda = \frac{R\Omega}{U_\infty},$$

the rotational frequencies can be written as:

$$\omega_{1P} = \Omega = \frac{\lambda U_\infty}{R}, \tag{4.62}$$

$$\omega_{B.P} = B\,\Omega = B\,\frac{\lambda U_\infty}{R}. \tag{4.63}$$

Note that we always have:

$$\omega_{B.P} = B\,\omega_{1P}.$$

The fundamental rotor frequency ω_{1P} typically varies with wind speed.

Tower design considerations If ω_{1P} or $\omega_{B.P}$ coincide with the tower eigenfrequencies, resonance can occur. This must be avoided through:

1. tower design, and

2. controller design.

Given the range of operational speeds, the tower can be classified into three frequency domains (see Figure 4.25):

- **"soft–soft"**: if the lowest tower eigenfrequency ω_{tower} is below the rotor frequency range.
- **"soft–stiff"**: if ω_{tower} lies between ω_{1P} and $\omega_{B.P}$.
- **"stiff–stiff"**: if ω_{tower} is higher than $\omega_{B.P}$, i.e., all tower eigenfrequencies are above the blade passing frequency.

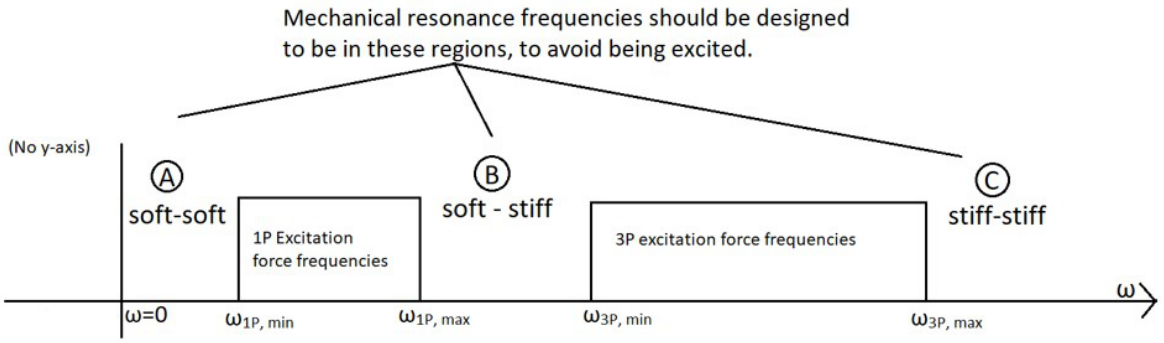

Figure 4.25: Classification of towers into "soft–soft", "soft–stiff", and "stiff–stiff" based on their eigenfrequencies relative to rotor and blade passing frequencies.

Example: MHI–Vestas V164 For the MHI–Vestas V164 turbine:

- Tip speed ratio: $\lambda = 8$
- Rotor radius: $R = 80\,\text{m}$
- Wind speed: $U_\infty = 10\,\text{m}\,\text{s}^{-1}$
- Rotor speed: $\Omega = 1\,\text{rad}\,\text{s}^{-1}$

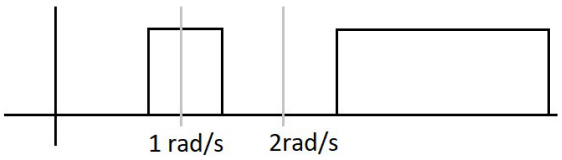

Figure 4.26: Excitation frequency ranges and tower classification for the MHI–Vestas V164.

4.7 Blade oscillation & centrifugal stiffening

Blade oscillations mostly occur flapwise, meaning forward–backward motion (see Figure 4.27).

Interestingly, due to rotation, the blades stiffen and have higher eigenfrequencies than they would have without rotating. The following sections explain why.

Figure 4.27: Flapwise blade oscillation mode.

4.7.1 Rotating, hinged beam (no elasticity)

Consider a beam rotating about a hinge.

The moment of inertia I [kg m^2] about the hinge is:

$$I = \int_0^R \mu(r) r^2 dr, \tag{4.64}$$

where $\mu(r)$ [kg m^{-1}] is the mass per unit length and R [m] is the blade length.

Define:

- ϕ [rad]: flapwise oscillation angle,
- Ω [rad s^{-1}]: rotation frequency,
- $M(\phi)$ [N m]: restoring moment.

The equation of motion is:

$$I\ddot{\phi} = M(\phi). \tag{4.65}$$

The restoring moment $M(\phi)$ comes from centrifugal forces:

$$M(\phi) = -\int_0^R \underbrace{\mu(r)\Omega^2 r \cos(\phi)\sin(\phi)}_{\approx\phi} r\, dr, \tag{4.66a}$$

$$\approx -\phi\Omega^2 \int_0^R \mu(r) r^2 dr, \tag{4.66b}$$

$$= -\phi\, \Omega^2\, I. \tag{4.66c}$$

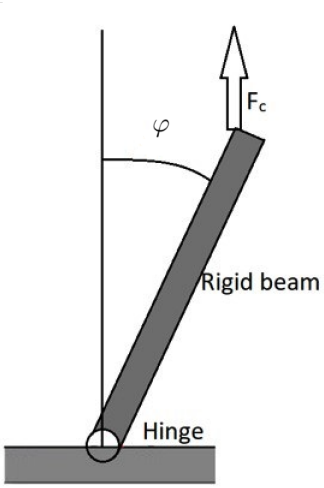

Figure 4.28: Rotating, hinged beam model for flapwise blade oscillations.

Substituting into Equation (4.65) gives:

$$I\ddot{\phi} = -\Omega^2 I\phi \quad \Leftrightarrow \quad \phi(t) = A\sin(\Omega t). \tag{4.67}$$

Thus, the eigenfrequency equals the rotor frequency.

4.7.2 Rotating beam with torsional spring

Now assume the beam is attached to a torsional spring with stiffness K [$\mathrm{N\,m\,rad^{-1}}$] (see Figure 4.29).

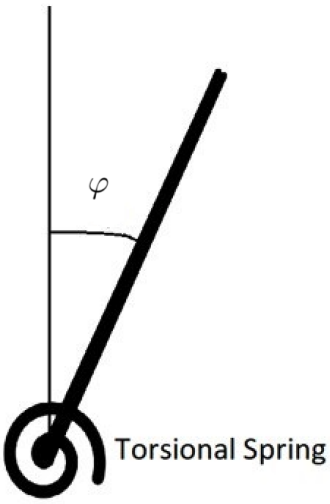

Figure 4.29: Rotating beam with torsional spring stiffness K.

The natural resonance frequency due to the spring alone is:

$$\omega_{NR} = \sqrt{\frac{K}{I}}, \tag{4.68}$$

and the moment becomes:

$$M(\phi) = -\Omega^2 I\phi - K\phi. \tag{4.69}$$

The equation of motion is:

$$I\ddot{\phi} = -\left(\Omega^2 I + K\right)\phi. \tag{4.70}$$

Dividing by I:

$$\ddot{\phi} = -\left(\Omega^2 + \frac{K}{I}\right)\phi, \tag{4.71a}$$

$$= -\left(\Omega^2 + \omega_{NR}^2\right)\phi, \tag{4.71b}$$

where $\omega_{NR}^2 = K/I$.

Finally, the total resonant frequency of the rotating beam is:

$$\omega_R^2 = \omega_{NR}^2 + \Omega^2, \tag{4.72}$$

showing the effect of centrifugal stiffening: rotation adds an extra Ω^2 term, increasing the overall eigenfrequency of the blade.

Chapter 5

Control of Wind Turbines

There are two different ways of controlling wind turbines:

1. **Passive control by mechanical design.** For example, some turbines rely on passive elements such as tails and vanes to orient themselves into the wind.

Figure 5.1: Tail-rotor used for passive control of a wind turbine.

Figure 5.2: Vane used for passive orientation of a wind turbine.

2. **Active control by sensor–actuator systems.** This method typically uses digital controllers and actuators to actively manage turbine operation.

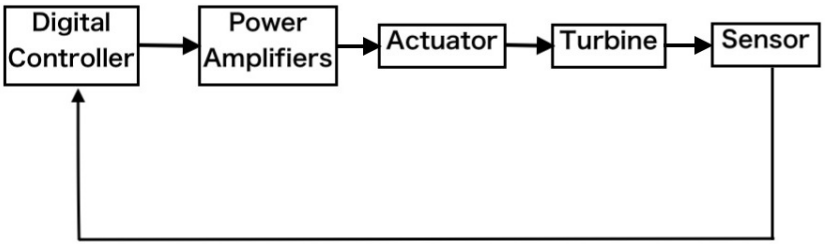

Figure 5.3: Example of an active control system using sensors and actuators.

5.1 Sensors and Actuators in wind turbines

Wind turbines rely on a variety of sensors and actuators to monitor their state and control their operation.

Sensors Typical sensors found in a modern wind turbine include:

- Generator speed, rotor speed, wind speed, yaw rate
- Temperature of gearbox oil, generator winding, ambient air, etc.
- Blade pitch, blade azimuth, yaw angle, wind direction
- Grid power, current, voltage, and grid frequency
- Tower top acceleration, gearbox vibration, shaft torque, blade root bending moment, etc.
- Environmental sensors for icing, humidity, and lightning detection

Actuators Common actuators used in wind turbines include:

- Generator (acting as both actuator and energy conversion device)
- Electric motors for pitch and yaw systems
- Linear motors, magnets, and switches
- Hydraulic power units and pistons (for high-power and high-speed control)
- Resistance heaters and fans for temperature regulation
- Mechanical brakes for the rotor and yaw system

5.2 Control system architecture

Usually, the **supervisory control** operates at a high level, determining the turbine operating status. The **dynamic control** operates at a lower level, handling fast-changing variables such as torque, pitch, and power.

5.3 Control of variable speed turbines

For speed control, the main actuators are:

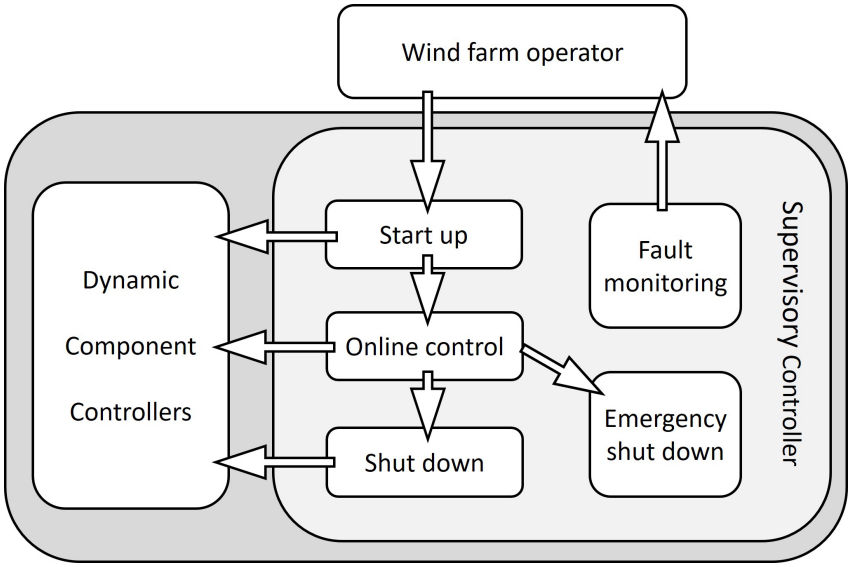

Figure 5.4: Overview of control system architecture for a wind turbine.

- Blade pitch
- Generator torque (this is controlled slowly to avoid drive-train oscillations)

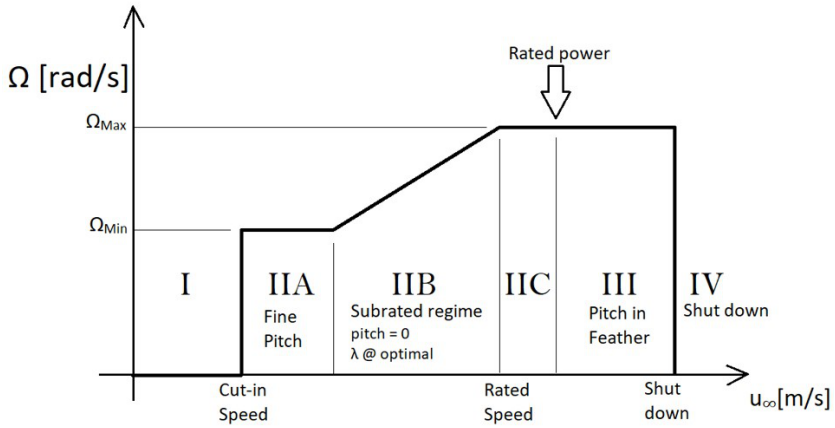

Figure 5.5: Rotation speed as a function of wind speed.

Because the wind speed on the rotor disc cannot be perfectly known, we must consider what the maximum power production and power coefficient $C_P(\lambda, \beta)$ can be.

The power function is given by:

$$P = \frac{1}{2}\rho A U_\infty^3 C_P(\lambda, \beta), \tag{5.1}$$

where:

- P [W] is the mechanical power,
- ρ [kg m^{-3}] is air density,
- A [m^2] is the swept area of the rotor,

- U_∞ [$\mathrm{m\,s^{-1}}$] is the free-stream wind speed,
- C_P [–] is the power coefficient,
- $\lambda = \frac{\Omega R}{U_\infty}$ is the tip-speed ratio, and
- β [°] is the collective blade pitch angle.

The power coefficient C_P is maximized at $\lambda = \lambda^*$ (e.g. $\lambda^* = 7$) and $\beta = \beta^*$. The optimal power coefficient is denoted $C_P^* = C_P(\lambda^*, \beta^*)$. (Note: The asterisk * denotes the optimal value.)

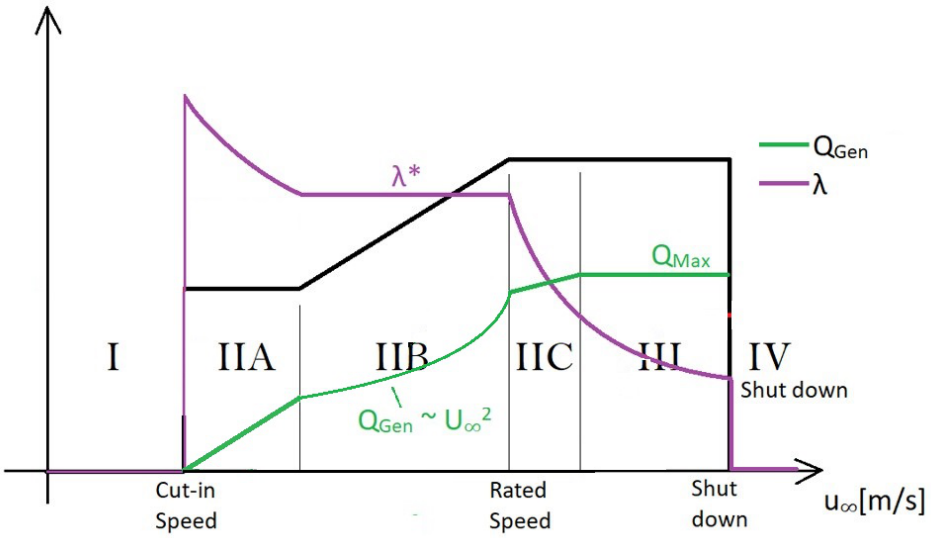

Figure 5.6: Pitch angle β, generator torque Q_{Gen}, and tip-speed ratio λ as functions of wind speed, in the different control regions.

The generator torque is denoted Q_{Gen}, and in equilibrium we have:

$$Q_{Gen} = Q_{Aero}.$$

Operating regions The turbine's operation is divided into several wind speed regions:

- **Region IIA:** The tip-speed ratio λ is fixed to $\lambda_{fix}^{IIA} = \frac{\Omega_{min} R}{U_\infty}$, and the blade pitch β is maximized. The power coefficient is then:

$$C_P = C_P(\lambda_{fix}^{IIA}, \beta).$$

- **Region IIB (subrated):** $\lambda = \lambda^*$ and $\beta = \beta^*$. The power coefficient is optimal:

$$C_P = C_P^* = C_P(\lambda^*, \beta^*).$$

  This means that:

$$P \propto U_\infty^3.$$

- **Region IIC & III:** The tip-speed ratio λ is again fixed to $\lambda_{fix}^{IIC} = \frac{\Omega_{max} R}{U_\infty}$, and β is regulated to control power. Region III is the maximum power region.

The blade pitch β^* is centered at 0 degrees because the blades are designed such that the power coefficient is maximized at that pitch.

5.4 Torque control at partial load (in region IIB)

The generator torque Q_{Gen} [N m] can be controlled directly and should counteract the aerodynamic torque Q_{Aero} [N m].

Given the rotor inertia I [kg m^2], the rotor speed Ω [rad s^{-1}] satisfies the ordinary differential equation:

$$I\dot{\Omega} = Q_{Aero} - Q_{Gen}. \tag{5.2}$$

The aerodynamic torque Q_{Aero} depends on wind speed U_∞, rotor speed Ω, and blade pitch angle β.

The aerodynamic power is given by:

$$P_{Aero} = \Omega\, Q_{Aero},$$

and since $\Omega = \frac{\lambda U_\infty}{R}$ we can express Q_{Aero} as:

$$Q_{Aero} = \frac{P_{Aero}}{\Omega} = \frac{1}{2}\rho(\pi R^2)U_\infty^3 \frac{C_P(\lambda,\beta)}{\lambda U_\infty}, \tag{5.3a}$$

$$= \frac{1}{2}\rho\pi R^3 U_\infty^2 \underbrace{\frac{C_P(\lambda,\beta)}{\lambda}}_{:=C_Q(\lambda,\beta)}, \tag{5.3b}$$

$$= \frac{1}{2}\rho\pi R^5 \Omega^2 \frac{C_P(\lambda,\beta)}{\lambda^3}. \tag{5.3c}$$

How to choose Q_{Gen} when only Ω is measured? The goal is to find the function $Q_{Gen}(\Omega)$ that keeps the turbine at the optimal tip speed ratio λ^* in Region IIB.

Intuitively:

- Apply a higher Q_{Gen} if Ω is too high.
- Apply a lower Q_{Gen} if Ω is too low.

At the optimal speed $\Omega^* = \frac{\lambda^* U_\infty}{R}$ we must have:

$$Q_{Aero}(\Omega^*, U_\infty, \beta^*) = Q_{Gen}(\Omega^*). \tag{5.4}$$

Thus, the generator torque control law is defined as:

$$Q_{Gen}(\Omega) := Q_{Aero}\left(\Omega, \frac{R\Omega}{\lambda^*}, \beta^*\right), \tag{5.5a}$$

$$= \frac{1}{2}\rho\pi R^5 \frac{C_P(\lambda^*, \beta^*)}{(\lambda^*)^3}\Omega^2, \tag{5.5b}$$

where the term

$$\underbrace{\frac{1}{2}\rho\pi R^5 \frac{C_P(\lambda^*, \beta^*)}{(\lambda^*)^3}}_{=:K_{Gen}}$$

is a constant torque coefficient.

Stability at Ω^* From Equation (5.2) we write the rotor speed derivative:

$$\dot{\Omega} = f(\Omega) = \frac{1}{I}\left(Q_{Aero}(\Omega, U_\infty, \beta^*) - Q_{Gen}(\Omega)\right). \tag{5.6}$$

Question 1: Is $f(\Omega^*) = 0$?

Yes. If $\Omega^* = \frac{\lambda^* U_\infty}{R}$, then by construction:

$$Q_{Aero}(\Omega^*, U_\infty, \beta^*) = K_{Gen}(\Omega^*)^2,$$

so indeed $f(\Omega^*) = 0$.

Question 2: Is the equilibrium stable?

We look at the derivative of f with respect to Ω:

$$\frac{df}{d\Omega} = \frac{1}{I}\left(\frac{dQ_{Aero}}{d\Omega} - \frac{dQ_{Gen}}{d\Omega}\right).$$

At $\Omega = \Omega^*$, we evaluate:

$$\frac{dQ_{Gen}}{d\Omega} = 2K_{Gen}\Omega,$$

and similarly:

$$\frac{dQ_{Aero}}{d\Omega} = 2K_{Gen}\Omega,$$

but because Q_{Gen} is actively controlled, the net slope is negative.

Simplifying:

$$\left.\frac{df}{d\Omega}\right|_{\Omega^*} = -\frac{1}{I}\frac{1}{2}\rho\pi R^5 \frac{3C_P^*\Omega^*}{(\lambda^*)^3}.$$

This derivative is strictly negative, meaning the control law is stable.

The settling time is inversely proportional to Ω^* (or equivalently, proportional to $\frac{1}{\Omega^*}$ or $\frac{R}{U_\infty}$).

5.5 Thrust jump at nominal wind speed

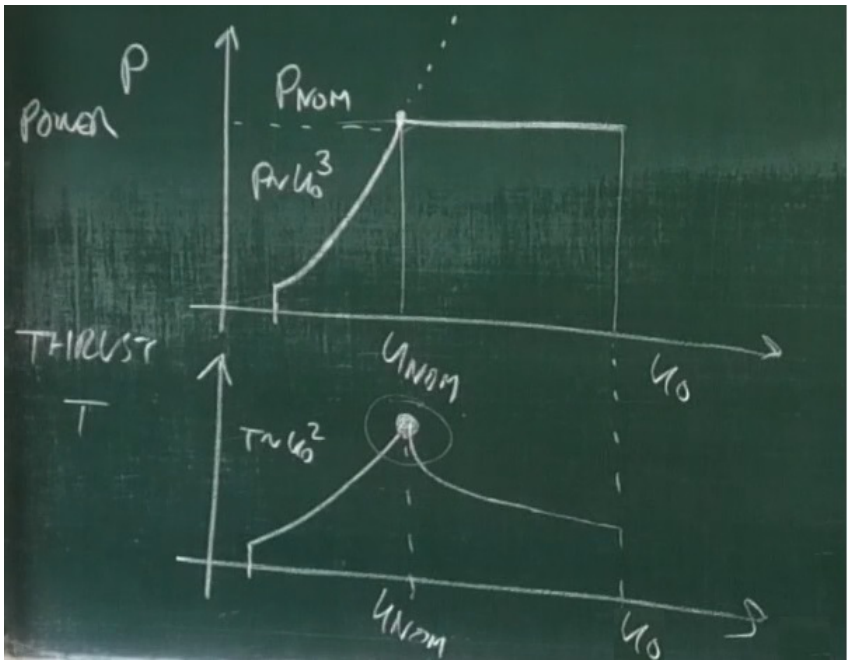

Figure 5.7: Power and thrust as functions of wind speed.

The reason for the reduction in thrust for $U_0 > U_{\text{nom}}$ is the reduction of the induction factor a.

Recall some facts from Betz theory The power coefficient and thrust coefficient are given by:

$$C_P = \frac{P}{\frac{1}{2}\rho A U_0^3} = 4a(1-a)^2,$$

$$C_T = \frac{T}{\frac{1}{2}\rho A U_0^2} = 4a(1-a),$$

$$T = \frac{P}{(1-a)U_0}.$$

The optimal power harvesting is achieved for induction factor $a^* = \frac{1}{3}$.

How does a depend on U_0? At the Betz limit we have:

$$C_P^* := C_P(a^*) = \frac{16}{27},$$

and

$$\left.\frac{\mathrm{d}C_P}{\mathrm{d}a}\right|_{a^*} = 0.$$

For $U_0 \geq U_{\text{nom}}$ we must ensure $P = P_{\text{nom}}$, which is only possible if we reduce C_P.

In a pitch-controlled system, C_P is reduced by reducing the induction factor a (alternatively, one could also increase the induction factor to reduce the power).

For $C_P < C_P^*$ we have $a < a^*$. Applying a Taylor expansion:

$$C_P = 4a(1-a)^2 = C_P^* + \frac{1}{2}\frac{\mathrm{d}^2 C_P}{\mathrm{d}a^2}(a-a^*)^2 + \text{higher order terms.} \tag{5.7}$$

The derivatives are:

$$\frac{\mathrm{d}C_P}{\mathrm{d}a} = 4(1-a)^2 - 8a(1-a),$$

$$\frac{\mathrm{d}^2 C_P}{\mathrm{d}a^2} = -16(1-a) + 8a \quad \rightarrow \quad \left.\frac{\mathrm{d}^2 C_P}{\mathrm{d}a^2}\right|_{a^*} = -8.$$

Plugging this into Equation (5.7) gives:

$$C_P = C_P^* - 4(a-a^*)^2,$$

so that:

$$a - a^* = -\sqrt{\frac{C_P^* - C_P}{4}}. \tag{5.8}$$

How does T depend on $U_0 - U_{\text{nom}} > 0$? Starting from:

$$C_P = C_P^* + \frac{\mathrm{d}C_P}{\mathrm{d}U_0}(U_0 - U_{\text{nom}}) + \text{higher order terms.} \tag{5.9}$$

For $P = P_{\max}$ and $U_0 = U_{\text{nom}}$:

$$C_P = \frac{P_{\max}}{\frac{1}{2}\rho A U_0^3}.$$

Differentiating:

$$\frac{\mathrm{d}C_P}{\mathrm{d}U_0} = -\frac{3P_{\max}}{\frac{1}{2}\rho A U_0^4} \quad \rightarrow \quad \frac{\mathrm{d}C_P}{\mathrm{d}U_0} = -\frac{3C_P^*}{U_{\mathrm{nom}}}.$$

Plugging into Equation (5.9):

$$C_P = C_P^* - 3C_P^* \frac{(U_0 - U_{\mathrm{nom}})}{U_{\mathrm{nom}}},$$

or equivalently:

$$C_P^* - C_P = 3C_P^* \frac{(U_0 - U_{\mathrm{nom}})}{U_{\mathrm{nom}}}.$$

Substitute this result into Equation (5.8) to get the relationship between induction factor and wind speed:

$$a - a^* = -\sqrt{\frac{3C_P^*}{4U_{\mathrm{nom}}\,(U_0 - U_{\mathrm{nom}})}}. \tag{5.10}$$

Effect on thrust The thrust is given by:

$$T = C_T \cdot \frac{1}{2}\rho A U_0^2 = 4a(1-a) \cdot \frac{1}{2}\rho A U_0^2.$$

Differentiating thrust with respect to U_0:

$$\frac{\mathrm{d}T}{\mathrm{d}U_0} = T_{\mathrm{nom}} + \frac{P_{\max}}{2U_{\mathrm{nom}}(1-a)}(U_0 - U_{\mathrm{nom}}) + (a(U_0) - a^*)\frac{U_0}{(1-a)U_{\mathrm{nom}}},$$

which simplifies to:

$$T = T_{\mathrm{nom}} \left[1 - \frac{U_0 - U_{\mathrm{nom}}}{U_{\mathrm{nom}}} - \sqrt{\frac{3C_P^*}{4U_{\mathrm{nom}}}(U_0 - U_{\mathrm{nom}})} \right].$$

Chapter 6

Alternative Concepts

6.1 Vertical axis wind turbines

There are two main differences between horizontal axis wind turbines (HAWTs), which we have been studying so far, and vertical axis wind turbines (VAWTs):

- A VAWT's generator is mounted at ground-level, simplifying the structural requirements on the tower and also making construction easier.
- HAWT blades are always passing through similarly 'fresh' flow, whereas VAWT blades have a 'front pass' through fresh flow, and a 'back pass' through a slowed (and turbulent) flow. This usually makes VAWTs less effecient (smaller C_P) that HAWTs.

Two main vertical axis wind turbine types are presented here: the Darrieus rotor and the Savonius turbine.

There main difference between the two, is in how each system produces power. In the case of the Savonius turbine, it's a drag force from the wind on the "cup" side of the blades that causes the rotor to turn. In the case of the Darrieus turbine, the blades pass perpendicular to the freestream (as they do in the 'normal' horizontal axis wind turbines (HAWTs)), meaning that it's a lift force that drives rotation. But, different from HAWTs and Savonius rotors, when Darrieus rotors are not rotating, there generally is not enough aerodynamic force pointed in the tangential rotation for the turbine to start on it's own. Because of this, it's common practice to pair the two systems, with a more-efficient (higher C_P) Darrieus turbine intended to produce power in normal operation mounted in combination with a small Savonius turbine intended to start the system.

6.2 Airborne wind energy (AWE)

For further detail, see the lecture slides (link provided in the notes): `https://www.syscop.de/files/2018ss/WES/lectures/20180711WES-AWE.key.pdf`

There are two main system concepts:

- In the first, there are generators and propellers on-board the kite, whose generated electricity is sent down through an electrified tether to the ground. This concept is

(a) Side view of a Darrieus vertical axis wind turbine.

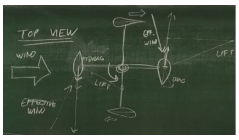

(b) Top view of a Darrieus rotor.

(c) Side view of a Savonius wind turbine.

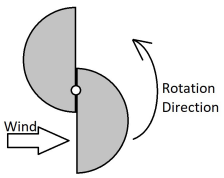

(d) Top view of a Savonius rotor.

Figure 6.1: Typical vertical axis wind turbine system types

variously called: "drag-mode" or "ground-gen" or "on-board generation".

- In the second, the tether is wrapped around the generator drum, and the kite flies variable-lift trajectories, so that the tether unwinds the generator at high tension before the tether gets re-wound at low tension. This concept is variously called: "lift-mode" or "fly-gen" or "pumping-cycle".

Variant 2: Generator on ground (pumping cycle) We assume the following:

- The effect of gravity is neglected.
- The cable is parallel to the wind W.
- The kite flies crosswind with high speed.

Where the variables are defined as:

- $V = \lambda \cdot W$
- W: real wind speed $[\mathrm{m\,s^{-1}}]$
- V: kite speed $[\mathrm{m\,s^{-1}}]$
- α: roll-out speed as a fraction of the real wind speed

6.2.1 Loyd's formula

Regard a kite or airfoil under idealized conditions:

- The tether is parallel to the wind.
- Gravity is neglected, steady wind $W \equiv U_\infty$.
- Steady crosswind flight with downward components.

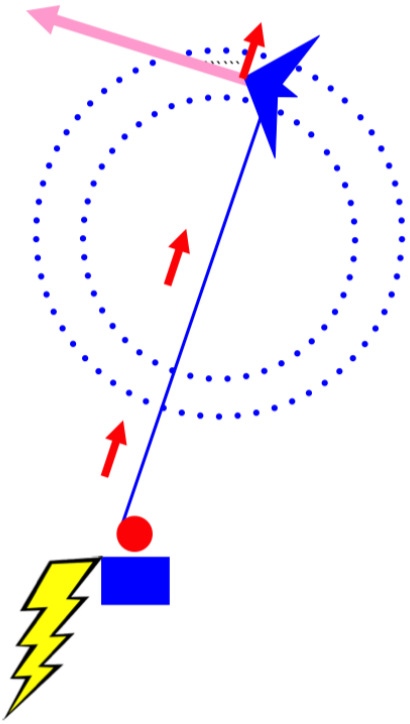

Figure 6.2: Ground-based airborne wind energy concept with a pumping cycle.

Given C_L, C_D, roll-out speed αW, wing area A, and tip speed ratio λ, the wind and motion vectors in the x–y frame are:

$$\mathbf{W} = \begin{bmatrix} -W \\ 0 \end{bmatrix} \tag{6.1}$$

$$\mathbf{V} = \begin{bmatrix} -\alpha W \\ \lambda W \end{bmatrix} \tag{6.2}$$

The effective wind is:

$$\mathbf{V}_e = \mathbf{W} - \mathbf{V} = \begin{bmatrix} (1-\alpha)W \\ -\lambda W \end{bmatrix} \tag{6.3}$$

with magnitude:

$$\|\mathbf{V}_e\| = W\sqrt{(1-\alpha)^2 + \lambda^2}.$$

Drag and lift forces The drag force is:

$$\mathbf{F}_D = \frac{1}{2}\rho A \|\mathbf{V}_e\|^2 C_D \frac{\mathbf{V}_e}{\|\mathbf{V}_e\|} \tag{6.4a}$$

$$= \frac{1}{2}\rho A V_e^2 C_D \begin{bmatrix} (1-\alpha) \\ -\lambda \end{bmatrix} \frac{1}{\sqrt{(1-\alpha)^2 + \lambda^2}} \tag{6.4b}$$

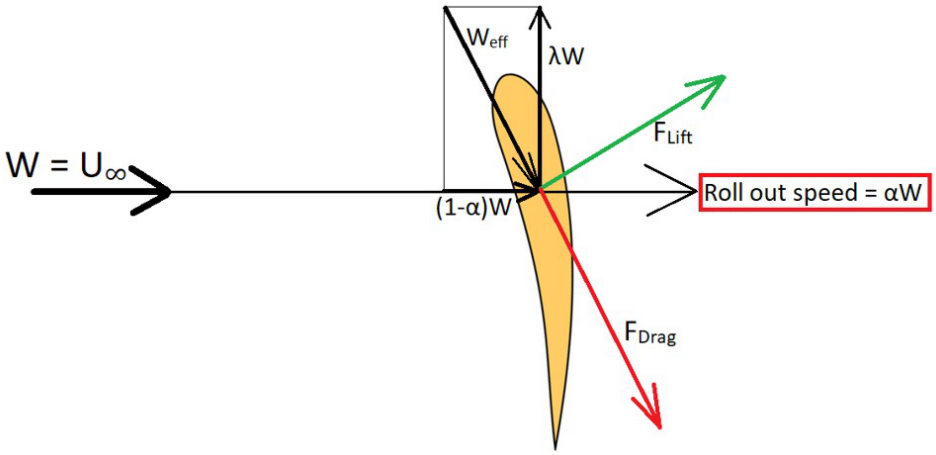

Figure 6.3: Kite crosswind configuration for Loyd's formula.

and the lift force is:

$$\mathbf{F}_L = \frac{1}{2}\rho A \|\mathbf{V}_e\|^2 C_L \frac{\mathbf{V}_e}{\|\mathbf{V}_e\|} \tag{6.5a}$$

$$= \frac{1}{2}\rho A V_e^2 C_L \begin{bmatrix} \lambda \\ (1-\alpha) \end{bmatrix} \frac{1}{\sqrt{(1-\alpha)^2+\lambda^2}} \tag{6.5b}$$

Sum of forces

$$\mathbf{F}_L + \mathbf{F}_D = \frac{1}{2}\rho A V_e^2 \frac{1}{\sqrt{(1-\alpha)^2+\lambda^2}} \begin{bmatrix} C_D(1-\alpha)+C_L\lambda \\ -C_D\lambda + C_L(1-\alpha) \end{bmatrix}. \tag{6.6}$$

Force balance In steady state there is no acceleration, so the force in the y-direction must be zero. This yields:

$$\lambda C_D = (1-\alpha)C_L. \tag{6.7}$$

Rearranging:

$$\lambda = \frac{C_L}{C_D}(1-\alpha). \tag{6.8}$$

Power generation The generated power is equal to roll-out speed αW times the x-component of tether tension F_T:

$$P = \alpha W F_T \tag{6.9a}$$

$$= \alpha W \cdot \frac{1}{2}\rho A W^2 \sqrt{(1-\alpha)^2+\lambda^2}\,(C_D(1-\alpha)+C_L\lambda) \tag{6.9b}$$

$$= \frac{1}{2}\rho A W^3 \alpha(1-\alpha)^2 \left(\frac{C_L^3}{C_D}\right) \tag{6.9c}$$

$$= \frac{1}{2}\rho A W^3 \frac{C_L^2}{C_D}\left(1+2\alpha(1-\alpha)^2\right). \tag{6.9d}$$

Optimization The maximum power is reached when $\alpha(1-\alpha)^2$ is maximized:

$$f(\alpha) = \alpha(1-\alpha)^2. \tag{6.10}$$

Differentiating:

$$f'(\alpha) = (1-\alpha)^2 - 2\alpha(1-\alpha) = 0. \tag{6.11}$$

From Equation (6.11), we find:

$$(1-\alpha) = 2\alpha \quad \Rightarrow \quad \alpha^* = \frac{1}{3}.$$

Evaluating at α^*:

$$f(\alpha^*) = \frac{4}{27}.$$

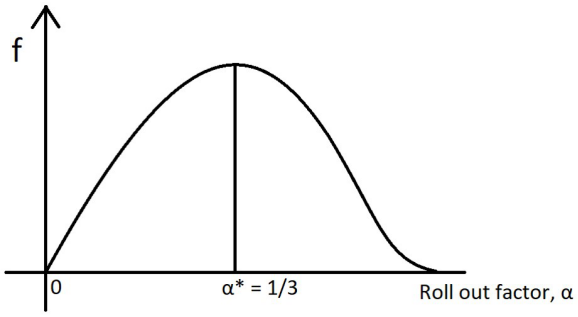

Figure 6.4: Optimal reel-out factor α^* and Loyd's formula derivation.

Loyd's formula The final Loyd's formula for maximum power is:

$$P = \frac{1}{2}\rho A W^3 \cdot \frac{4}{27} \cdot \frac{C_L^2}{C_D} \underbrace{\left(1 + \frac{C_D^2}{C_L^2}\right)}_{\approx 1} \tag{6.12}$$

Example Consider $C_L = 1$, $C_D = 0.05$, $W = 10$ m/s, and $\rho = 1.2$ kg/m^3.

We compute:

$$\frac{C_L^2}{C_D} = \frac{1^2}{0.05} = 20.$$

Substituting:

$$\frac{P}{A} = \underbrace{\frac{1}{2}\rho W^3 \cdot \frac{4}{27} \cdot C_L \frac{C_L^2}{C_D}\left(1 + \frac{C_D^2}{C_L^2}\right)}_{\zeta \text{ "Harvesting factor zeta"}}$$

$$\zeta = \frac{4}{27} \cdot 400 \left(1 + \frac{1}{400}\right) \approx 59$$

This yields a harvesting factor ("zeta") of approximately 59 and a maximum specific power:

$$P/A \approx 36 \text{ kW/m}^2.$$

Acknowledgement

This document was producing by transcribing and expanding on a previous (2020) edition. This transcription, including figure extraction, was completed with the assistance of OpenAI's ChatGPT, a language model. ChatGPT was used to convert the contents from pdf into LaTeXformat, extract and label figures, generate three illustrative plots (e.g., Weibull, Rayleigh, and Normal distributions), and improve the flow of text by completing partial sentences into full, coherent statements. The contents were reviewed and edited, and in many cases re-written by Rachel Leuthold. For future TAs, please find the LaTeXcode for this version at `https://gitlab.syscop.de/teaching/WIND-ENERGY-SYSTEMS`.
- Freiburg, July 2025